CONTRACT REQUIREMENTS	CONTRACT ITEM	MODEL	CONTRACT NO.	DATE
Exhibit E, Para. 5.1	13	LEM	NAS 9-1100	14 Jan 63

TYPE II

#693

REPORT

NO. LED-500-5

DATE: 22 April 1965

LMS MATH MODEL - EQUATIONS OF MOTION, SUBSYSTEM INTERFACES AND VISUAL DISPLAY DRIVE EQUATIONS

CODE 26512

M. Shapiro
F. Murra

PREPARED BY:

M. Shapiro
F. Murra

A.B. Whitaker

Approved By
A.B. Whitaker

Ross Fleisig

APPROVED BY:
Ross Fleisig

V. Speiser

CHECKED BY:
V. Speiser

H. Levin

Approved By
H. Levin

REVISIONS

DATE	REV. BY	REVISIONS & ADDED PAGES	REMARKS

~~AVAILABLE TO NASA HEADQUARTERS ONLY~~

GRUMMAN AIRCRAFT ENGINEERING CORPORATION

FORWARD

The LEM Guidance, Navigation and Control-Analysis and Integration Section has the responsibility of supplying major portions of the LEM Mission Simulator (LMS) Math Model to the LEM Training Equipment Section. Report LED-500-5 represents a partial fulfillment of this obligation.

Where possible, all equations are derived in the most general form to reflect an exact model of the physical system. These equations are subsequently simplified in the text to the extent that the ensuing simulation is compatible with the prime mission objective, namely astronaut training. A few of the more important simplifications, that are discussed in the text, are listed below:

1. During lunar mission exercises, the LEM equations of motion should include lunar triaxiality perturbations only.
2. The fuel slosh computational loop should be based on a constant damping ratio. It is recommended that additional simplifications be sought with respect to the series of second order differential equations that represent the fuel-slosh-pendulum analog model.
3. During all independent LMS mission modes, the CSM trajectory should be represented by 2-body motion.
4. During all Earth mission exercises, LEM motion should be defined by relative motion equations, wherein the coordinate origin is located at the CSM mass center. Thus, Earth oblateness perturbations and CSM aerodynamic perturbations are never computed by the LEM Mission Simulator.
5. During lunar mission exercises, relative motion equations should be used to describe the LEM trajectory whenever the LEM is located within some small, predetermined sphere of influence measured from the CSM mass center.

6. Jet damping forces and torques should be deleted.

7. Stage separation forces and torques should be represented by a linear function rather than a third order polynomial.

8. The lunar libration matrix and the regression of the Moon's node should be maintained constant during the course of a run.

9. During any given run, the Moon's radius should be a constant specified by the Land-Mass Simulator datum surface.

10. Lunar surface velocities due to the Moon's libration and nodal regression rate are small and should be neglected.

11. The incremental LEM velocity relative to the lunar surface due to a displacement between the LEM-CG and the landing radar-CG is small and should be neglected.

12. Ground tracker elevation constraints should be assumed constant rather than computed as a function of the tracker azimuth angle.

13. Fuel and oxidizer inertias should be based on point-mass considerations.

TABLE OF CONTENTS

I. Summary

The purpose of this report is to present the rationale, assumptions and derivations used to generate the following sets of equations for the LMS.

A. LEM Translational Equations of Motion (Lunar)

B. CSM and LEM Relative Equations of Motion

C. Rotational Equations of Motion

D. General Transformations

E. Ephemeris

F. Rendezvous Radar Subsystem Interface Equations

G. Landing Radar Subsystem Interface Equations

H. Communications Antenna Interface Equations

I. Weights and Balance

J. External Visual Display Drive Equations

Sets A through J represent detailed equations that provide "true" (error free) trajectory information to all major subsystems and the instructor. These equations are also used to generate true visual cues for the astronaut.

II. Introduction

A. General. The Apollo Mission Simulation Complex will be used to train all personnel directly connected with the landing of two men on the Moon and their safe return to Earth. This complex consists of three simulators; namely, the Manned Spaceflight Control Center (MSCC), the Apollo Mission Simulator (AMS), and the LEM Mission Simulator (LMS). Briefly, the MSCC coordinates all aspects of the Apollo Mission, while the AMS and LMS are concerned primarily with those functions performed by the Command and Service Modules and the Lunar Excursion Module, respectively. Only the LMS functions are described herein.

The LMS Math Model has been written in accordance with the ground rules established in reference 1. These are:

1. The LMS must operate either independently of the AMS and MSCC or in conjunction with the AMS and/or MSCC (integrated mode).
2. The LMS must be capable of simulating either Lunar Mission or Earth Mission phases.
3. The LMS must describe all LEM operational functions.

B. Report Format. The detailed equations and information contained herein is outlined in accordance with the Index Diagram given in sheet AAA (see Section VI). This summary sheet contains 10 sets of equations and 1 set of figures. Each set of equations corresponds to a particular simulation function such as rotational equations of motion, or subsystem interface equations, or external visual display drive equations. Specific simulation functions are lettered from A to J. Furthermore, each set or simulation function is partitioned into subsets numbered from 10 to 90. With this breakdown it is possible to quickly locate a particular equation. For example, F - 20 describes the rendezvous radar gimbal angle and gimbal rate equations, since, from sheet AAA, set F denotes the rendezvous radar and subset 2^1 denotes gimbal angle and rate computations.

Sheet AAA also presents required inputs from other math models. External math model inputs are indicated by arrows entering from the left of each set. The more important outputs, computed within each set, are shown by arrows leaving the set.

A more detailed breakdown of the flow between sets, subsets, and other math models are given in sheets AA. Sheets AA were generated as an aid to programming the equations on a digital computer.

Discussed in Section III of this report are all the detailed eqations developed on sheets A through J. Section III is divided into subsections. Each subsection is lettered from A to J to correspond to those sets (simulation functions) shown in index sheet AAA. Thus, report subsection III-J discusses the derivations required to generate the visual display drive equations. Each report subsection is complete and includes:

a. the purpose or reasons for simulating each set

b. derivations and assumptions related to the subset equations

c. recommendations or need for future work

d. conclusions

Equations, given in the text, that are designated by a capital letter followed by a number can be found on the corresponding sheets lettered from A to J. These equations do not necessarily follow a sequential order in the text since the complete flow diagrams were generated prior to documentation. Text equations designated by small letters are used either as intermediaries to derive a set or subset equation or to present an alternate approach not listed on the detailed flow diagrams.

References are listed in Section IV. Symbols, units and range of variables are defined in Section V. Index sheet AAA, flow sheets AA and detailed equation sheets A through J are given in Section VI. All Figures are presented in Section VII.

III. Detailed Equations - Sheets A through J

A. LEM Translational Equations (M-Frame).

1. Purpose. The purpose of Set A equations is to accurately represent all significant external forces acting on the LEM vehicle during the lunar mission phase. Integrating these forces provides a "true" LEM trajectory governed by the accuracy of the physical assumptions and the numerical integration scheme employed. These equations will be used during independent or integrated lunar operational modes only. Earth operational modes and CSM motion equations during the independent mode are discussed in Subsection III-B.

2. Primary Reference System and Generalized Equations of Motion. NASA has suggested (reference 2) that the primary reference frame be defined by the mean Earth equator of date, where, axis X is directed along the mean equinox of date and axis Z lies along the Earth's mean spin vector. During lunar missions, the reference set will be Moon centered (X_M, Y_M, Z_M; see Figure 1) whereas, during Earth training missions the reference set will be earth centered (X_E, Y_E, Z_E).

The equations of motion of a point of mass relative to an inertial frame centered at a massive body, n, are well known:

$$\ddot{\bar{r}}_L = -K^2(m_n+m_L)\frac{\bar{r}_L}{r_L^3} - K^2\sum_{\substack{j=1 \\ j\neq L}}^{n-1} m_j\left[\frac{\bar{r}_L-\bar{r}_j}{r_{jL}^3}+\frac{\bar{r}_j}{r_j^3}\right]+\bar{P}+\sum\frac{\bar{F}}{m_L} \qquad (a\text{-}1)$$

Subscript L denotes LEM. Let the massive body represent the moon, n = M. The bracketed term contains both the direct attraction of body m_j on the vehicle m_L and the indirect attraction of body m_j (i.e. Earth, Jupiter, etc.) on the Moon's origin m_M. Vector $\bar{P}$ denotes the lunar triaxiality acceleration. All external forces such as main engine thrust, RCS thrust, fuel slosh, separation forces and jet damping forces are lumped into the term $\sum \frac{\bar{F}}{m_L}$.

3. Gravitational Perturbations. During the lunar mission phase all gravitational forces except those due to lunar triaxiality are neglected. The reasons for this statement are listed below.

a. "M or E" - Frame Perturbation. Lunar-solar forces acting on the Earth's equatorial bulge cause the Earth's mean equator of date, and hence the mean equinox, to precess at an average rate of about 0.015 degrees/year. Accordingly, the reference M or E-frame is non-inertial. For the LMS, however, an inertial set is assumed. Solution accuracy is not compromised by this assumption because it can be shown that the apparent coriolis and centrifugal errors induced are less than those perturbative accelerations due to either Mars or Jupiter (reference 3). The LMS-LEM trajectory calculations are therefore unaffected.

b. Solar-Perturbation. An extensive numerical study has been conducted at GAEC (reference 4) to ascertain the effect of lunar triaxiality, Earth, Sun and planet perturbations on the motion of a close lunar satellite. This report clearly indicates that the effect of solar and planetary (Earth excluded) perturbations on satellite motion are approximately 3 to 4 orders of magnitude smaller than the combined Earth-Lunar triaxiality perturbations. This is in general agreement with the order of magnitude obtained by simply ratioing the Sun and triaxiality perturbations. Since, as shown below, the Earth perturbation can be neglected for purposes of LMS simulation, it is safe to neglect the solar and planetary perturbations.

c. Earth Perturbation. The influence of the Earth's perturbative acceleration on the motion of a near lunar satellite has a smaller effect than does the Moon's triaxiality perturbation. This is evidenced either from inspecting the Earth-Moon potential function or by comparing the data given in reference 4. Numerical data from reference 4 indicate that the Earth perturbation has approximately a 1 to 2 order of magnitude smaller effect on short period radial, semi-major axis, and eccentricity excursions (for a low altitude, circular, equatorial lunar satellite orbit) than does lunar triaxiality perturbation. For example, the Earth's contribution to the radial excursion is .009 n. mi. during a 14 day mission. Thus, by neglecting the Earth perturbation, a maximum short period radial excursion error of .009 n.m. is introduced.

LEM orbital inclination and right ascension of the ascending node long period and secular excursions must also be considered. Reference 4 indicates that for a lunar equatorial satellite orbit, the Earth has a more predominant influence on these parameters then does the lunar triaxiality. This result appears reasonable since to the first order there is no lunar triaxiality perturbation normal to the equatorial plane. The Earth perturbation, however, does produce a disturbing force component normal to this plane. Thus, inclination or nodal excursions, for a lunar equatorial orbit, reflect the effect of the Earth's influence rather than the influence of a triaxial Moon.

Although the Earth perturbation on satellite inclination exceeds that of the Moon, the resultant multibody inclination excursions are still small. For example, the equivalent angular satellite position error due to neglecting the Earth, based on representative initial conditions (low altitude, circular, lunar equatorial orbit), is approximately .01 n. mi. after each satellite revolution (reference 4). As the LEM orbit inclination with respect to the lunar equator increases, the Earth's secular perturbative influence diminishes relative to the lunar triaxiality perturbation. Since the LEM lunar mission is of the order of a few days, and since the resultant Earth induced excursions are well within "spec limits" (reference 1), the Earth has been deleted as a perturbing body during lunar separation-to-descent and ascent-to-rendezvous mission phases.

4. LEM Equations of Motion. In the absence of solar and Earth perturbations, the LEM translational equations (a-1) with respect to a Moon centered M-Frame become:

$$\ddot{\bar{r}}_{M/L} = \frac{-\mu_M \bar{r}_{M/L}}{r^3_{M/L}} + \bar{P}_{M/L} + \sum \frac{\bar{F}_{M/L}}{m_L} \qquad \text{(A-10)}$$

a. Lunar Triaxiality Perturbation. The recommended form of the lunar triaxiality potential is (reference 2):

$$\Phi_M = C\left[A\left(1 - \frac{3Z^2_{S/L}}{r^2_{M/L}}\right) + B\left(1 - \frac{3Y^2_{S/L}}{r^2_{M/L}}\right)\right] \qquad \text{(a-2)}$$

Constants A, B and C have been determined by a NASA Earth Model Meeting and are given as (reference 2):

$$A = \frac{I_C - I_A}{I_C} = 619.36 \times 10^{-6}$$

$$B = \frac{I_B - I_A}{I_C} = 202.70 \times 10^{-6} \qquad \text{(A-01)}$$

$$C = \left(\frac{3}{2}\frac{I_C}{m_M R_M^2}\right)\left(\frac{M_M R_M^2}{3}\right) = 2.815995 \times 10^{25} \frac{FT^5}{SEC^2} \qquad (A\text{-}01)$$

Principal moments of inertia, I_A, I_B, I_C, are measured along the Moon's long, intermediate and short axis, respectively.

The triaxiality perturbation acting on the LEM vehicle is given by the gradient of (a-2), thus:

$$\bar{P}_S = P_{X_S}\hat{i}_S + P_{Y_S}\hat{j}_S + P_{Z_S}\hat{k}_S$$

where:

$$P_{X_S} = \frac{3CX_{S/L}}{r_{M/L}^5} F_L$$

$$P_{Y_S} = \frac{3CY_{S/L}}{r_{M/L}^5}(F_L - 2B) \qquad (A\text{-}21)$$

$$P_{Z_S} = \frac{3CZ_{S/L}}{r_{M/L}^5}(F_L - 2A)$$

and where:

$$F_L = A\left[5\left(\frac{Z_{S/L}}{r_{M/L}}\right)^2 - 1\right] + B\left[5\left(\frac{Y_{S/L}}{r_{M/L}}\right)^2 - 1\right] \qquad (A\text{-}23)$$

Equations (A-21, see sheet A) require that the LEM position vector be measured relative to selenographic coordinates ($\bar{r}_{S/L}$). The LEM position vector relative to M-frame coordinates ($\bar{r}_{M/L}$) is known from the solution of the equation of motion (A-10). Hence, these coordinates must be transformed from the M-frame to the selenographic S-frame. This is accomplished by matrix operator a_{ij} (see Section III-D, equations D-10):

$$\bar{r}_{S/L} = a_{ij}\, \bar{r}_{M/L} \qquad (D\text{-}10)$$

Once having determined the triaxiality accelerations in the S-frame, (A-21), then these accelerations must be transformed back to the M-frame equations of motion; therefore:

$$\bar{P}_M = a_{ij}^T \ \bar{P}_S \qquad \text{(A-20)}$$

This completes the triaxiality perturbation computations.

b. Main Engine Thrust Forces. Descent or ascent engine thrust forces (T_k; k = D or A) are supplied by the Propulsion Math Model Section of the LMS. The descent engine nozzle is gimballed to provide trimming moments in addition to translational forces. Descent engine gimbal angles $\delta\theta_D$ and $\delta\psi_D$ are depicted in Figure 2. These angles are generated by the Stabilization and Control Math Model Section of the LMS.

The ascent engine nozzle is fixed to the body. Angles $\delta\theta_A$ and $\delta\psi_A$ are math model input constants that reflect any angular misalignment between the thrust axis $\hat{T}_A$ and the body axis $\hat{X}_B$. Main engine thrust forces resolved along the body axes take the following form:

$$\begin{aligned} T_{X_{BK}} &= T_K \cos\delta_{\psi_K} \cos\delta_{\theta_K} \\ T_{Y_{BK}} &= T_K \sin\delta_{\psi_K} \qquad \text{(A-30)} \\ T_{Z_{BK}} &= T_K \cos\delta_{\psi_K} \sin\delta_{\theta_K} \end{aligned}$$

c. RCS Thrust Forces. The reaction control system consists of 16 thrusters mounted on support booms in clusters of four as shown in Figure 3. Two separate propellant feed systems, "a" and "b" are provided. Systems a and b are denoted in Figure 3 by unshaded and shaded thruster nozzles, respectively. Each thruster is designated by a number (T_u, u = 1, 2, ...16). Translational forces and/or moments are generated by appropriate thrust commands issued from the Reaction Control System Math Model.

RCS force components along the body axes are:

$$T_{X_{BR}} = T_2 + T_6 + T_{10} + T_{14} - (T_1 + T_5 + T_9 + T_{13})$$
$$T_{Y_{BR}} = T_{12} + T_{16} - (T_4 + T_8) \qquad (A\text{-}50)$$
$$T_{Z_{BR}} = T_7 + T_{11} - (T_3 + T_{15})$$

d. Fuel and Oxidizer Slosh Forces Vehicle torques induced by main engine propellant oscillations during the powered descent and ascent maneuvers have a significant effect on RCS propellant consumption and limit cycle characteristics (references 5, 39). Thus, any meaningful math model should have provisions to simulate propellant slosh force and torque perturbations. A detailed description and derivation of the mechanical analog used to simulate slosh forces is given in references 6, 7 and 8. A brief description of these equations, as related to the LMS math model (A-40), is given below.

Fuel and oxidizer slosh forces depend on the accelerations acting on each tank. The tanks are not located at the vehicle CG (see Figure 4). It is therefore necessary to transform the known linear acceleration acting at the vehicle CG to an applied linear acceleration acting at each tank CG. Component tank accelerations acting along the body Y_B direction ($\ddot{V}_{SK_j}$) and Z_B direction ($\ddot{W}_{SK_j}$) are computed in equation (A-45). Descent stage slosh forces, in each of four tanks ($j = 1, 2, 3, 4$), are generated whenever the descent engine is activated ($K = D$). Ascent stage slosh forces, in each of two tanks, ($j = 1, 2$), are generated whenever the ascent engine is activated ($K = A$).

Consider a tank coordinate reference system fixed to the liquid mass and parallel to the LEM body axes system at main engine ignition. As the LEM yaws* about its X_B axis, the liquid mass is assumed to remain stationary; consequently, a yaw displacement will exist between the tank axes and the vehicle axes. Let this yaw excursion be denoted by angle ϕ_k, where:

$$\phi_K = \int_{t_{1_K}}^{t_{2_K}} p_B \, dt \qquad (A\text{-}44)$$

The limits of integration extend from the initiation of main engine burn until shutdown.

Angle ϕ_k is used in equation (A-43) to transform the perturbing acceleration acting on each tank from body coordinates to liquid coordinates. Accelerations $\ddot{\bar{V}}_{SK_j}$ are forcing function inputs to the equivalent mechanical slosh model. The slosh model (A-42) is represented by a pendulum whose mass and support position is designed to generate forces equivalent to the amount of propellant that sloshes.

The solution of (A-42) depends on the slosh natural frequency, $\omega_{n_{K_j}}$, and damping ratio, ρ_{j_K}. Values for $\omega_{n_{K_j}}$ are given in equations A-46 and A-47 in terms of total longitudinal thrust acceleration $\frac{T_{X_{BS}}}{m_L}$, tank radius, R_{K_T}, and a non-dimensional parameter, M_{K_j}. Parameter M_{K_j} is

---

* Normally this motion is referred to as vehicle roll. With respect to the LEM astronaut, however, this motion is sensed as vehicle yaw.

supplied as a tabular function of oxidizer or fuel mass ratio (mass remaining to total tank mass capacity, $\frac{m_{K_j}}{(m_{K_j})_0}$, see A-46a, 47a). Loop A-49 a, b, c, d is employed to define damping ratio, ρ_{j_K}. As shown, this involved loop depends on the fluid height h_{j_K} (A-46a, A-47a), tank shape (A-49d), number of baffles in each tank β_K, baffle height h_{β_K} (see Figure 4), baffle width W_{β_K}, the equivalent pendulum motion (A-42), and ω_{nK_j}. Note that logic A-49d applies only to the descent tanks since $\beta_A = 0$.

Slosh forces in tank coordinates are represented by set A-41. Slosh mass is computed in A-46, A-47 based on experimental data given in A-46a, A-47a. A final transformation yields slosh forces $S_{Y_{K_j}}$, $S_{Z_{K_j}}$ (A-40) in body coordinates.

It is assumed (references 5, 6 and 7) that the instantaneous propellant mass CG remains fixed at the center of each spherical ascent tank but varies relative to the center of each non-spherical descent tank. Hence, the composite descent propellant mass CG depends on the representative "slosh" mass CG and "rigid" mass CG (see Figure 4). Component slosh and rigid mass CG distances are measured relative to the center of each descent tank along the X_B body direction and are tabulated in tables A-46a, 47a). The composite CG of each descent tank is calculated in equations A-48 for subsequent use in the Weights and Balance Section (Section III-I).

It is recommended that additional effort be expended to simplify the damping ratio computations. Sufficient LMS realism may be achieved, for example, by assuming a linear and/or constant damping ratio variation as a function of liquid height for some "typical" wall slosh amplitudes.

e. Stage Separation Forces. Substantial separation forces exist whenever the descent stage is separated from the ascent stage. A detailed derivation of the separation forces are given in reference 9 and will not be repeated herein. Instead, a brief description of the logic flow is presented.

Staging forces are considered as a perturbation to the total thrust and are activated at the instant of ascent engine ignition. Staging forces have a characteristic shape shown in the accompanying sketch (see A-60, 61):

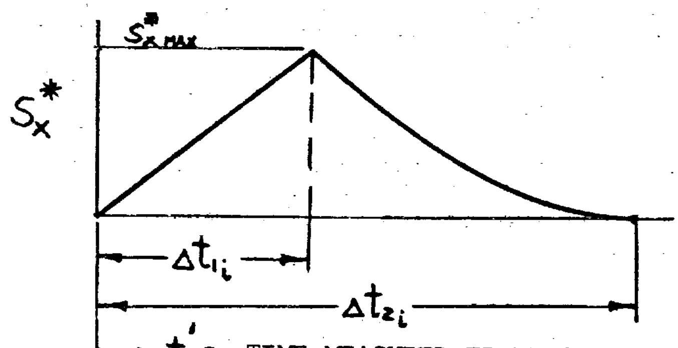

At ascent engine ignition, the stage separation force increases linearly to a maximum value. The thrust decay characteristic is represented by a third order polynomial that has a zero value at Δt_{2_i}. All stage separation coefficients and timing events depend on whether an abort, with partial (i = PP) or full (i = FP) tank pressure, or a lunar lift-off (i = LO) is being performed (A-61).

f. Jet Damping Forces. Jet damping forces are introduced during main engine burning whenever the LEM rotates about the transverse Y_B or Z_B body axes. It is assumed that the exhaust gases leave the nozzle with lateral velocity components equivalent to $q_B \bar{\alpha}_{NK}$ and $r_B \bar{\alpha}_{NK}$, where $\bar{\alpha}_{NK}$ is the distance measured from the vehicle CG to the nozzle exit. The rate of change of linear momentum of the exhaust gases induce a force which opposes vehicle rotation. If rotational coupling and nozzle asymmetry are neglected then the first order damping forces can be approximated by (A-70).

Jet forces are small compared to an RCS thruster capability of 100 pounds. Conservative values for mass flow rate, body angular rate and $\bar{\alpha}_{N_K}$ are 1 slug/sec., 10 deg/sec. and 10 feet, respectively. Substituting these data into A-70 gives damping forces less than 2 pounds. Thus, jet damping forces can be safely neglected.

g. Non-Gravity Force Summation. All external, non-gravitational forces are summed in A-81 and transformed from body axes coordinates to inertial M-Frame coordinates in block A-80 for direct use in the equations of motion (A-10).

5. Conclusions.

a. The LEM equations of motion are defined with respect to the M-Frame and include lunar triaxiality perturbations only. This set will be used during independent or integrated LMS lunar mission phases.

b. Jet damping forces are deleted.

c. The third order polynomial thrust separation decay characteristic will be represented by a linear decay characteristic. No loss in realism results.

d. The damping ratio loop, required to compute the slosh forces, (A-49), will be represented by a tabular function depending on the height of fluid in each tank. It is recommended that further simplifications be sought for LMS implementation.

B. LEM-CSM Relative Equations of Motion and CSM Trajectory Computations.

1. Purpose. The purpose of Set B is to formulate LMS motion equations that simplify computer mechanization and retain trajectory precision consistant with overall LMS mission dictates. In particular, it is desired to:

a. Provide CSM state variables during independent LMS operation (no interface with MSCC or AMS).

b. Accurately describe relative motion coordinates of the LEM with respect to the CSM during lunar rendezvous and separation phases.

c. Accurately describe relative motion coordinates of the LEM with respect to the CSM during all Earth operation phases.

Justification for selecting a two-body CSM orbit as a reference for meeting many of these requirements while neglecting most perturbations follow.

2. CSM Equation of Motion Considerations.

a. General. During independent LMS operation the coordinates of the CSM must be known in order to provide inputs to the visual displays, the LEM Rendezvous Radar Math Model and the LGC steering equations. It is proposed to generate CSM coordinates based on two-body, Kepler motion. This approach seems reasonable because:

i. A ground rule has been established that the CSM will not thrust during independent operation (references 1 and 10).

ii. Two-body CSM solutions are required to simulate the LEM Guidance Computer (LGC) - CSM state vector computation (see sheets N, O, P, refs. 13, 41).

Suppose a two body CSM solution was not employed. On this basis the LMS must effectively perform an AMS function. This would require a sharp increase in LMS computer storage to numerically integrate the CSM trajectory including lunar perturbations during the lunar phase (A-10), and

Earth perturbations during the Earth mission phase (See Section III-3-32). The additional computer cost and complexity is not commensurate with the gain in trajectory precision, over and above the two body solution, for the following reasons:

i. Precision CSM trajectories will always be available during all phases of the LMS-AMS, LMS-MSCC, or LMS-AMS-MSCC integrated operation.

ii. During lunar descent to touchdown, or even ascent to terminal rendezvous initiation, small errors in the CSM position from what the CSM position would have been had all perturbations been included, would be imperceptible to the pilot and inconsequential to the training mission. This statement is made because only as the relative distance approaches zero is it essential that the position of the CSM relative to the LEM be known with great precision. But, it is for this very reason that relative coordinates are employed.

iii. For Earth missions, positional accuracy of the CSM and LEM relative to inertial space is compromised; however, the positional accuracy of the CSM relative to the LEM will not be compromised provided mission time and relative distances remain small.

Consider the implication of all relevant Earth perturbations on the LEM orbit during the independent mode. Admittedly, inertial errors must accrue if a two body CSM solution is adhered to. However, it must also be realized that the LEM has no re-entry capability. Accordingly, safety considerations would dictate that during Earth training exercises, the relative excursions between the LEM and CSM be constrained to some maximum value. Thus, with regard to equation synthesization, any perturbative influence on the CSM orbit will not substantially influence the coordinate representation of the LEM with respect to the CSM since the LEM equations of motion are described with respect to the CSM (B-10). Instead, as mentioned previously, CSM perturbative influences will be reflected in the LEM coordinates with respect to the Earth centered inertial or Earth fixed coordinate system. In terms of math modeling this means that the communication equations (H-30) and the visual display MEP equations (J-40) will be slightly in error. Should this be deemed important, then system operation can always be checked by integrated LMS-AMS or LMS-MSCC or LMS-AMS-MSCC operation.

b. CSM First Order Oblateness and Aerodynamics Perturbation Considerations.

The two-body solution does not reflect the influence of oblateness and aerodynamic forces acting on the CSM orbit. Oblateness perturbations can cause significant secular nodal and possibly perigee excursions relative to an inertial frame over a one day period (on the order of 5 deg/day for a close earth satellite launched within Cape Kennedy azimuth constraints). The consequence of the nodal drift is a shift in the subsatellite point with respect to ground tracking stations.

Aerodynamic drag alters all six elements of the CSM orbit; however, the the significant perturbations are a secular decrease in semi-major axis and circularization of the orbit. A few simple calculations will place the aerodynamic perturbations in the proper perspective. Assume a conservative CSM ballistic coefficient ($\frac{W}{C_d S}$) equal to 200 lbs/ft^2 and circular CSM orbits whose altitudes are 100, 200, and 300 n.m. After each Earth circuit the constant aerodynamic drag acceleration will reduce the CSM altitude by 0.3 n.m., 8×10^{-3} n.m. and 8×10^{-4} n.m. respectively (reference 11). It is felt that errors of this magnitude can be tolerated over a time period of $1\frac{1}{2}$ hours without imposing any restrictions on the prime mission objective, namely astronaut training.

Three techniques may be employed to account for first order oblateness and aerodynamic perturbations for independent LMS operations. These are:

i. Technique 1 - Exact integration of the equations of motion.

ii. Technique 2 - A simplified CSM solution with perturbative influences.

iii. Technique 3 - A two-body CSM solution with no up date. Approximate communication and MEP phase relations between the Earth and the LEM can be achieved by altering the Earth's rotation rate.

Techniques 2 and 3 require that LEM motion be synthesized relative to the CSM. Each technique is subsequently discussed.

3. Technique 1 - Exact CSM Equations of Motion. Obviously, triaxiality, oblateness and aerodynamic perturbations can be computed by the direct integration of the CSM and LEM equations of motion during independent LMS operations. For the sake of completeness, these equations are given:

$$\ddot{\bar{r}}_{n/v} = -\frac{\mu_n}{r^3_{n/v}}\bar{r}_{n/v} + \bar{P}_{n/v} + \bar{A}_v \quad ; \begin{matrix} V = L \text{ or } C \\ n = M \text{ or } E \end{matrix} \qquad (b\text{-}1)$$

Vector $\bar{P}_{n/v}$ denotes either the Moon's triaxiality acceleration (A-20) or the Earth's non-central gravitational acceleration. The latter is derived from the gradient of the potential function (Φ_V). Considering only zonal harmonics, $\bar{P}_{E/V}$ is:

$$\bar{P}_{E/V} = \nabla\Phi_V = \frac{\partial\Phi_V}{\partial X_{E/V}}\hat{i}_E + \frac{\partial\Phi_V}{\partial Y_{E/V}}\hat{j}_E + \frac{\partial\Phi_V}{\partial Z_{E/V}}\hat{k}_E \qquad (b\text{-}2)$$

where:

$$\Phi_V = \frac{\mu_E}{r_{E/V}}\left\{-\left(\frac{R_E}{r_{E/V}}\right)^2 J_2\left[\frac{3}{2}\left(\frac{Z_{E/V}}{r_{E/V}}\right)^2 - \frac{1}{2}\right] - \left(\frac{R_E}{r_{E/V}}\right)^3 J_3\left[\frac{5}{2}\left(\frac{Z_{E/V}}{r_{E/V}}\right)^3 - \frac{3}{2}\left(\frac{Z_{E/V}}{r_{E/V}}\right)\right] + \cdots\cdots\right\}$$

Vehicle aerodynamic accelerations $\bar{A}_V$ (C_D = constant) are:

$$\bar{A}_V = \frac{\frac{1}{2}\rho(h_V)V^2_{R/V}C_{D_V}S_V}{m_V}\frac{\bar{V}_{R/V}}{|\bar{V}_{R/V}|} \qquad (B\text{-}30,31)$$

Where the velocity of the CSM or LEM relative to a rotating atmosphere is:

$$\bar{V}_{R/V} = \dot{\bar{r}}_{E/V} - \bar{\omega}_E \times \bar{r}_{E/V} \qquad \text{(B-32)}$$

Equations b-1 require the use of a sophisticated numerical integration scheme in order to insure that integration errors do not exceed the perturbation accelerations. It is felt that the use of such a scheme would require more computer storage and longer solution times than would the implementation of the first order perturbation equations. In essence, mechanization of equations b-1 would be somewhat analogous to building an AMS computer within the LMS computer for use during independent LEM operations. Moreover, it is also felt that within the constraint of realistic astronaut training there is no need to include any perturbations on the CSM two-body trajectory, since, as implied earlier, these perturbations will have a second order effect on the LEM-CSM relative distance.

4. Technique 2 - A Simplified CSM Solution With Perturbation Influences.

a. Earth Oblateness (CSM Orbit). The principal effect of Earth oblateness is to alter the mean motion, cause a secular nodal regression, and a perigee advance given by the following expressions (reference 14):

$$\Delta\Omega = -\frac{J_2 \bar{n}}{\left[\frac{a_o}{R_E}(1-e_o^2)\right]^2} \cos i_o \, t \qquad \text{Nodal Regression}$$

$$\Delta\omega = \frac{J_2 \bar{n}}{\left[\frac{a_o}{R_E}(1-e_o^2)\right]^2}\left(2-\frac{5}{2}\sin^2 i_o\right)t \qquad \text{Perigee Advance} \qquad \text{(b-3)}$$

$$\bar{n} = n_o\left[1 + \frac{J_2}{\left[\frac{a_o}{R_E}(1-e_o^2)\right]^2}\left(1-\frac{3}{2}\sin^2 i_o\right)\sqrt{1-e_o^2}\right] \qquad \text{Perturbed Mean Motion}$$

$$n_o = \sqrt{\frac{\mu_E}{a_o^3}}$$

Subscript o denotes initial or rectified values of the osculating CSM orbit. Long and short period variations in the six orbital elements are neglected.

b. Aerodynamic Perturbations (CSM Orbit). Secular excursions result in all orbit elements due to aerodynamic perturbations. Nodal and inclination secular changes are caused by the rotating atmosphere. These terms as well as $\Delta\omega$ are small for a large variety of "typical missions" (reference 15) and will be neglected. Based on a non-rotating atmosphere, the secular perturbation in semi-major axis and eccentricity are (reference 16):

$$\Delta a_A = -\frac{C_{D_c} S_c}{m_c}\int_{E_0}^{E} \rho(h_c)\, a_c^2 \left[\frac{(1+e_0\cos E)^3}{1-e_0\cos E}\right]^{\frac{1}{2}} dE \qquad \text{(b-4)}$$

$$\Delta e_A = -\frac{C_{D_c} S_c}{m_c}\int_{E_0}^{E} \rho(h_c)\, a_0^2 (1-e_0^2)\left[\frac{1+e_0\cos E}{1-e_0\cos E}\right]^{\frac{1}{2}} dE$$

Perturbations Δa_A and Δe_A can be found by integrating equations (b-4) over a complete or partial revolution (Simpson's rule is sufficient).

c. CSM Orbital Elements. In order to define the osculating orbit, it is first necessary to compute the initial CSM orbit elements. At problem initialization the CSM orbit elements can be found in terms of $\bar{r}_{E/C_0}$ and $\dot{\bar{r}}_{E/C_0}$. Semi-major axis and eccentricity are given by the visviva and angular momentum equations:

$$a_0 = \left[\frac{2}{r_{E/C_0}} - \frac{V_{E/C_0}^2}{\mu_E}\right]^{-1} \qquad \text{(B-23)}$$

$$e_0 = \left[1 - \frac{H_{E/C}^2}{a_0 \mu_E}\right]^{\frac{1}{2}} \qquad \text{(b-5)}$$

Orbit inclination is defined as the angle between the mean Earth spin axis ($\hat{Z}_E = \hat{k}$) and the CSM angular momentum vector:

$$\cos i_o = \frac{\hat{k} \cdot \bar{H}_{E/C}}{|\bar{H}_{E/C}|} = \frac{H_{X_{E/C}}}{H_{E/C}} \tag{b-6}$$

$$0 \leq i_o \leq \pi$$

Let the acending node direction be given as:

$$\bar{N} = \hat{k} \times \bar{H}_{E/C}$$

Then, the longitude of the ascending node is:

$$\tan \Omega_o = \frac{\bar{N} \cdot \hat{j}}{\bar{N} \cdot \hat{i}} = \frac{H_{X_{E/C}}}{-H_{Y_{E/C}}} \tag{b-7}$$

Finally, the argument of perigee is the difference between the argument of latitude and the true anomaly:

$$\omega_o = u_o - \theta_o \tag{b-8}$$

where:

$$\tan u_o = \frac{(H_{E/C} \times \bar{N}) \cdot \bar{r}_{E/C_o}}{H_{E/C}[\bar{N} \cdot \bar{r}_{E/C_o}]} \tag{b-9}$$

and:

$$\tan \frac{\theta_o}{2} = \sqrt{\frac{1+e_o}{1-e_o}} \tan \frac{E_o}{2} \tag{b-10}$$

The eccentric anomaly at epoch (E_o) is defined at problem start when t = 0 (B-25) or after each rectification interval.

The instantaneous orbit elements are given by equation b-5 through b-10:

$$\begin{aligned} a &= a_o + \Delta a_A \\ e &= e_o + \Delta e_A \\ \Omega &= \Omega_o + \Delta \Omega \\ \omega &= \omega_o + \Delta \omega \\ i &= i_o \end{aligned} \tag{b-11}$$

The first order osculating orbit elements given above are used to approximate the CSM state vector in inertial coordinates.

d. <u>CSM State Vector Computations</u>. Consider a fixed inertial axes (E-Frame) X, Y, Z and an orbital axis x, y. Let x denote the perigee direction and let y lie in the osculating orbit plane in the latus rectum direction. If the orbit is circular, then direct $\hat{x}$ along the ascending node, if the orbit is circular equatorial, then direct $\hat{x}$ along $\hat{X}$. Orient axes x, y with respect to axes X, Y, Z by the standard angle rotations Ω, i and ω. Then, any vector described in the XYZ set will have $\hat{x}$ and $\hat{y}$ projections given by:

$$\begin{aligned}\hat{x} = {} & [\cos\omega\cos\Omega - \sin\omega\sin\Omega\cos i]\hat{X} \\ & + [\cos\omega\sin\Omega + \sin\omega\cos\Omega\cos i]\hat{Y} \\ & + \sin\omega\sin i\,\hat{Z}\end{aligned} \qquad (b\text{-}12)$$

$$\begin{aligned}\hat{y} = {} & -[\sin\omega\cos\Omega + \cos\omega\sin\Omega\cos i]\hat{X} \\ & - [\sin\omega\sin\Omega - \cos\omega\cos\Omega\cos i]\hat{Y} \\ & + \cos\omega\sin i\,\hat{Z}\end{aligned} \qquad (b\text{-}13)$$

The CSM radius can be defined in terms of the eccentric anomaly and projected on the $\hat{x}$ and $\hat{y}$ axes. This gives:

$$\bar{r}_{E/C} = a\left[(\cos E - e)\hat{x} + \sin E\sqrt{1-e^2}\,\hat{y}\right] \qquad (b\text{-}14)$$

Where, the eccentric anomaly E can be defined in terms of the perturbed mean motion and eccentricity. Substitution of (b-12) and (b-13) into (b-14) gives an approximate specification of $X_{E/C}$, $Y_{E/C}$ and $Z_{E/C}$ at time t.

Differentiation of (b-14) yields the required velocity components:

$$\dot{\bar{r}}_{E/C} = a\left[-\sin E\,\hat{x} + \sqrt{1-e^2}\cos E\,\hat{y}\right]\dot{E} \qquad (b\text{-}15)$$

where:

$$\dot{E} = \frac{\bar{n}}{1 - e\cos E}$$

A more sophisticated representation of the CSM state vector, which include second order effects, can be found in the literature.

5. Technique 3 - Recommended Two-Body CSM Equations of Motion With Alteration of Earth Rotation Rate.

a. CSM Two-Body Equation of Motion. During integrated operation the AMS or MSCC will generate the CSM state vector interface with block B-20. Whenever the LMS operates independently, however, it is proposed to generate the CSM state vector based on a spherical symmetric force field:

$$\ddot{\bar{r}}_{n/c} = -\frac{\mu_n}{r^3_{n/c}}\,\bar{r}_{n/c} \qquad \text{(b-16)}$$

The solution for central force motion can be written in terms of four scalar parameters (reference 12):

$$\begin{aligned} \bar{r}_{n/c} &= f\,\bar{r}_{n/c_0} + g\,\dot{\bar{r}}_{n/c_0} \\ \dot{\bar{r}}_{n/c} &= \dot{f}\,\bar{r}_{n/c_0} + \dot{g}\,\dot{\bar{r}}_{n/c_0} \end{aligned} \qquad \text{(B-20)}$$

Scalar parameters f, g, $\dot{f}$, $\dot{g}$, (B-26) depend on the instantaneous orbit radius, appropriate orbit constants and the difference in eccentric anomaly $(E-E_o)$ measured from epoch (problem start $t = 0$). The delta eccentric anomaly $(E-E_o)$ is computed from Kepler's equation, using a Newton-Raphson iteration technique, at any desired interval of time t measured from problem start (see B-25). Thus, CSM motion is known once CSM initial conditions $\bar{r}_{n/c_o}$, $\dot{\bar{r}}_{n/c_o}$ are specified. Subsidiary calculations are performed to define the initial CSM radius, radius rate, velocity and angular momentum components for use in other subset equations.

Equations B-20, in the form shown, will be used as inputs to the LGC during the ascent-to-terminal rendezvous maneuver (see reference 13, 41, sheets N, O, P).

b. Alteration of Earth Rotation Rate. Technique 3 assumes that during the independent mode an accurate representation of LEM motion relative to the CSM is essential; but the LEM-CSM motion with respect to both geographic coordinates and inertial coordinates can be compromised. Thus, it is proposed to retain the CSM mean motion at its constant two-body value but alter the rotation rate of the Earth to artificially compensate for the nodal shift due to the difference between Kepler motion and perturbed motion. Obviously this technique introduces an error because the CSM will not occupy a position it should occupy if a true ephemeris were generated. This has no profound implication on astronaut training but it definitely has a profound implication on computer size. The instructor, the subsystems, and the visual displays interpret the two-body trajectory as a true trajectory and issue commands accordingly. Trajectories influenced by all perturbations will always be available during the integrated mode.

Technique 3 demands no change to the equations given on Sheet B. Instead, whenever a transformation from the inertial E-Frame to the geographic G-Frame is required, the effective Earth rotation rate could be given by:

$$\omega_E' = \omega_E + \dot{\Omega} \qquad (b\text{-}17)$$

where:

$$\dot{\Omega} = -\frac{J_2 \bar{n}}{[a_o(1-e_o^2)]^2} \cos i_o$$

6. LEM Relative Equations of Motion.

a. General. As the relative LEM-CSM distance diminishes, relative motion accuracy cannot be achieved by differencing LEM inertial M-Frame coordinates (A-11, A-12) from AMS or MSCC generated CSM inertial M-Frame coordinates. Precision must be lost due to numerical round-off and integration errors implicit in differencing two large numbers of equal magnitude. Furthermore, additional errors would accrue during independent LMS operation since $\bar{r}_{M/L}$ includes triaxiality (A-10) whereas $\bar{r}_{M/C}$ (B-20) does not. Thus, the primary motivation for introducing a LEM relative coordinate system is to obtain an accurate representation of LEM motion relative to the CSM during lunar separation, terminal rendezvous, and docking maneuvers without resorting to double mission techniques. Relative motion equations are also extended to all Earth mission phases, since during Earth operations, it is of prime importance to determine the LEM position with respect to an Earth-fixed frame. This technique results in equation simplifications.

b. Relative Reference Frames. The origin of relative coordinates is selected at the CSM center of mass. This choice is based on the consideration that during integrated operation (LMS, MSCC and AMS), the CSM coordinates supplied by the AMS will reflect triaxiality or oblateness and aerodynamic effects. Hence, the perturbative accelerations on the moving origin located at the CSM will automatically be included in the motion simulation.

Two reference frames are particularly desireable to describe the LEM relative equations of motion. These are a rotating local horizon, local vertical H-Frame, or an accelerated but non-rotating M or E-Frame (see Figure 5). With regard to LMS mechanization, a study was conducted to ascertain which frame:

i. Simplifies LMS-AMS interface requirements

ii. Minimizes computer storage requirements

iii. Provides an accurate motion simulation

Results of this study (reference 17) imply that:

i. The accuracy requirements should be comparable regardless of which coordinate system is programmed.

ii. Additional AMS interface data are required for H-Frame mechanization.

iii. Computer storage requirements are reduced if relative M or E-Frame rather than relative H-Frame equations are mechanized.

Accordingly, a relative n-frame (n = M or E) will be employed to define LEM relative motion equations.

Consider a non-rotating coordinate frame located at the origin of the CSM mass center (Figure 5). Note that:

$$\begin{aligned} \bar{r}_{n/L} &= \bar{r}_{n/C} + \bar{\rho} \\ \dot{\bar{r}}_{n/L} &= \dot{\bar{r}}_{n/C} + \dot{\bar{\rho}} \\ \ddot{\bar{r}}_{n/L} &= \ddot{\bar{r}}_{n/C} + \ddot{\bar{\rho}} \end{aligned} \qquad (b\text{-}18)$$

With respect to the non-rotating n-frame (see b-1):

$$\ddot{\bar{r}}_{n/V} = -\frac{\mu_n}{r^3_{n/V}}\,\bar{r}_{n/V} + \bar{P}_{n/V} + \sum\left(\frac{\bar{F}_n}{m_n}\right)_V + \bar{A}_V \qquad (b\text{-}19)$$

Substituting (b-18) into (b-19) gives the desired LEM relative motion equations:

$$\begin{aligned} \ddot{\bar{\rho}} = &-\frac{\mu_n}{r^3_{n/L}}\left[\bar{\rho} + \left\{1 - \left(\frac{r_{n/L}}{r_{n/C}}\right)^3\right\}\bar{r}_{n/C}\right] && \text{relative central force gravitational acceleration} \\ &+ \sum\left[\left(\frac{\bar{F}_n}{m}\right)_L - \left(\frac{\bar{F}_n}{m}\right)_C\right] && \text{relative external acceleration} \\ &+ (\bar{A}_L - \bar{A}_C) && \text{relative aerodynamic acceleration} \\ &+ (\bar{P}_{n/L} - \bar{P}_{n/C}) && \text{relative triaxiality or oblateness perturbation} \end{aligned} \qquad (b\text{-}20)$$

Reference 17 concludes that, during the LMS training mission, the relative triaxiality and oblateness accelerations $(\bar{P}_{n/L} - \bar{P}_{n/C})$ are small and can be neglected.

Inherent in numerically integrating equation (b-20) is the loss of significant figures in the bracketed gravitational term. This arises because the radius from the central body to the LEM and to the CSM are almost identical. Numerical significance can be preserved, however, by redefining $\left\{(r_{n/L}/r_{n/C})^3 - 1\right\}$ as follows (reference 12): Let:

$$f(P) = \left(\frac{r_{n/L}}{r_{n/C}}\right)^3 - 1 \qquad \text{(b-21)}$$

where:

$$P = \frac{\rho}{r_{n/C}}\left[\frac{\rho}{r_{n/C}} - 2\cos\alpha\right] \qquad \text{(B-13)}$$

$$\cos\alpha = \frac{\rho_X X_{n/C} + \rho_Y Y_{n/C} + \rho_Z Z_{n/C}}{\rho\, r_{n/C}}$$

Then, by combining (b-21) and (B-13), $f(P)$ takes the form:

$$f(P) = (1+P)^{\frac{3}{2}} - 1 \qquad \text{(b-22)}$$

The numerical difficulty can be resolved by either expanding equation (b-22) in an infinite series in terms of P, or by rewriting equation (b-22) in a more suitable form. The latter tack is taken:

$$f(P) = \frac{(1+P)^3 - 1}{(1+P)^{\frac{3}{2}} + 1}$$

or:

$$f(P) = P\left[\frac{P^2 + 3P + 3}{1 + (1+P)^{\frac{3}{2}}}\right] \qquad \text{(B-14)}$$

Note that equation (B-14) does not depend upon the difference between numbers of equal magnitude. The final form of the relative motion M or E-Frame equations can now be obtained:

$$\ddot{\bar{\rho}} = -\frac{\mu_n}{r^3_{n/L}}\left[\bar{\rho} - f(\rho)\,\bar{r}_{n/C}\right] + \left[\left(\frac{\bar{F}_n}{m}\right)_L - \left(\frac{\bar{F}_n}{m}\right)_C\right] + \left[\bar{A}_L - \bar{A}_C\right] \quad \text{(B-10)}$$

c. Switch Logic. Consider the lunar mission. Let two spheres of radii D_1 and D_2 be drawn with the CSM as origin. Whenever the LEM lies within the inner sphere, relative motion equations will be used to define the trajectory. Conversely, LEM motion outside the outer sphere is described by inertial equations A-10. As the LEM crosses either boundary $\rho_{LS} = D_1, D_2$, switch logic must be included to switch from one set of equations to the other without interrupting a computer run. Automatic re-initialization is readily accomplished by using equations (B-18). Note that CSM vectors $\bar{r}_{M/C}$ and $\dot{\bar{r}}_{M/C}$ are always known. Consequently, as ρ_{LS} decreases and satisfies $\rho_{LS} \leq D$, then equations B-10 can be initialized:

$$\bar{\rho} = \bar{r}_{M/L} - \bar{r}_{M/C}$$
$$\dot{\bar{\rho}} = \dot{\bar{r}}_{M/L} - \dot{\bar{r}}_{M/C} \quad \text{(B-02)}$$

As ρ_{LS} increases, until $\rho_{LS} \geq D_2$ is satisfied, then equations A-10 can be initialized:

$$\bar{r}_{M/L} = \bar{r}_{M/C} + \bar{\rho}$$
$$\dot{\bar{r}}_{M/L} = \dot{\bar{r}}_{M/C} + \dot{\bar{\rho}} \quad \text{(B-02)}$$

Two distances, D_1 and D_2, are inputted in order to eliminate any possibility of hunting between relative and inertial LEM equations.

It is proposed to always employ relative motion equations during Earth training exercises and therefore switch logic is irrelevant.

7. Relative Aerodynamic Accelerations

a. General - Relative aerodynamic perturbations between the vehicles diminishes as the relative distance closes. These perturbations are meaningful only if the vehicles are separated by a large distance for an extended time duration. Once again a simple numerical example will be instructive. Let the ballistic coefficients for the CSM and LEM be 200 and 100 lbs/ft^2. Consider an extreme case where the CSM altitude is 100 n. mi. and the LEM is at an altitude of 200 n. mi. or greater. A relative aerodynamic acceleration of 5×10^{-5} ft/sec^2 is estimated for this configuration. This value is orders of magnitude smaller than the acceleration available from LEM's translational attitude jets and therefore should have no influence on pilot technique, system operation, or the ΔV budget during Earth training rendezvous maneuvers. It is recommended that relative aerodynamic perturbations be deleted during independent LMS operation, but included during integrated LMS operation. The justification for including relative aerodynamics is that the AMS already contains the CSM aerodynamic forces and these forces can readily be interfaced with equations (B-10).

b. LEM Aerodynamics - A simplified aerodynamic model is proposed. This model must be consistant with the AMS aerodynamics otherwise interface errors will result. The LEM drag coefficient is assumed constant. All other aerodynamic forces are neglected. Moreover, diurnal, seasonal and solar activity effects on density variations are also neglected. Thus, the LEM drag acceleration for insertion into equations (B-10), during the integrated mode, is given as:

$$\bar{A}_L = \frac{\frac{1}{2}\rho(h_L)V_{R/L}^2 C_{D_L} S_L}{m_L} \frac{\bar{V}_{R/L}}{|\bar{V}_{R/L}|} \qquad \text{(B-30,31)}$$

Vector $\bar{V}_{R/L}$ represents the relative velocity of the LEM vehicle with respect to a rotating earth atmosphere:

$$\bar{V}_{R/L} = \bar{V}_{E/L} - \bar{\omega}_E \times \bar{r}_E \qquad \text{(B-32)}$$

$$\bar{\omega}_E = \omega_E \hat{K}$$

The density variation (ρ_L) with altitude (h_L) is approximated by a series of experimental curve fits (B-34). Altitude above a spheroidal Earth (reference 18) is represented by equation (B-33). The second order flattening term can be neglected since it has a maximum value of approximately 90 feet and consequently is trivial with respect to density calculations. CSM aerodynamic accelerations required in equations (B-10) must be supplied by the AMS during integrated operations.

8. Conclusions And Recommendations

a. During integrated LMS operations, computer storage requirements can be minimized and double precision problems can possibly be avoided by:

1. Describing LEM motion relative to the CSM by a relative M-frame coordinate system located at the CSM center of mass for lunar mission operations whenever the line-of-sight distance is less than approximately one to four nautical miles.
2. Describing LEM motion relative to the CSM by a relative E-frame coordinate system located at the CSM center of mass for all Earth orbit missions.
3. Never computing relative lunar triaxiality perturbations.
4. Never computing Earth oblateness perturbations.
5. Computing LEM aerodynamics based on a constant drag coefficient and standard density tables. CSM aerodynamics will be supplied by the AMS.

b. During <u>independent LMS operations</u>, a loss in trajectory fidelity will be accepted. To summarize, this loss in fidelity:

i. Does not affect the LEM state variables with respect to the M-frame whenever equations (A-10) are activated.

ii. Does not affect LEM motion relative to the CSM whenever relative equations B-10 are activated except through the relative perturbations which are trivial on a short term basis and trivial based on the LMS mission objective - astronaut training.

Conversely, this loss in fidelity:

i. Does affect the CSM position relative to the M-frame whenever equations A-10 are activated. Since the CSM cannot thrust, the initial CSM state vector can always be adjusted to compensate, on a short term basis, for secular differences between Kepler motion (B-20) and n-body motion.

ii. Does affect the inertial position of the LEM and the CSM with respect to the M-frame or E-frame whenever relative motion equations (B-10) are activated. This is of no consequence during lunar training exercises. During Earth training exercises, this means that the local Earth terrain (MEP) as seen by the astronaut would vary slightly from what the astronaut would see if he were <u>actually</u> in orbit.

Based on the foregoing, it is concluded that, during <u>independent LMS operation</u>:

1. The CSM trajectory be computed using Kepler motion.
2. Relative aerodynamic perturbations be deleted.
3. The rotation rate of the earth be altered to compensate for CSM nodal regression.

C. LEM Rotational Equations of Motion

1. Purpose. - The purpose of Set "C" equations is to accurately represent the rotational dynamics of the LEM vehicle during all LMS mission phases.

2. Rotational Equations. The standard, rigid-body, rotational equations of motion are given by equations C-10. These equations are written with respect to a non-principal, body axis system located at the instantaneous C.G. Body axes X_B, Y_B, Z_B are oriented parallel to the symmetry axes as shown in Figures 3 and 4. The more important time derivative moment of momentum terms, representing fluid particle motions (fuel slosh) and particles being transferred out of the system (damping), are combined into the moment components L_B, M_B, and N_B. Instantaneous moments and products of inertia are generated in Subsection III-I, titled, Weights and Balance. Product of inertia terms are retained to account for non-symmetric loading conditions resulting, for example, from a fuel or oxidizer leak or pump malfunction.

Equations C-11 are the first integrals of equations C-10 and represent inertial angular rates p_B, q_B, r_B about the vehicle X_B, Y_B, and Z_B directions, respectively.

3. External Torques.

a. RCS Torques. Equations (C-51) define the RCS torques with respect to a fixed reference point. This point lies in the RCS plane of symmetry at distances l_1, and l_2 measured from the inner and outer thruster arms (see Figure 3). Moments about the fixed reference point are subsequently transferred to the vehicle CG (C-50), which is displaced from the reference point by component distances† $\bar{\alpha}_R$, $\bar{\beta}_R$, $\bar{\delta}_R$ along symmetry directions X_B, Y_B, Z_B. Transferring the moments, rather than computing the moments directly about the CG, results in algebraic simplification.

† Bars in this instance do not represent vectors but component distances measured from the instantaneous CG.

b. Main Engine Torques. Thrust components resulting from descent engine gimbal nozzle action or ascent engine misalignment have been ascertained (A-30). The moment arm from the nozzle throat to the vehicle CG is computed by subset equation I-30:

$$\bar{d}_K = \bar{\alpha}_K \hat{\imath}_B + \bar{\beta}_K \hat{\jmath}_B + \bar{\gamma}_K \hat{k}_B \qquad \text{(c-1)}$$

Hence, the total moment about the CG is:

$$\bar{M}_K = \bar{d}_K \times \bar{\bar{T}}_{B_K} \qquad \text{(C-30)}$$

c. Fuel Slosh Torques. The perturbative ascent slosh force acts at the geometric center of the empty spherical fuel and oxidizer tanks (reference 8). Consequently, ascent slosh moments induced (C-40) are defined by the perturbative slosh forces (A-40) and their corresponding distances $\bar{\alpha}_{A_j}$, $\bar{\beta}_{A_j}$, $\bar{\gamma}_{A_j}$, measured from the empty ascent tank centroid to the composite vehicle CG. This does not apply to the descent tank slosh perturbations. Instead, the pendulum support, that characterizes the origin of descent slosh perturbations, varies along the longitudinal tank symmetry axis by a distance $\Delta\alpha_{S_j}$ (A-47, see Figure 4) measured from the tank centroid. Accordingly, descent slosh torques depend on distances $\bar{\alpha}'_{D_j}$ $(= \alpha^*_{D_j} + \Delta\alpha_{S_j} - \alpha_{CG})$, $\bar{\beta}_{D_j}$ and $\bar{\gamma}_{D_j}$ which are computed by equations (I-20) and (I-30). Parameter $\Delta\alpha_{S_j}$ can vary by approximately ±.5 feet.

Any simplification made to the slosh forces (Subsection III - A - 4d) will be reflected in the slosh moments.

d. Jet Damping Torques

I. Jet Torque Contributions. Jet damping torques are induced by the rate of which mass particles leaving the vehicle are transferring moment of momentum to the vehicle. Two factors contribute to the jet torques during the powered descent and ascent maneuvers. First, jet torques about the instantaneous vehicle CG are generated by jet forces (A-70). Moment arm components which reflect lateral vehicle CG motion relative to the exhaust nozzle $\left(\bar{\beta}_{N_K},\ \bar{\gamma}_{N_K}\right)$ are small and neglected. Thus, the first jet torque contribution is represented as:

$$
\begin{aligned}
L'_{D_K} &= \bar{\beta}_{N_K} D_{Z_K} - \bar{\gamma}_{N_K} D_{Y_K} = 0 \\
M'_{D_K} &= -\bar{\alpha}_{N_K} D_{Z_K} = -q_B\, \dot{m}\, \bar{\alpha}^2_{N_K} \\
N'_{D_K} &= \bar{\alpha}_{N_K} D_{Y_K} = -r_B\, \dot{m}\, \bar{\alpha}^2_{N_K}
\end{aligned}
\qquad (c\text{-}2)
$$

The second damping contribution results from the time rate of change of fuel or oxidizer inertia relative to the vehicle CG. This is equivalent to the rate of change of fuel or oxidizer CG relative to each tank CG plus a transfer term from the tank CG to the vehicle CG. Prior to expanding these terms, previous assumptions are reiterated:

i. The local CG of the ascent propellants is invariant regardless of propellant mass left in the tank.

ii. The local CG of the non-spherical descent tank propellants vary within small limits.

iii. Lateral tank CG excursions are non-existent.

Within this framework, the rate of change of propellant inertia relative to the local CG of each tank is zero. Moreover, only longitudinal excursions are considered in defining the rate of change of tank propellant inertia relative to the vehicle CG. Let distances $\bar{\alpha}_{A_1}$ and $\bar{\alpha}_{D_1}$ define the plane of the composite ascent tank CG's and descent tank CG's. Then, the inertia transfer terms are simply (see references 19 and 20):

$$M''_{D_K} = q_B \, \dot{m} \, \overline{\alpha}^2_{K_1}$$
$$N''_{D_K} = r_B \, \dot{m} \, \overline{\alpha}^2_{K_1} \qquad (c\text{-}3)$$

Combining contributions c-2 and c-3 yields the desired result:

$$M_{D_K} = - q_B \, \dot{m} \, (\overline{\alpha}^2_{N_K} - \overline{\alpha}^2_{K_1})$$
$$N_{D_K} = - r_B \, \dot{m} \, (\overline{\alpha}^2_{N_K} - \overline{\alpha}^2_{K_1}) \qquad (C\text{-}70)$$

e. Order of Magnitude Check. Equation (C-70) depends on the distance parameter $(\overline{\alpha}^2_{NK} - \overline{\alpha}^2_{K_1})$ which can vary between limits of approximately 50 to 75 ft^2 and 13 to 17 ft^2 for the descent and ascent phases, respectively (see reference 21). Nominal mission profiles require controlled body rates on the order of 1 deg/sec. These data when combined with a mass flow rate of 1 slug/sec. and substituted into (C-70) give representative damping moments that vary between approximately .2 ft-lbs to 1.2 ft-lbs. Increasing the body rates by an order of magnitude (10°/sec) causes the moments to increase by an order of magnitude (12 ft-lbs).

It is recommended that jet torques be deleted since:

i. Even for an extreme case the jet torques are negligible compared to the RCS torque capability of 2200 ft-lbs.

ii. Jet torques have no influence on the primary mission objective - astronaut training.

f. Engine Separation Torques. An extensive investigation is being conducted to ascertain the stage separation torque perturbations (references 9 and 22). Present indications are that these torques are large and cannot be neglected. Furthermore, the moment arm relating the position of force application to the vehicle CG is a time dependent variable. For this reason, the moment perturbations (C-60) are not represented by a constant arm times the stage separation force (equations A-60). The moment time transient, however, has a shape similar to the stage separation force profile.

Should future refined studies indicate a small moment arm variation with time, then stage separation torques could be computed using an average, constant moment arm times the stage force (A-60).

g. <u>Moment Summation</u>. All external LEM torques are summed in subset (C-80) for insertion into the rotational equations of motion.

During the integrated mode in the docked configuration, both the LMS and AMS will solve the rotational equations of motion. This requires that the AMS provide CSM external torques (C-81) relative to the LEM body axes about the composite LEM-CSM center of mass. When docked, the LEM $\hat{X}_B$ axis is directed opposite to the CSM $\hat{X}_B$ axis. Also, an arbitrary fixed roll angle ($\phi_{CSM} + \phi$) may exist between the LEM and CSM $\hat{Y}_B$ axes (see sketch). Accordingly, CSM external torques (L_{LSM}, M_{CSM}, N_{CSM}),

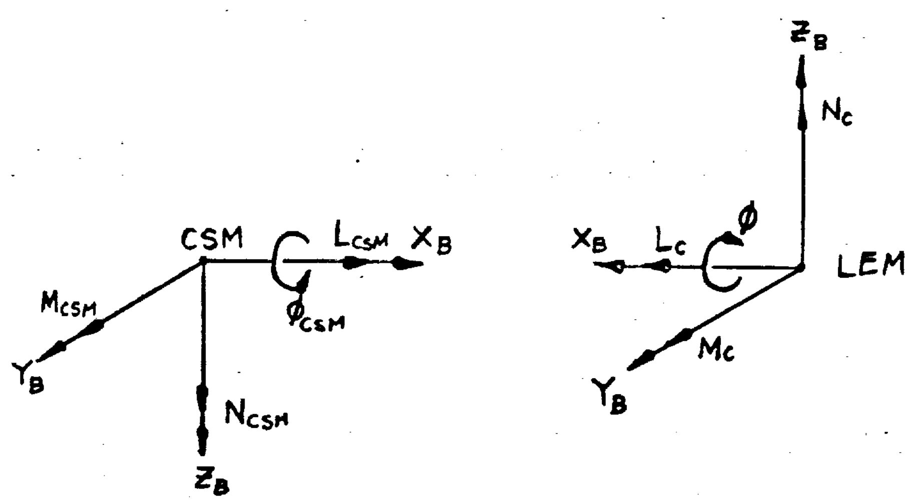

computed by the AMS relative to the CSM body axes are transformed as follows prior to insertion into (C-10):

$$
\begin{aligned}
L_c &= -L_{CSM} \\
M_c &= M_{CSM}\cos(\phi_c+\phi) - N_{CSM}\sin(\phi_c+\phi) \\
N_c &= -N_{CSM}\cos(\phi_c+\phi) - M_{CSM}\sin(\phi_c+\phi)
\end{aligned}
\qquad \text{(C-81)}
$$

4. LEM Orientation Computations

a. General. Basic to all rigid body simulation problems is the specification of vehicle orientation with respect to a known coordinate reference. The coordinate reference selected, for purpose of LMS simulation, is the inertial M or E - frame rather than the true IMU reference frame. This choice is made to simplify LMS-AMS interface requirements and to prevent erratic visual display motion whenever the true reference frame, computed within the LGC, is altered.

Vehicle orientation is simulated by integrating the rotational equations of motion to obtain body rates p_B, q_B, r_B. Once body rates are obtained (C-11), then the time dependent direction cosine matrix can be generated from either:

i. the Euler rate equations ($\dot{\theta}, \dot{\psi}, \dot{\phi}$).

ii. the direction cosine rate equations ($\dot{a}_{ij}$; $i=1,2,3$; $j=1,2,3$).

iii. the quaternion rate equations ($\dot{e}_i$; $i = 1,2,3,4$).

Euler rate equations are simple to implement; however, these equations introduce inaccuracies as the middle angle or second ordered rotation approaches $\pm\frac{\pi}{2}$. This condition is normally referred to as "gimbal lock." In a gimbal lock configuration, the inner and outer rotation axes coincide resulting in infinite inner and outer angular rates. Euler rate equations are inappropriate for mechanization since an all attitude capability is desired for complete LMS digital simulation.

Resort to an analytic description of a redundant four gimbal set is not considered because of unwarranted complexity.

The direction cosine rate equations and the quaternion rate equations do not exhibit any singularities. It remains, therefore, to determine which of these two techniques are best suited for IMS mechanization.

b. Selection Criteria. An empirical study (references 23, 24 and 25) was conducted on the 7094 digital computer to ascertain the relative advantage between using either direction cosine or quaternion rate equations to define vehicle orientation angles for digital simulation. The relative advantage of each technique was evaluated by comparing computer storage requirements, solution speed and Euler angle output accuracy for a variety of numerical integration schemes and integration intervals. Accuracy comparisons were made by matching digital outputs to an analytical Euler angle solution for coning motion. Study results indicated that the quaternion rate equations were slightly superior in all categories. Hence, the quaternion rate equations, given below, will be mechanized for simulation (reference 26):

$$\begin{aligned} \dot{e}_1 &= \tfrac{1}{2}(-e_4 p_B - e_3 q_B - e_2 r_B) \\ \dot{e}_2 &= \tfrac{1}{2}(-e_3 p_B + e_4 q_B + e_1 r_B) \\ \dot{e}_3 &= \tfrac{1}{2}(e_2 p_B + e_1 q_B - e_4 r_B) \\ \dot{e}_4 &= \tfrac{1}{2}(e_1 p_B - e_2 q_B + e_3 r_B) \end{aligned} \qquad \text{(C-20)}$$

c. Euler Angle Matrix Operator. Physically, parameters e_i represent trigonometric functions of three direction cosines and a rotation angle. The three direction cosines position a rotation axis about which the rotation angle carries the rigid body from an arbitrary initial orientation to an arbitrary final orientation. Starting values for e_1, e_2, e_3, and e_4 are required in order to initialize (C-20). In addition, the inverse problem of specifying a body axes orientation, given instantaneous values of e_i must also be defined. Initial e_i values are not known directly since it is assumed that the LEM vehicle orientation will be given in terms of Euler angles θ, ψ and ϕ. Thus, the correspondence between the four parameter set and the Euler angle set must be ascertained. Prior to defining this correspondence, it is first necessary to define the LEM Euler angles.

LEM Euler angles are specified by a specific sequence of ordered rotations which differ from standard aircraft usage. The transformation from the inertial axes (X_n, Y_n, Z_n) to the body axes (X_B, Y_B, Z_B) is given by the following ordered counterclockwise rotations:

i. Pitch (θ) about the Y_n reference axis.

ii. Roll (ψ) about the new Z' axis so formed.

iii. Yaw (ϕ) about the new X" axis so formed to give X_B, Y_B, Z_B directions.

The foregoing rotations are represented in matrix form as follows:

$$\bar{r}_B = g_{ij_n} \bar{r}_n \tag{D-40}$$

where:

$$g_{ij_n} = \begin{pmatrix} g_{11} & g_{12} & g_{13} \\ g_{21} & g_{22} & g_{23} \\ g_{31} & g_{32} & g_{33} \end{pmatrix}$$

and where:

$$g_{ij_n} = \begin{bmatrix} \cos\psi\cos\theta & \sin\psi & -\cos\psi\sin\theta \\ -\cos\phi\sin\psi\cos\theta + \sin\phi\sin\theta & \cos\phi\cos\psi & \cos\phi\sin\psi\sin\theta + \sin\phi\cos\theta \\ \sin\phi\sin\psi\cos\theta - \cos\phi\sin\theta & -\sin\phi\cos\psi & -\sin\theta\sin\phi\sin\psi + \cos\phi\cos\theta \end{bmatrix} \tag{C-4}$$

It must be mentioned that Euler angles θ, ψ, ϕ described above are not used to orient the astronaut's "8-ball" display. The "8-ball" display is activated by indicated Euler angles (θ_{IMU}, ψ_{IMU}, ϕ_{IMU}, Sheet L, references 13, 41). These indicated angles correspond to gimbal pick-off resolvers and reflect the LEM body orientation with respect to the physical, onboard, platform.

d. Quaternion Initialization. It can be shown (references 26 and 27), that for each real, three-dimensional, orthogonal transformation matrix (c-4) there is an associated two by two imaginary matrix that relates the initial vehicle orientation to the final vehicle orientation. The complex matrix must; a) be unitary, the product of the matrix and the transpose of its complex conjugate is unity, and b) have a determinant = +1. These conditions lead to the following operator form:

$$H = \begin{pmatrix} e_1 + i e_2 & e_3 + i e_4 \\ -e_3 + i e_4 & e_1 - i e_2 \end{pmatrix} \qquad \text{(c-5)}$$

Real numbers e_i are the quaternions or Euler parameters.

Proof is given in reference 26 that the following similarity transformation;

$$P' = H\,(P)\,(H)^{-1}$$

$$P = \begin{pmatrix} Z & X - iY \\ X + iY & -Z \end{pmatrix} \qquad \text{(c-6)}$$

satisfies all the requirements of a real orthogonal transformation operator when X, Y, and Z are interpreted as vector components. Substituting (c-5) into (c-6) and expanding gives:

$$\bar{r}_B = g_{ij_n} \bar{r}_n$$

$$g_{ij_n} = \begin{pmatrix} e_1^2 - e_2^2 - e_3^2 + e_4^2 & 2(e_1 e_2 + e_3 e_4) & 2(e_2 e_4 - e_1 e_3) \\ 2(e_3 e_4 - e_1 e_2) & e_1^2 - e_2^2 + e_3^2 - e_4^2 & 2(e_2 e_3 + e_4 e_1) \\ 2(e_1 e_3 + e_2 e_4) & 2(e_2 e_3 - e_1 e_4) & e_1^2 + e_2^2 - e_3^2 - e_4^2 \end{pmatrix} \qquad \text{(D-40)}$$

Only three of the four quaternions are independent. The fourth is related to the other three by the equation:

$$e_1^2 + e_2^2 + e_3^2 + e_4^2 = 1 \qquad \text{(c-7)}$$

This dependency forms the basis of a rectification scheme which is used to maintain direction cosine orthonormality (reference 28).

Consider the first ordered rotation θ about Y_n ($\psi = \phi = 0$). There must be a one to one correspondence between matrix operator g_{ij_n} (c-4) and matrix operator g_{ij_n} (D-40). Comparing elements of each matrix gives:

$$\begin{aligned} e_1^2 - e_2^2 - e_3^2 + e_4^2 &= \cos\theta \\ 2(e_3 e_4 - e_1 e_2) &= 0 \\ 2(e_1 e_3 + e_2 e_4) &= \sin\theta \\ 2(e_1 e_2 + e_3 e_4) &= 0 \\ e_1^2 - e_2^2 + e_3^2 - e_4^2 &= 1 \\ 2(e_2 e_3 - e_1 e_4) &= 0 \\ 2(e_2 e_4 - e_1 e_3) &= -\sin\theta \\ 2(e_2 e_3 + e_1 e_4) &= 0 \\ e_1^2 + e_2^2 - e_3^2 - e_4^2 &= \cos\theta \end{aligned} \qquad \text{(c-8)}$$

Set (c-8) is satisfied if and only if:

$$e_2 = e_4 = 0 \tag{c-9}$$

whereupon elements (c-8) reduce to:

$$e_1 = \frac{\sin\theta}{2\sin\frac{\theta}{2}} = \cos\frac{\theta}{2}$$

$$e_3 = \sin\frac{\theta}{2} \tag{c-10}$$

But, it was indicated earlier that complex matrix H (c-5) represents a real rotation. Hence, substituting elements (c-9) and (c-10) into (c-5) gives:

$$H_\theta = \begin{pmatrix} \cos\frac{\theta}{2} & \sin\frac{\theta}{2} \\ -\sin\frac{\theta}{2} & \cos\frac{\theta}{2} \end{pmatrix} \tag{c-11}$$

Repeating this procedure for the second ordered rotation (ψ) and the third ordered rotation (ϕ) yields:

$$H_\psi = \begin{pmatrix} \cos\frac{\psi}{2} + i\sin\frac{\psi}{2} & 0 \\ 0 & \cos\frac{\psi}{2} - i\sin\frac{\psi}{2} \end{pmatrix} \tag{c-12}$$

$$H_\phi = \begin{pmatrix} \cos\frac{\phi}{2} & i\sin\frac{\phi}{2} \\ i\sin\frac{\phi}{2} & \cos\frac{\phi}{2} \end{pmatrix} \tag{c-13}$$

The final vehicle orientation, resulting from θ, ψ and ϕ rotations, is specified by rotation matrices c-11, c-12, c-13:

$$H = \begin{vmatrix} e_1 + i e_2 & e_3 + i e_4 \\ -e_3 + i e_4 & e_1 - i e_2 \end{vmatrix} = H_\phi H_\psi H_\theta \tag{c-14}$$

Expanding the right hand member of (c-14) and comparing each element to the left hand member gives the desired result:

$$
\begin{aligned}
e_{1_0} &= \cos\frac{\phi_0}{2}\cos\frac{\psi_0}{2}\cos\frac{\theta_0}{2} - \sin\frac{\phi_0}{2}\sin\frac{\psi_0}{2}\sin\frac{\theta_0}{2} \\
e_{2_0} &= \cos\frac{\phi_0}{2}\sin\frac{\psi_0}{2}\cos\frac{\theta_0}{2} - \sin\frac{\phi_0}{2}\cos\frac{\psi_0}{2}\sin\frac{\theta_0}{2} \\
e_{3_0} &= \cos\frac{\phi_0}{2}\cos\frac{\psi_0}{2}\sin\frac{\theta_0}{2} + \sin\frac{\phi_0}{2}\sin\frac{\psi_0}{2}\cos\frac{\theta_0}{2} \\
e_{4_0} &= \cos\frac{\phi_0}{2}\sin\frac{\psi_0}{2}\sin\frac{\theta_0}{2} + \sin\frac{\phi_0}{2}\cos\frac{\psi_0}{2}\cos\frac{\theta_0}{2}
\end{aligned}
\qquad (C\text{-}21)
$$

Equations (C-21) are used once during each run. They specify the quaternions at problem start based on known initial values of the LEM Euler angles with respect to the inertial M or E-frame.

e. Inverse Problem. Direction cosine matrix elements g_{ij_n} (D-40) are known at each instant of time. It is desired to determine the corresponding Euler angles to use as drive inputs for gimballed visual displays (see for example: J-10, J-41 and J-60). As mentioned earlier each element of (D-40) must be identical to each element of (c-4). With regard to the first ordered rotation, θ , it is seen that:

$$\tan\theta = \frac{-(-\sin\theta\cos\psi)}{\cos\theta\cos\psi} = \frac{-g_{13}}{g_{11}} \qquad (c\text{-}15)$$

The middle rotation ψ could be defined as:

$$\sin\psi = g_{12} \qquad (c\text{-}16)$$

or:

$$\tan\psi = \frac{\sin\psi}{(\cos\psi\cos\theta)\cos\theta - (-\cos\psi\sin\theta)\sin\theta} = \frac{g_{12}}{g_{11}\cos\theta - g_{13}\sin\theta} \qquad (c\text{-}17)$$

Similarly, the outer rotation angle could be given by:

$$\tan\phi = \frac{-(-\sin\phi\cos\psi)}{\cos\phi\cos\psi} = \frac{-g_{32}}{g_{22}} \qquad \text{(c-18)}$$

or:

$$\tan\phi = \frac{(\sin\phi\sin\theta - \cos\phi\cos\theta\sin\psi)\sin\theta + (\sin\phi\cos\theta + \cos\phi\sin\theta\sin\psi)\cos\theta}{(-\cos\phi\sin\theta + \sin\phi\cos\theta\sin\psi)\sin\theta + (\cos\phi\cos\theta - \sin\phi\sin\theta\sin\psi)\cos\theta}$$

$$= \frac{g_{21}\sin\theta + g_{23}\cos\theta}{g_{31}\sin\theta + g_{33}\cos\theta} \qquad \text{(c-19)}$$

Equations c-15, c-16 and c-18 have obvious advantages. However, as ψ approaches $\pm\frac{\pi}{2}$, θ and ϕ are undefined. This is not consistent with the requirement of an "all attitude capability."

"Gimbal lock" can be artificially circumvented by applying the following logic to equations c-15, c-17 and c-19. As the middle rotation (ψ) approaches $\frac{\pi}{2}$ (say $\frac{\pi}{2} \pm \epsilon^*$), freeze θ at its current value, but continue to compute ϕ. This technique will ensure that the sum $\theta + \phi$ is correct to order ϵ^*. Realize that in the neighborhood of $\psi = \pm\frac{\pi}{2}$, the inner and outer rotation axes are nearly coincident, therefore, the sum $\theta + \phi$ is sufficient to specify a true vehicle space orientation. Gimbal lock logic is not required whenever ψ leaves the neighborhood given by $\frac{\pi}{2} \pm \epsilon^*$, since algebraic equations c-15, c-17 and c-19 are self sufficient.

5. Conclusions

a. Retain product of inertia terms to account for non-symmetric loading conditions.

b. Reference RCS torques with respect to a fixed reference point. Subsequently, transform these torques to the instantaneous vehicle CG. This technique results in algebraic simplification.

c. Simplifications made to slosh forces will be reflected in the slosh torque loop.

d. Delete jet damping torques.

e. It is recommended that stage separation torques be computed from separation forces based on a constant moment arm. If future studies indicate that this is impractical, then approximate the third order decay characteristic by a linear decay characteristic.

f. Compute the vehicle-platform direction cosine matrix based on four quaternion rate equations rather than six direction cosine rate equations. It appears that the quaternions have a slight advantage over direction cosine rate equations with respect to digital storage capacity, solution speed and accuracy.

g. Incorporate "gimbal lock" logic in the visual display subsection to ensure an all attitude display capability.

h. A rectification technique to force direction cosine orthonormality is recommended (C-25, 26). Should this technique differ from that already programmed for the AMS, then discard equations (C-25), and (C-26).

D. GENERAL TRANSFORMATIONS

1. Purpose. - The purpose of Set D is to generate the more important transformation relationships used in the LMS Math Model. The transformation operators derived in this subsection are listed below:

Matrix Operator:	Transforms any vector measured in the:	to the:	thus:
a_{ij}	lunar inertial M-frame	Selenographic S-frame	$\overline{r}_S = a_{ij}\,\overline{r}_M$
c_{ij_E}	inertial earth E-frame	True IMU reference R-frame	$\overline{r}_R = c_{ij_E}\,\overline{r}_E$
c_{ij_M}	inertial lunar M-frame	True IMU reference R-frame	$\overline{r}_R = c_{ij_M}\,\overline{r}_M$
g_{ij_n}	inertial M or E - frame	LEM body B-frame	$\overline{r}_B = g_{ij_n}\,\overline{r}_n$
f_{ij}	inertial Earth E-frame	rotating geographic G-frame	$\overline{r}_G = f_{ij}\,\overline{r}_E$
l_{ij_n}	window or telescope optical pq-frame	inertial Earth-E or Moon - M frame	$\overline{r}_n = l_{ij_n}\,\overline{r}_{pq}$

2. Matrix Operator From Inertial M - Frame To Selenographic S - Frame. - During lunar missions it is essential to position the inertial platform, define the trajectory and provide visual cues with sufficient realism relative to known lunar landmarks. An accurate representation of the Moon's motion is required to accomplish these tasks.

Let the selenographic $\hat{Z}_S$ axis be defined by the Moon's rotation vector. Neglecting physical librations, axis $\hat{Z}_S$ makes a constant angle of $1^\circ 32.1'$ (Hayn's constant) with the ecliptic North Pole. Based on Cassini's laws (reference 29), the pole of the Moon's orbit, $\hat{P}$, describes a small circle about the ecliptic pole in about 18.6 years. The great circle arc $\widehat{Z_S P}$ contains the ecliptic pole, which lies between $\hat{Z}_S$ and $\hat{P}$. Thus, the lunar equator and the lunar orbit have a common line of nodes with respect to the ecliptic. Define the $\hat{X}_S$ axis to lie along the Moon - Earth line when the Moon is at the ascending node and concurrently at either apogee or perigee (reference 29). Ordered rotations necessary to establish the time dependent relationship between this fixed selenographic frame and the basic computational mean equinox, mean equator of date reference system is discussed next.

Refer to Figure 6. Rotate about the mean equinox $\hat{X}_M$ through the mean obliquity, ϵ. This establishes the ecliptic system:

$$\bar{r}_\epsilon = a_{n_j} \, \bar{r}_M \qquad \text{(D-13)}$$

Next, establish the Moon's mean ascending node by a rotation Ω about the ecliptic pole:

$$\bar{r}_\Omega = a_{mn} \, \bar{r}_\epsilon \qquad \text{(D-14)}$$

From Cassini's laws, the ascending node of the lunar orbit defines the descending node of the lunar equator. A clockwise rotation (I) about the node through Hayn's constant locates the lunar equator relative to the ecliptic plane:

$$\bar{r}_I = a_{\ell m} \, \bar{r}_\Omega \qquad \text{(D-15)}$$

Neglecting physical librations, the prime lunar meridian, which lies in the $\hat{X}_S - \hat{Z}_S$ plane and faces the Earth, rotates at a rate equivalent to the Moon's mean motion. At any instant, therefore, the prime meridian is at an angular distance of $\pi + (☾ - \Omega)$ measured from the mean ascending lunar orbit node. Symbol ☾ represents the mean lunar longitude. The final rotation operator is:

$$\bar{\Gamma}_{S_{MEAN}} = a_{K\ell}\ \bar{\Gamma}_I \qquad \text{(D-13)}$$

Combining equations D-13 through D-16 gives the transformation from the inertial M-frame (fixed at problem start) to a non-nutating, selenographic S-frame:

$$\bar{\Gamma}_{S_{MEAN}} = \left(a_{K\ell}\, a_{\ell m}\, a_{mn}\, a_{nj}\right) \bar{\Gamma}_M \qquad \text{(d-1)}$$

Equation (d-1) does not reflect the complex wobbling motion of the Moon, normally referred to as physical libration. Physical libration represents lunar oscillations which have total amplitude variations constrained to $\pm.04°$ and associated short and long period motions of 1 and 6 years, respectively. A first order description of this motion is given by the physical libration matrix presented below (references 29 and 30):

$$\bar{\Gamma}_S = L_{iK}\ \bar{\Gamma}_{S_{MEAN}} \qquad \text{(D-11, 12)}$$

The desired orientation of the selenographic axis relative to the inertial M-frame is found by substituting (d-1) into (D-11, 12):

$$\bar{\Gamma}_S = a_{ij}\ \bar{\Gamma}_M \qquad \text{(D-10)}$$

The libration matrix and operator (D-16) have an insignificant variation during the course of any training session. It is, therefore, recommended that these matrix operators be computed at problem start and maintained constant during any particular run.

3. Matrix Operator From True IMU R-Frame To Inertial E or M-Frame

a. Earth Mission. - At present, the desired LEM platform directions required for earth training exercises are not known. It is arbitrarily assumed that the LEM platform will be referenced to the Earth launch site at the time of launch. Let this position be specified by a known

Universal time measured in hours, H (E-01) from Greenwich Midnight to problem start and integer days D* (E-01) from Greenwich Midnight Dec. 31, of the launch year to Greenwich Midnight of the launch day. These constants define the Greenwich Hour Angle relative to the mean equinox of date (see loops E-01 and E-10). The position of the launch site at launch is:

$$RA_E = GHA_E + \lambda_E \tag{D-21}$$

Parameter λ_E denotes the launch site longitude measured Eastward from Greenwich. The assumed platform direction is space fixed and can now be found by the following three ordered rotations:

i. Rotate about the mean spin axis $\hat{Z}_E$ through RA_E.

ii. Rotate about the new $\hat{Y}'_E$ axis so formed through the launch site declination δ_E (positive North).

iii. Rotate about the new $\hat{X}''_E$ axis so formed through the intended launch azimuth angle ψ_E (measured positive East of North), to give assumed Earth mission platform directions X_R, Y_R, Z_R.

The ordered rotations specify the transformation:

$$\overline{F}_{R_E} = C_{ij_E} \overline{F}_E \tag{D-20}$$

b. <u>Lunar Mission</u>. - The desired platform orientation for all lunar mission modes, is based on references 31 and 32. These references state that the $\hat{X}_R$ platform axis will be directed from the Moon's center to the intended landing site at some nominal landing time, or take-off site at some nominal take-off time. Moreover, the $\hat{Z}_R$ platform axis shall be parallel to the CSM orbit plane in the direction of motion. A precise definition follows.

Consider a hypothetical mission. Assume CSM-LEM lunar injection has taken place and that the CSM platform is inertially aligned to the M-frame (or E-frame). Subsequent to separation, both LEM and CSM platforms must be aligned to new desired reference directions. These directions are specified by the desired landing site selenographic longitude (λ_s) and latitude (ϕ_s) as well as the desired nominal touchdown time, t*, measured from problem start to touchdown. Time t* specifies the inertial position of the Moon, and hence the landing site, at the nominal time of landing. This landing site position is fixed by:

i. First, computing ahead to ascertain the Julian date T* (E-01), and days from epoch d* (E-22) to touchdown.

ii. Second, computing the lunar and solar orbit elements based on future times T* and d* (E-20).

iii. Third, using elements (E-20) to compute the transformation matrix a_{ij}^* at times T* and d*.

Transformation matrix a_{ij}^* specifies the inertial orientation of the Moon at the nominal touchdown time t*. The landing site unit vector measured in selenographic coordinates is known:

$$\hat{r}_s = \cos\phi_s \cos\lambda_s \hat{i}_s + \cos\phi_s \sin\lambda_s \hat{j}_s + \sin\phi_s \hat{k}_s \qquad \text{(D-33)}$$

Thus, the components of $\hat{r}_s$ transformed to M-frame coordinates correspond exactly to the components of reference direction $\hat{x}_R$ measured in the M-frame:

$$\hat{x}_R = c_{11}\hat{i}_M + c_{12}\hat{j}_M + c_{13}\hat{k}_M - a_{ij}^* \hat{r}_M \qquad \text{(D-32)}$$

Reference direction $\hat{z}_R$ is parallel to the CSM orbit plane (references 31, 32). This direction is formed by the cross product of the CSM specific angular momentum ($\hat{H}_{M/C}$) and $\hat{x}_R$. Orbit determination techniques will be employed to define the CSM orbit prior to the separation maneuver; consequently, $\hat{H}_{M/C}$ is assumed known:

$$\hat{H}_{M/C} = b'_{21}\hat{\imath}_M + b'_{22}\hat{\jmath}_M + b'_{23}\hat{k}_M \quad \text{(D-35)}$$

Whereupon reference direction $\hat{Z}_R$ is:

$$\hat{Z}_R = \frac{\hat{H}_{M/C} \times \hat{X}_R}{|\hat{H}_{M/C} \times \hat{X}_R|}$$

or:

$$\hat{Z}_R = c_{31}\hat{\imath}_M + c_{32}\hat{\jmath}_M + c_{33}\hat{k}_M \quad \text{(D-30)}$$

Orthogonality forces $\hat{Y}_R$:

$$\hat{Y}_R = \hat{Z}_R \times \hat{X}_R \quad \text{(D-30)}$$

Combining the foregoing gives the desired transformation matrix:

$$\bar{\Gamma}_R = c_{ij}\,\bar{\Gamma}_M \quad \text{(D-30)}$$

Matrix C_{ij} is stored in the LGC computer and subsequently used to align the physical platform (see Sheet Q references 13, 41).

The LEM Platform is realigned prior to take-off. Once again, directions X_R, Y_R and Z_R are found, given the selenographic latitude and longitude of the take-off site and a nominal take-off time t* measured from problem start. Time t* is given by the allowable launch window variation which in turn is defined during prelaunch operations (see Sheet N references 13, 41).

4. Matrix Operator From Inertial M or E-Frame to LEM Body B-Frame

The transformation matrix $g_{i j_n}$ (D-40) has been defined in Subsection III-C-4. This matrix is used to position the visual displays:

$$\bar{r}_B = g_{ij_n} \bar{r}_n \tag{D-40}$$

5. Matrix Operator From Inertial E - Frame to Geographic G - Frame

Subset equations (D-60) relate the Greenwich meridian to the E-frame and are used to:

i. Specify the line-of-sight communication requirements between the LEM vehicle and each Earth tracking station.

ii. Position the mission effects projector (MEP) during Earth training exercises.

The Earth's mean equator is defined by the X_E - Y_E reference plane. Consequently, a single rotation about the Earth's mean spin axis ($\hat{Z}_E = \hat{Z}_G$) is sufficient to position the prime meridian relative to the E-frame.

6. Matrix Operator From the LEM Body B-Frame to the Optical Window W-Frame Or Telescope T-Frame

a. General. Lunar landmarks, the Earth, the CSM, and star positions are observed by the astronauts through either two forward windows, an upper window or one of three telescope positions. Window and telescope optical axes ($\hat{Z}_{pq}$) are shown schematically in Figure 7. Each optical axis has a fixed direction relative to the body axes. For each viewing mode, this direction extends from the flight station design eye to the center of each respective viewing device. All visual displays are positioned relative to this line-of-sight direction. Field of view constraints are automatically included in all visual displays.

Window and telescope transformations are generalized by use of dummy subscripts pq. Subscript p denotes the viewing device, either window (p = W) or telescope (p = T). Subscript q denotes the viewing mode, either left (q = l), right (q = r) or above (q = a). The generalized transformation matrix given below is based on ordered, right hand rotations specified by input constants ϕ_{pq}, θ_{pq}, ψ_{pq} (see J-01):

$$F_{pq} = (h_{ij})_{pq} F_B \qquad \text{(D-70)}$$

b. Window Transformations. The left hand window coordinate axes are derived as follows. Displace the body axes from the vehicle CG to the flight station design eye. Rotate about X_B through $+\phi_{Wl}$. Rotate about the new $Y_{B'}$ axis so formed through a negative angle $-\theta_{Wl}$. This positions the left window axis frame X_{Wl}, Y_{Wl}, Z_{Wl}. Note that $\psi_{Wq} = 0$.

A similar procedure is repeated for the right window. A negative rotation $-\phi_{Wr}$ is followed by a negative rotation $-\theta_{Wr}$.

Only one rotation is required to specify the above window optical axes, namely, a positive rotation about Y_B through θ_{Wa}.

c. Telescope Transformations. The center or above telescope axes are given by a single rotation $+\theta_{Ta}$ about the Y_B axis. Three rotations, however, are required to specify the left or right telescope axes relative to the body axes. Consider the left telescope. Axes X_{Tl}, Y_{Tl}, Z_{Tl} are defined by a positive rotation ϕ_{Tl} about X_B, followed by $+\theta_{Tl}$ about Y_B', followed by $-\psi_{Tl}$ about Z_B''. The latter transformation is necessary to synthesize prism rotation whenever the Alignment Optical Telescope is slewed. Right telescope ordered rotations are $-\phi_{Tr}$, $+\theta_{Tr}$, $+\psi_{Tr}$.

The optical axes can be transformed directly into M or E-frame. coordinates by employing known matrix operators D-70 and D-40. Hence:

$$\overline{T}_n = (\ell_{ij})_{p\gamma_n} \overline{T}_{p\gamma} \qquad \text{(D-80)}$$

where:

$$(\ell_{ij})_{p\gamma_n} = (g_{ik})_n^T (h_{kj})_{p\gamma}^T$$

Additional transformations, when required for particular subsystem applications, will be discussed in the following report subsections.

7. Conclusions

a. Matrix operator a_{ij} transforms M-frame coordinates to selenographic coordinates and is initialized at problem start. Negligible errors will accrue if the libration matrix and lunar orbit element Ω are held constant during the course of a run. Element Ω changes by approximately .053 deg/day.

b. For Earth training exercises, the LEM platform is assumed fixed to the launch site at launch. Reference directions $\hat{X}_R$ and $\hat{Z}_R$ are given by the launch site vertical and azimuth heading direction, respectively.

E. Ephemeris.

1. Purpose. The purpose of Set E is to define the Moon and Sun positions in mean Earth equator of date coordinates (E-frame), determine the Moon's orbital elements, and generate the Greenwich Hour Angle. Lunar and solar coordinates will be supplied by JPL Ephemeris Tapes (Reference 33).

2. Problem Start Initialization.

a. Time. The JPL tapes are referenced to a 1950.0 epoch and require Julian Date inputs at problem start. It is assumed that training exercises will be initialized by the specification of Universal Time measured in hours H, and days D* of the launch year. Thus, these data must be transformed to Julian Days. This may require counting the number of mean solar days from epoch January 1, 4713 B.C. to problem start.

Consider a reference epoch of 1950.0 (midnight December 31, 1949). Excluding leap years the number of days from this epoch to problem start is $365\ (Y - 1950) + D^* + \frac{H}{24}$. Leap year days, during the time span (Y - 1950), are determined by the integer value of N, where:

$$N + \Delta N = 1 + \frac{Y - 1953}{4} \qquad 0 \leq \Delta N < 1 \tag{E-01}$$

The total number of days from the reference epoch can now be found:

$$d_o = 365(Y - 1950) + D^* + \frac{H}{24} + N \tag{E-01}$$

Having defined d_o, Julian time measured in terms of Julian centuries from epoch 1950.0 is simply:

$$T_o = \frac{d_o}{36{,}525} \tag{E-01}$$

This time is fixed at problem start and does not vary during the length of any training mission.

Julian days, measured from January 1, 4713 B.C. to date, are given by equation E-22. This number may be required as an input to the JPL program.

b. Greenwich Hour Angle. The right ascension of the mean Sun, corrected for aberration and referenced to the mean equinox of 1950.0 was obtained from reference 16 and is given by subset equation E-10. The Sun 's meridian at problem start is employed to specify the time varying Greenwich meridian with respect to the fixed mean equinox of date (E-10).

3. Lunar-Solar Positional and Orbital Elements. The position coordinates of the Moon, $\bar{r}_{E/M}$, and Sun $\bar{r}_{E/\odot}$, relative to the mean equinox of date are outputs of the JPL ephemeris program. Therefore, subset equations E-30 and E-31 should not be programmed.

Lunar orbital elements $(\Omega, ☾, \Gamma')$, and solar elements $(\epsilon, g_{\odot})$ were obtained from reference 34 and updated from epoch January 0.5, 1900 to reference epoch 1950.0. These elements are given by E-20. They are employed to define the selenographic transformation matrix a_{ij}. Also included are the Moon's mean longitude rate $\dot{☾}$, and nodal regression rate $\dot{\Omega}$. These data are employed later to define the linear velocity of the LEM's subsatellite point relative to the lunar surface.

4. Conclusions

a. All planetary elements are computed with respect to the mean equinox of date based on a fundamental epoch of 1950.0.

b. The JPL Ephemeris Program will supply the Sun and Moon position coordinates. If this program also outputs the appropriate lunar orbit elements and GHA, then Set E equations should not be programmed.

F. Rendezvous Radar.

1. Purpose. The purpose of Set F is define the line-of-sight vector, measured from the LEM to the CSM, in LEM body coordinates and to provide required inputs to the Rendezvous Radar Subsystem Math Model.

2. Relative Range and Velocity Vectors Measured In LEM Body Axes.

a. Scalar Range and Range Rate. Scalar range defines the linear CG-to-CG distance between the LEM and CSM vehicles:

$$\rho_{LS} = |\bar{\rho}| = +\sqrt{\rho_X^2 + \rho_Y^2 + \rho_Z^2} \qquad \text{(F-10)}$$

Scalar range rate denotes the relative separation or closing speed between the vehicles and is given by:

$$\dot{\rho}_{LS} = \frac{\bar{\rho} \cdot \dot{\bar{\rho}}}{|\bar{\rho}|} = \frac{d}{dt}\sqrt{\rho_X^2 + \rho_Y^2 + \rho_Z^2} = \frac{\rho_X \dot{\rho}_X + \rho_Y \dot{\rho}_Y + \rho_Z \dot{\rho}_Z}{\rho_{LS}} \qquad \text{(F-10)}$$

Parameter $\dot{\rho}_{LS}$ is a required rendezvous and docking display unit.

b. M or E-Frame Relative Components. Component distances and velocities must be ascertained in order to activate equations (F-10). These data are computed from two separate sources. As mentioned in Subsections A and B, LEM motion is generated with respect to either the inertial M-frame or a non-rotating, but accelerated, relative frame centered at the CSM.

Inertial M-frame LEM equations are activated during lunar mission exercises whenever $\rho_{LS} \geq D_2$ (B-02). CSM motion is supplied in M-frame coordinates regardless of whether the mission mode is integrated or independent. Accordingly, CSM motion relative to the LEM, expressed in M-frame coordinates, is:

$$\bar{\rho}_M = \bar{r}_{M/C} - \bar{r}_{M/L} = \bar{\rho}^*$$
$$\dot{\bar{\rho}}_M = \dot{\bar{r}}_{M/C} - \dot{\bar{r}}_{M/L} = \dot{\bar{\rho}}^* \qquad \text{(F-11,12,25)}$$

Relative motion coordinates are direct outputs of equation (B-10). These data are always computed during Earth mission operations, and during lunar operations whenever $\rho_{LS} < D_1$. Relative motion vectors

$\bar{\rho}$ and $\dot{\bar{\rho}}$, thus computed, describe LEM motion with respect to the CSM. A change in sign is therefore required to describe CSM motion relative to the LEM. This generalized vector, measured in E or M-frame coordinates, is given as:

$$\bar{\rho}^* = -\bar{\rho} \qquad \dot{\bar{\rho}}^* = -\dot{\bar{\rho}} \tag{F-25}$$

Switching logic is provided in subset equation (F-25) to discriminate between $\bar{\rho}$ * and $\dot{\bar{\rho}}$ * calculations based on inputs from subset equations (A-10) or (B-10).

Once $\bar{\rho}$ * and $\dot{\bar{\rho}}$ * are obtained, a single transformation relates the relative motion vectors to LEM body axes:

$$\bar{\rho}_B = g_{ij_n} \bar{\rho}^* \tag{F-23}$$

$$\dot{\bar{\rho}}_B = g_{ij_n} \dot{\bar{\rho}}^* \tag{F-24}$$

Motion measured between the LEM-CG and the CSM-CG is defined by vectors $\bar{\rho}_B$ and $\dot{\bar{\rho}}_B$. The following transformations are required to describe relative motion between the LEM radar dish and the CSM-CG:

$$\bar{\rho}_B' = \bar{\rho}_B - \bar{d}_{RR} \qquad \dot{\bar{\rho}}_B' = \dot{\bar{\rho}}_B - \bar{\omega}_B \times \bar{\rho}_B' \tag{f-1}$$

Vectors $\bar{d}_{RR}$ and ω_B represent the displacement between the LEM-CG and rendezvous radar dish, and the total LEM angular velocity. Thus:

$$\bar{d}_{RR} = (\alpha_{RR} - \alpha_{CG})\hat{i}_B + (\beta_{RR} - \beta_{CG})\hat{j}_B + (\gamma_{RR} - \gamma_{CG})\hat{k}_B \qquad \bar{\omega}_B = p_B\hat{i}_B + q_B\hat{j}_B + r_B\hat{k}_B \tag{f-2}$$

It is recommended that equations (f-1) and (f-2) not be programmed because:

i. At large distances parallax errors are overshadowed by rendezvous radar system errors.

ii. At relative distances less than approximately 50 feet, where parallax errors can be significant, the rendezvous radar is no longer operative (reference 35).

Parallax corrections will be made, however, to the rendezvous and docking visual display drive equations.

3. Rendezvous Radar Interface Parameters.

a. Gimbal Angles. Presented in Figure 8 is a schematic representation of the rendezvous radar gimballing geometry. Consider a rendezvous radar axes system (x_{RR}, y_{RR}, z_{RR}) fixed to the radar dish. Let the radar axes coincide with the LEM body axes. Define $\hat{x}_{RR}$, $\hat{y}_{RR}$ and $\hat{z}_{RR}$ directions as the outboard, inboard and boresight axis, respectively. Position the radar axes by a rotation E_{LS} about Y_B , followed by a second rotation A_{LS} about the new X_B' axis so formed. The transformation matrix reduces to:

$$\bar{r}_{RR} = M(E_{LS}, A_{LS})\,\bar{r}_B \qquad \text{(f-3)}$$

or, in expanded form:

$$\begin{bmatrix} x_{RR} \\ y_{RR} \\ z_{RR} \end{bmatrix} = \begin{bmatrix} \cos E_{LS} & 0 & -\sin E_{LS} \\ \sin A_{LS}\sin E_{LS} & \cos A_{LS} & \sin A_{LS}\cos E_{LS} \\ \cos A_{LS}\sin E_{LS} & -\sin A_{LS} & \cos A_{LS}\cos E_{LS} \end{bmatrix} \begin{bmatrix} \rho_{x_B} \\ \rho_{Y_B} \\ \rho_{z_B} \end{bmatrix}$$

Realize that z_{RR} specifies the line-of-sight direction between the vehicles. Hence, component distances x_{RR} and y_{RR} must be zero. Therefore:

$$0 = \rho_{x_B}\cos E_{LS} - \rho_{z_B}\sin E_{LS} \qquad \text{(f-4)}$$

$$0 = \rho_{x_B}\sin A_{LS}\sin E_{LS} + \rho_{Y_B}\cos A_{LS} + \rho_{z_B}\sin A_{LS}\cos E_{LS} \qquad \text{(f-5)}$$

Solving equations (f-4) and (f-5) for E_{LS} and A_{LS} gives:

$$\tan E_{LS} = \frac{\rho_{x_B}}{\rho_{z_B}} \qquad \text{(F-20)}$$

$$\tan A_{LS} = \frac{-\rho_{Y_B}}{\rho_{x_B}\sin E_{LS} + \rho_{z_B}\cos E_{LS}} \qquad \text{(F-21)}$$

Gimbal angle E_{LS} exhibits a singularity when the CSM line-of-sight lies along the LEM Y_B body axis ($\rho_{X_B} = \rho_{Z_B} = 0$). Geometrically, this condition corresponds to $A_{LS} = \pm \frac{\pi}{2}$ and $E_{LS} = 0$. The indeterminacy, tan $E_{LS} = \frac{0}{0}$, is circumvented by introducing logic (F-22) that forces $E_{LS} = 0$ when $\rho_{X_B} = \rho_{Z_B} = 0$.

The line-of-sight gimbal angle rates relative to the body axes are generated by differentiating E_{LS} and A_{LS} with respect to time (See equations F-20, 21). Infinite rates exist when ρ_{Y_B} and ρ_{Z_B} approach zero. Infinite rates are ameliorated by the addition of logic commands (F-22) that force either $\dot{A}_{LS}$ or $\dot{E}_{LS}$ to zero values whenever ρ_{Y_B} or ρ_{Z_B} equal zero, respectively.

b. Radar Subsystem Math Model Rate Inputs. Five angular rate inputs are required to interface with the Rendezvous Radar Subsystem Math Model. Two of these rates represent total inertial angular velocities measured along the radar line-of-sight inboard and outboard axes. This includes the motion of the gimbal axes relative to the body axes plus the motion of the body axes relative to inertial space. Expressed mathematically:

$$\begin{bmatrix} \omega_{LS_{ob}} \\ \omega_{LS_{ib}} \\ 0 \end{bmatrix} = \begin{bmatrix} \dot{A}_{LS} \\ 0 \\ 0 \end{bmatrix} + M(E_{LS}, A_{LS}) \begin{bmatrix} p_B \\ q_B + \dot{E}_{LS} \\ r_B \end{bmatrix} \qquad \text{(F-30)}$$

The last three required rate inputs (p_B, q_B, r_B) reflect inertial angular velocities of the LEM body† resolved along the rendezvous radar tracking axis. A distinction must be made between the line-of-sight axes and the tracking axes. The line-of-sight axes represents a hypothetical radar dish which continually points at the CSM. Boresight

† Does not include radar gimbal angle rates.

errors and servo system lags prevent the hardware radar dish, and hence the tracking line axes, from continually pointing at the CSM. Physical system gimbal angles and angle rates are computed in the Rendezvous Radar Subsystem Math Model and are designated by subscript TL rather than subscript LS.

Radar Subsystem Math Model inputs E_{TL} and A_{TL} provide the link required to define total LEM angular rates resolved along radar tracking line axes:

$$\begin{bmatrix} \omega_{B_{cb}} \\ \omega_{B_{ib}} \\ \omega_{TL} \end{bmatrix} = \begin{bmatrix} \cos E_{TL} & 0 & -\sin E_{TL} \\ \sin A_{TL} \sin E_{TL} & \cos A_{TL} & \sin A_{TL} \cos E_{TL} \\ \cos A_{TL} \sin E_{TL} & -\sin A_{TL} & \cos A_{TL} \cos E_{TL} \end{bmatrix} \begin{bmatrix} p_B \\ q_B \\ r_B \end{bmatrix} \tag{F-31}$$

4. <u>Conclusions</u>

a. True line-of-sight distances and velocities, used as inputs to the R.R. Math Model, represent CSM-CG motion relative to the B-frame located at the instantaneous LEM-CG. Parallax corrections, to compensate for radar dish displacements relative to the LEM-CG, are not included because:

i. radar uncertainties overshadow the parallax correction.

ii. the radar is inoperative at relative distances less than 50 feet.

iii. if parallax corrections are included then CSM skin track errors should also be included. This represents unnecessary complications.

G. Landing Radar

1. Purpose. The purpose of Set G is to determine velocity and altitude inputs for the Landing Radar Subsystem Math Model and for the Land Mass Simulator. In addition, subsidiary calculations are made to determine the slant range of each landing radar beam measured from the LEM vehicle to the lunar surface. Set G equations are not activated during Earth mission exercises.

2. Doppler Input Velocities

a. The Moon's Shape. The Moon's surface velocity at the subsatellite point and LEM altitude depend on the Moon's shape. A Land-Mass Simulator will be employed to generate surface irregularities above an assumed spherical datum reference (R_{LM}). The datum reference will vary depending on the latitude and longitude of intended landing site (ϕ_{LM}, λ_{LM}). Since the Land-Mass Simulator is designed for 10 specific landing sites, 10 spherical datum references are envisioned (R_{LM_j}; j = 1, 2, 3, 4, 5, 6, 7, 8, 9, 10).

It is common practice to represent the Moon's surface by a triaxial ellipsoid (reference 8):

$$R_{LM} = a_M \left[1 - f'(\cos\phi_{LM} \sin\lambda_{LM})^2 - f^* \sin^2\phi_{LM}\right] \qquad \text{(g-1)}$$

Parameters f' and f* denote the Moon's equatorial and polar flattening constants, while a_M represents the Moon's semi-major axis. Both the semi-minor equatorial axis and semi-polar axis are foreshortened by approximately 0.2 n.m. and 0.6 n.m., respectively, when compared to a_M. Equation (g-1) may be used to establish the spherical datum reference at problem start. Thus, if the first intended landing sight is at the pole, then the Moon's constant radius would be $R_{LM_1} = a_M [1-f^*]$.

Altitude errors introduced by the foregoing assumption are small as illustrated by the following example. The landing radar is activated at altitudes below 30,000 feet. Assume the maximum surface range, measured from the subsatellite point to the landing site will always be less than 110 n.m.* A 110 n.m. shift in surface location on the reference triaxial ellipsoid causes a maximum selenographic radius change of approximately 45 feet. Surface irregularities included in the simulation will overshadow 45 feet. Moreover, the spherical datum reference is approached as the LEM approaches the landing site. Consequently, all subsequent calculations are referenced to the spherical datum.

b. Velocity of Subsatellite Point. At any instant, the LEM's subsatellite point in terms of selenographic latitude and longitude is known:

$$\sin\phi_{S/L} = \frac{Z_{S/L}}{r_{M/L}} \qquad ; -\frac{\pi}{2} \le \phi_{S/L} \le \frac{\pi}{2}$$
$$\tan\lambda_{S/L} = \frac{Y_{S/L}}{X_{S/L}} \tag{G-12}$$

Hence, the vector components of the subsatellite point, measured in selenographic coordinates, can be found:

$$\bar{R}_{S/L} = R_{LM}\left[\cos\phi_{S/L}\cos\lambda_{S/L}\,\hat{i}_s + \cos\phi_{S/L}\sin\lambda_{S/L}\,\hat{j}_s + \sin\phi_{S/L}\,\hat{k}_s\right] \tag{G-14}$$

Accordingly, the lunar surface velocity is given by:

$$\dot{\bar{R}}_{S/L} = \bar{\omega}_s \times \bar{R}_{S/L} \tag{G-16}$$

It remains to determine the Moon's total angular velocity $\bar{\omega}_s$.

* Actually, for the nominal mission, the downrange distance at 30,000 feet altitude is about 35 n.m.

Refer to Figure 6. Note that the Moon's nodal regression rate vector is parallel to the ecliptic plane. Also, note that the mean position of the Moon is given by the mean longitude, ☾ , which is measured from the mean equinox along the ecliptic to the mean ascending node, and then along the lunar orbit. Since measurements are made with respect to the mean equinox of date, which is assumed fixed, vector $\dot{☾}$ reflects the change of the mean Moon's position relative to the regressing mean ascending node. Consequently, $\dot{☾}$ is directed normal to the lunar orbit. From Cassini's Laws, however, the Moon's rate about the north-south axis is equal to the Moon's mean rotation in its orbit. Thus, $\dot{☾}$ is also directed along $\hat{Z}_s$. Transforming vectors $\dot{\Omega}$ and $\dot{☾}$ to selenographic coordinates gives:

$$\begin{bmatrix} \omega_{X_s} \\ \omega_{Y_s} \\ \omega_{Z_s} \end{bmatrix} = a_{kl} a_{lm} \begin{bmatrix} 0 \\ 0 \\ \dot{\Omega} \end{bmatrix} + \begin{bmatrix} 0 \\ 0 \\ \dot{☾} \end{bmatrix} \qquad \text{(G-15)}$$

Matrix operators a_{kl} and a_{lm} are given by subset equations D-13 and D-15.

Equation (G-15) does not include velocities induced by physical librations. These terms are neglected because, even if a conservative libration amplitude of .06 deg/year is assumed, then the resulting surface velocity due to libration is approximately 2×10^{-4} ft/sec, which is insignificant when compared to a surface velocity of about .06 ft/sec. for nodal regression and about 13 to 14 ft/sec for $\dot{☾}$. NASA has recommended (reference 40) that the surface velocity due to $\dot{\Omega}$ be neglected. This is reasonable since the $\dot{\Omega}$ contribution is 20 times smaller than the $\dot{☾}$ contribution and will have no effect on astronaut training.

Lunar surface velocity components, measured in M-frame coordinates, are now found as follows:

$$\dot{\bar{r}}_{M/S} = a_{ij} \dot{\bar{R}}_{S/L} \tag{G-10}$$

c. Velocity of LEM Relative to Lunar Surface. LEM inertial M-frame velocity components are computed from equations A-11. The LEM velocity vector relative to the Moon's surface is, therefore:

$$\dot{\bar{r}}_{M/R} = \dot{\bar{r}}_{M/L} - \dot{\bar{r}}_{M/S} \tag{G-21}$$

This relative velocity vector is transformed into body axes using matrix operator g_{ij_M}:

$$\dot{\bar{r}}_{B/S} = g_{ij_M} \dot{\bar{r}}_{M/R} \tag{G-20}$$

An additional transformation is required to generate doppler velocity signals measured along landing radar beam directions.

d. Landing Radar Beam Directions. The Landing Radar Subsystem computes three components of relative velocity and altitude above the lunar terrain. Effectively, these state parameters are measured by four doppler signals that are transmitted to the surface in a fixed beam pattern relative to a landing radar plate (see Figure 9). Moreover, the landing radar plate can be positioned in one of two known orientations (α_1 or α_2) relative to the LEM X_B-Z_B body axes. Two landing radar plate detent positions ensure that the altitude beam ($\hat{D}_4$) will be approximately normal to the lunar surface, as the LEM orientation is altered during the powered descent and hover-to-touchdown mission phases.

Consider the ordered rotations necessary to establish the matrix operator between body axes directions $\hat{X}_B$, $\hat{Y}_B$, $\hat{Z}_B$ and landing radar beam directions $\hat{D}_1$, $\hat{D}_2$, $\hat{D}_3$, and $\hat{D}_4$ (see Figure 9). A single negative rotation ($\alpha_j + \xi_K + \frac{\pi}{2}$; j = 1, 2; k = 1, 2, 3, 4) about the Y_B body axis defines the altimeter beam direction $\hat{D}_4$, and locates the plane formed by $\hat{D}_1$ and $\hat{D}_2$. A positive (Λ_2) or negative (Λ_1) rotation about the new X_B' axis is sufficient to describe $\hat{D}_2$ or $\hat{D}_1$. A similar procedure is used to locate $\hat{D}_3$. Combining all rotations yield:

$$\begin{bmatrix} \hat{D}_1 \\ \hat{D}_2 \\ \hat{D}_3 \\ \hat{D}_4 \end{bmatrix} = g_{ij} \begin{bmatrix} \hat{X}_B \\ \hat{Y}_B \\ \hat{Z}_B \end{bmatrix}$$

where, (g-2)

$$g_{ij} = \begin{bmatrix} a_1 & b_1 & c_1 \\ a_2 & b_2 & c_2 \\ a_3 & b_3 & c_3 \\ a_4 & 0 & c_4 \end{bmatrix}$$

Fixed matrix elements a, b and c (equations G-47, 48 and 49) are trignometric combinations of the positive-valued, geometric pattern angles ξ_K and Λ_i . Input angles, $\xi_K = \xi_0 + \Delta \xi_K$ and $\Lambda_i = \Lambda_0 + \Delta \Lambda_i$, reflect the nominal design angles of each radar beam relative to the landing plate, plus calibration errors.

Finally, doppler velocity input signals to the Landing Radar Math Model are found from equations (g-2) and (G-20):

$$\begin{bmatrix} D_{S_1} \\ D_{S_2} \\ D_{S_3} \\ 0 \end{bmatrix} = g_{ij} \begin{bmatrix} \dot{X}_{B/S} \\ \dot{Y}_{B/S} \\ \dot{Z}_{B/S} \end{bmatrix} \qquad \text{(G-40)}$$

Doppler signals D_{s1}, D_{s_2}, D_{s_3} do not include spurious velocity signals, transmitted to the landing plate, due to vehicle CG rotation rates p_B, q_B, r_B. These velocities are small, have an average value of zero and are therefore neglected.

It remains to determine the actual altitude above the lunar terrain as well as the slant range of each radar beam.

3. Slant Range Measured Along Radar Beams

a. General. Slant range calculations depend on two geometric angles. These are:

i. the angle μ_K measured between each doppler beam direction and the LEM local vertical (see Figure 10).

ii. the angle θ_{o_k} measured between each doppler beam direction and the local vertical formed by the intersection of each doppler beam with the lunar surface (see Figure 10).

b. Local Vertical Angle. Angle μ_K is formed by taking the dot product of each beam direction (g-2) with the LEM radius vector defined with respect to the landing radar plate rather than the vehicle CG:

$$\cos \mu_k = \frac{\overline{r}'_{B/L} \cdot \hat{D}_k}{|\overline{r}'_{B/L}|} \;; 0 \le \mu_k \le \frac{\pi}{2} \qquad \text{(G-43)}$$

where, the radius vector from the Moon to the radar plate origin is:

$$\overline{r}'_{B/L} = \overline{r}_{B/L} + \overline{\alpha}_{LR} \hat{i}_B + \overline{\beta}_{LR} \hat{j}_B + \overline{\delta}_{LR} \hat{k}_B \qquad \text{(G-41)}$$

and where:

$$\overline{r}_{B/L} = g_{ij_M} \overline{r}_{M/L} \qquad \text{(G-42)}$$

Vectors $\bar{r}_{B/L}$ and $\bar{r}'_{B/L}$ are illustrated below:

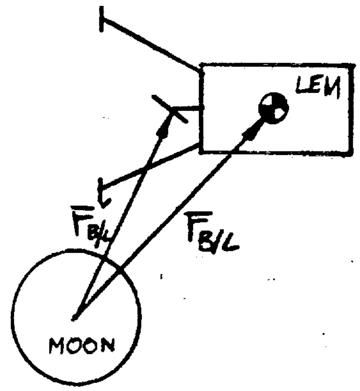

Should μ_K be greater than $\frac{\pi}{2}$, than an intersection between the k^{th} radar beam and the lunar surface is impossible. In fact, the limiting condition is specified by the angle measured between the LEM local vertical at the landing plate and a line drawn from the LEM tangent to the lunar surface. Call this angle μ_{MAX}, hence:

$$\sin \mu_{MAX} = \frac{R_{LM}}{r'_{B/L}}$$

$$0 \leq \mu_{MAX} \leq \frac{\pi}{2} \qquad \text{(G-43b)}$$

If $\mu_K > \mu_{MAX}$, then the k^{th} beam will not intersect the lunar surface; consequently, $R_K = \infty$(G-43a). Logic given by (G-43a) must be programmed to prevent a singularity from occuring in loops G-44 and G-45.

c. Surface Intersection Angle and Slant Range. Angle θ_{o_k} is computed from the law of sines whenever $\mu_K \leq \mu_{MAX}$:

$$\sin \theta_{o_k} = \frac{r'_{B/L}}{R_{LM}} \sin \mu_k$$

$$0 \leq \theta_{o_k} \leq \frac{\pi}{2} \qquad \text{(G-44)}$$

Angle θ_{o_k} is a Landing Radar Math Model input that characterizes the backscattering effect as each doppler beam makes contact with the lunar surface.

The slant range, measured from the radar plate origin along each doppler beam to its intersection with the assumed datum surface is:

$$R_{\ell} = R_{LM} \frac{\sin(\theta_{o\ell} - \mu_{\ell})}{\sin \mu_{\ell}} \tag{G-45}$$

d. Altitude Above Reference Datum. Two idealized altitude signals relative to the spherical datum surface are computed for use on the instructor's console. Altitudes $h_{M/L}$ and $h_{M/LR}$ are measured from the datum surface to the vehicle CG and landing radar plate, respectively:

$$h_{M/L} = r_{M/L} - R_{LM}$$

$$h_{M/LR} = r'_{B/L} - R_{LM} \tag{G-30}$$

The difference in altitude ($h_{M/L}$ - $h_{M/LR}$) may be as large as 8 feet. Altitude rate is given by:

$$\dot{h}_{M/L} = \frac{\bar{r}_{M/L} \cdot \bar{V}_{M/L}}{|\bar{r}_{M/L}|} = \dot{r}_{M/L} \tag{G-30}$$

Local Surface irregularities are not reflected by equations (G-30, 45). Terrain elevation above the reference datum will be specified by the Land Mass Simulator to modify the ideal altimeter range signal R_{ℓ}. Corrections will not be made to slant range measured along doppler velocity beams R_1, R_2 and R_3.

4. Land Mass Simulator.

a. General. A Land Mass Simulator, consisting of a film plate transport and an optical-electrical system, provides local elevation information for 10 specific areas of the Moon. The film transport represents a planar surface tangent to the Moon at one of the ten intended landing sites. Each site is referenced by a known selenographic latitude (ϕ_{LM}) and longitude (λ_{LM}) which forms the origin of a topocentric, two dimensional coordinate frame $\hat{J}_{LM}$, $\hat{K}_{LM}$. Vectors $\hat{J}_{LM}$ and $\hat{K}_{LM}$ are directed due East and North, respectively.

Surface irregularities above the reference datum are projected onto the flat film transport (see sketch) and subsequently read by an optical-electrical system. In essence, the optical-electrical system is positioned relative to the LEM subsatellite point, where-upon an additional signal (ψ_{LM}) is generated to locate the vector drawn from the

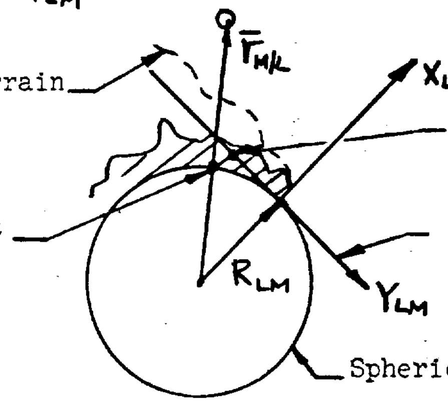

subsatellite point to the altimeter beam intersection point ($\Delta \bar{r}_{S/4}$, see Figure 11). The amount of radiant flux that passes through the film plate along the altimeter beam is ascertained by the Land Mass Simulator and used to produce a voltage proportional to surface elevation (e_T - see Figure 10).

b. Drive Coordinates Y_{LM} and Z_{LM}. In order to position the optical-electrical system, it is necessary to determine the excursion of the subsatellite point relative to the film plate origin in film transport (flat plate) coordinates. The required manipulations are discussed below.

Consider the transformation between land mass coordinates and S-frame coordinates. Rotate about Z_S through the longitude of the landing site (λ_{LM}). Rotate again about the new Y_S' axis so formed through the desired landing site latitude ϕ_{LM} to give desired land mass coordinates X_{LM}, Y_{LM}, Z_{LM}. In vector form:

$$\overline{F}_{LM} = p_{ij}\,\overline{r}_s \qquad \text{(g-3)}$$

where:

$$p_{ij} = \begin{bmatrix} \cos\phi_{LM}\cos\lambda_{LM} & \cos\phi_{LM}\sin\lambda_{LM} & \sin\phi_{LM} \\ -\sin\lambda_{LM} & \cos\lambda_{LM} & 0 \\ -\sin\phi_{LM}\cos\lambda_{LM} & -\sin\phi_{LM}\sin\lambda_{LM} & \cos\phi_{LM} \end{bmatrix} \qquad \text{(g-4)}$$

LEM subsatellite point coordinates are known from previous calculations:

$$\overline{R}_{S/L} = R_{X_{S/L}}\,\hat{i}_s + R_{Y_{S/L}}\,\hat{j}_s + R_{Z_{S/L}}\,\hat{k}_s \qquad \text{(G-14)}$$

Moreover, the constant radius vector to the film transport origin (landing site), is also known:

$$\overline{R}_{LM} = R_{LM}\left[\cos\phi_{LM}\cos\lambda_{LM}\,\hat{i}_s + \cos\phi_{LM}\sin\lambda_{LM}\,\hat{j}_s + \sin\phi_{LM}\,\hat{k}_s\right] \qquad \text{(G-51)}$$

or:

$$\overline{R}_{LM} = R_{X_{LM}}\,\hat{i}_s + R_{Y_{LM}}\,\hat{j}_s + R_{Z_{LM}}\,\hat{k}_s$$

Consequently, equations (G-14) and (G-51) define the subsatellite point relative to the land mass origin measured in S-frame coordinates (Figure 11):

$$\Delta\overline{r}_s = \overline{R}_{S/L} - \overline{R}_{LM} \qquad \text{(g-5)}$$

Transforming $\Delta\overline{r}_s$ to land mass coordinates, $\overline{r}_{LM} = P_{ij}\,\Delta\overline{r}_s$, gives the desired result, namely:

$$Y_{LM} = -\Delta X_s \sin\lambda_{LM} + \Delta Y_s \cos\lambda_{LM}$$

$$Z_{LM} = -\Delta X_s \sin\phi_{LM} \cos\lambda_{LM} - \Delta Y_s \sin\phi_{LM} \sin\lambda_{LM} + \Delta Z_s \cos\phi_{LM} \qquad \text{(G-50)}$$

Component X_{LM} is normal to the film transport and hence is not required to drive the optical-electrical system.

Equation (G-50) reflects the difference ($\Delta \bar{r}_s$) between two large numbers of equal magnitude (6×10^6 feet). If the digital computer is scaled to accommodate a variable range from 0 to 6×10^6 feet, then the least significant bit is about .7 feet. This means that as the LEM approaches the landing site, the scene as viewed by the astronaut would exhibit an erratic or jerk motion equivalent to approximately 1 foot. To eliminate this erratic motion it is recommended that equation (g-5) be reformulated.

When the Land Mass Simulator, or Landing and Ascent Image Generator becomes active, initialize equation (g-5):

$$\Delta \bar{r}_{s_0} = \bar{R}_{S/L_0} - \bar{R}_{LM} \qquad \text{(G-52)}$$

Vector $\Delta \bar{r}_s$ can be computed by integrating the LEM velocity relative to the lunar surface in selenographic coordinates, hence:

$$\Delta \bar{r}_s = \Delta \bar{r}_{s_0} - \int \dot{\bar{r}}_s \, dt \qquad \text{(G-53)}$$

Where:

$$\dot{\bar{r}}_s = a_{ij}\,\dot{\bar{r}}_{M/R}$$

Vector $\Delta \bar{r}_s$ as computed in (G-53) is inserted into equation (G-50).

With regard to computer scaling, $\Delta \bar{r}_{so}$ is on the order of 12×10^4 feet. Hence, $\int \dot{\bar{r}}_s dt$ also varies between 0 and 12×10^4 feet. The least significant bit therefore is about .01 feet. Visual display irregularities of .01 feet are imperceptible to the astronaut.

c. Azimuth Drive Angle, ψ_{LM}. Azimuth angle ψ_{LM} depends on $\Delta \bar{r}_4$. Vector $\Delta \bar{r}_4$ is measured from the subsatellite point to the intersection of the altimeter beam with the reference lunar surface in Land Mass coordinates. This vector is found as follows. Determine the slant range vector in body coordinates:

$$\begin{bmatrix} X_{B/4} \\ 0 \\ Z_{B/4} \end{bmatrix} = \begin{bmatrix} \cos(\xi_4 + \alpha_j) \\ 0 \\ -\sin(\xi_4 + \alpha_j) \end{bmatrix} \begin{bmatrix} R_4 \\ 0 \\ 0 \end{bmatrix} \qquad \text{(G-61)}$$

Use matrix operator D-10 and D-40 to resolve $\bar{r}_{B/4}$ from body coordinates to selenographic coordinates:

$$\bar{r}_{S/4} = \begin{bmatrix} X_{S/4} \\ Y_{S/4} \\ Z_{S/4} \end{bmatrix} = a_{ij}\, g^T_{ij_M} \begin{bmatrix} X_{B/4} \\ 0 \\ Y_{B/4} \end{bmatrix} = S_{ij} \begin{bmatrix} X_{B/4} \\ Z_{B/4} \end{bmatrix} \qquad \text{(G-62)}$$

Given the nominal altitude beam vector $\bar{r}_{s/4}$, the drive vector in selenographic coordinates can now be determined:

$$\Delta \bar{r}_{S/4} = (\bar{r}_{S/L} - \bar{R}_{S/L}) + \bar{r}_{S/4} \qquad \text{(G-63)}$$

Transforming to land mass coordinates gives:

$$\begin{bmatrix} \Delta X_4 \\ \Delta Y_4 \\ \Delta Z_4 \end{bmatrix} = p_{ij} \begin{bmatrix} X_{S/L} - R_{X_{S/L}} + X_{S/4} \\ Y_{S/L} - R_{Y_{S/L}} + Y_{S/4} \\ Z_{S/L} - R_{Z_{S/L}} + Z_{S/4} \end{bmatrix} \qquad \text{(g-6)}$$

Whereupon the desired vector measured in land mass coordinates is:

$$\overline{\Delta r_4} = \Delta Y_4 \, j_{LM} + \Delta Z_4 \, k_{LM} \qquad \text{(G-64)}$$

Hence, the azimuth angle drive measured East of North reduces to:

$$\tan \psi_{LM} = \frac{\Delta Y_4}{\Delta Z_4} \qquad \text{(G-60)}$$

The significant figure problem discussed earlier is also evident in equation (G-63). Equation (G-63) is not modified. The reason for this is that vector $\Delta \bar{r}_{s/4}$ (G-63) is not used as a visual display drive parameter. Instead $\Delta \bar{r}_{s/4}$ defines a terrain scan azimuth direction. Thus , erratic motion (on the order of 1 foot) in $\Delta \bar{r}_{s/4}$ cannot be sensed by the astronaut in any of the visual displays.

Given ψ_{LM}, Y_{LM}, Z_{LM} and μ_4 , the Land Mass Simulator automatically outputs surface elevation, e_T (see Figure 10), normal to the film transport. This signal is resolved along the altimeter beam and mixed with R_4 to yield an indicated altitude R_4' :

$$R_4' = R_4 - \frac{e_T}{\cos \theta_{04}} \qquad \text{(G-46)}$$

5. Conclusions

a. Lunar surface velocities due to the Moon's libration and the Moon's regression rate $\dot{\Omega}$ are small and neglected.

b. The lunar radius at the subsatellite point is based on a spherical model. During any run, the lunar radius (R_{LM}) is specified by the reference radius of a particular landing site. This reference radius represents the Land-Mass Simulator datum surface used to generate local terrain irregularities.

c. Spurious doppler velocity signals are neglected. These velocities are caused by LEM-CG rotations coupled with a displacement between the landing radar plate and the LEM-CG.

H. LEM Communication Requirements

1. Purpose. The purpose of Set H is to determine whether or not the LEM can communicate with either the CSM or Earth tracking stations. LEM-VHF antennas are used to communicate with the CSM. An S-band antenna or two fixed, conical log antennas are used for Earth communications while in lunar orbit or in Earth orbit, respectively.

2. LEM-CSM Communication Capability

a. Line-of-Sight Viewing. LEM-CSM visibility constraints are based on the orientation of the line-of-sight vector $\bar{\rho}^*$ relative to the central body. During lunar or terrestrial operations the Moon or Earth, respectively, is regarded as the central body. Geometric visibility constraints are generalized and apply to either mission mode.

As shown in Figure 12a, visibility is assured if R_c^* is greater than the central body radius. Distance R_c^* is computed below:

$$R_c^* = r_{n/c} \sin B_c \tag{h-1}$$

But:

$$\sin B_c = \frac{r_{n/L} \sin \sigma_c}{\rho_{LS}} \tag{h-2}$$

Substituting (h-2) into (h-1) gives:

$$R_c^* = \frac{r_{n/c}\, r_{n/L} \sin \sigma_c}{\rho_{LS}} \tag{H-11}$$

Angle σ_c is defined by the scalar product of $\bar{r}_{n/c}$ and $\bar{r}_{n/L}$, or:

$$\cos \sigma_c = \frac{\bar{r}_{n/c} \cdot \bar{r}_{n/L}}{|\bar{r}_{n/c}|\,|\bar{r}_{n/L}|} \tag{H-12}$$

$$0 \le \sigma_c \le \pi$$

Visibility may also be possible when R_c^* is less than R_n. This condition is tested based on a comparison between angles σ_c and σ_c^*, defined in Figure 12a. Note that:

$$\cos \sigma_c^* = \frac{R_n}{r_{n/c}} \tag{H-11}$$

$$0 \le \sigma_c^* \le \frac{\pi}{2}$$

Equations H-11 and H-12 are interpreted as follows:

i. Visibility always exists if $R_c^* \angle R_n$ provided $\sigma_c \leq \sigma_c^*$.

ii. Visibility never exists if $R_c^* \angle R_n$ and $\sigma_c > \sigma_c^*$.

iii. Visibility always exists whenever $R_c^* \geq R_n$.

b. VHF Antenna Orientations. Even though the CSM and LEM are visible to one another, the CSM and LEM-VHF antennas may be misaligned such that a high noise to signal strength ratio precludes communication. A requirement is established, therefore, to define VHF antenna orientations. These orientations are specified by the angles:

i. ξL_i, measured between the LEM antenna and the line-of-sight.

ii. ξC_i, measured between the CSM antenna and the line-of-sight.

iii. ξ_{ii}, measured between the LEM and CSM antennas projected on a plane perpendicular to the line-of-sight.

Angles ξL_i, ξC_i, and ξ_{ii} are required inputs to the Communication Math Model.

Each vehicle has two VHF antennas. At any instant, only one antenna on either vehicle, selected by the astronauts, will be used for communication. The choice of antennas must be inputted to the IMS Math Model.

Consider angle ξL_i calculations. The direction cosines of each LEM antenna relative to the LEM body axes is known:

$$\hat{l}_i = l_{1_i} \hat{\imath}_B + l_{2_i} \hat{\jmath}_B + l_{3_i} \hat{k}_B \qquad \text{(H-51)}$$
$$i = 1,2$$

Similarly, the direction cosines of each CSM antenna relative to the CSM body axes is known:

$$\hat{c}_i = c_{1_i} \hat{\imath}_{B_C} + c_{2_i} \hat{\jmath}_{B_C} + c_{3_i} \hat{k}_{B_C} \qquad \text{(H-51)}$$
$$i = 1,2$$

Vectors $\hat{l}_i$ and $\hat{c}_i$ are further resolved to M or E frame coordinates:

$$\hat{l}_{n_i} = g_{ij_n}^T \hat{l}_i \qquad \text{(H-52)}$$
$$\hat{c}_{n_i} = g_{ij_c}^T \hat{c}_i \qquad \text{(H-53)}$$

During independent operation, the CSM antenna direction cosines (H-51) are required LMS inputs. The LMS will compute the CSM, n-frame vector $\hat{C}_{ni}$ (H-53). During integrated operations, however, the AMS will compute all CSM-VHF antenna directions.

The desired angles measured between the line-of-sight direction, $\bar{\rho}^*$, and each antenna direction (see sketch) can now be found:

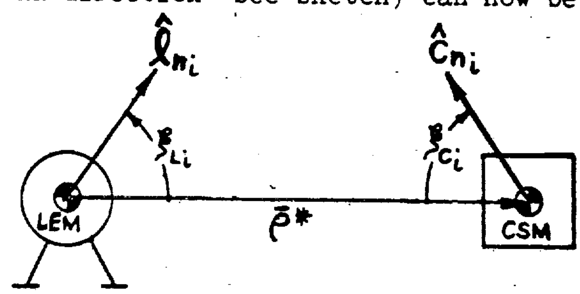

$$\cos \xi_{L_i} = \frac{\hat{\ell}_{n_i} \cdot \bar{\rho}^*}{|\bar{\rho}^*|} \qquad 0 \le \xi_{L_i} \le \pi$$

$$\cos \xi_{C_i} = \frac{-\hat{C}_{n_i} \cdot \bar{\rho}^*}{|\bar{\rho}^*|} \qquad 0 \le \xi_{C_i} \le \pi \qquad \text{(H-50)}$$

In order to define angle ξ_{ii}, the directions normal to the planes formed by the LEM antennas and $\bar{\rho}^*$, and the CSM antennas and $\bar{\rho}^*$ must first be ascertained. These directions are:

$$\hat{\eta}_{L_i} = \frac{\hat{\ell}_{n_i} \times \bar{\rho}^*}{|\bar{\rho}^*| \sin \xi_{L_i}}$$

$$\hat{\eta}_{C_i} = \frac{\hat{C}_{n_i} \times \bar{\rho}^*}{|\bar{\rho}^*| \sin \xi_{C_i}} \qquad \text{(H-54)}$$

Now, ξ_{ii} is:

$$\cos \xi_{ii} = \hat{\eta}_{L_i} \cdot \hat{\eta}_{C_i} \qquad \text{(H-55)}$$

$$0 \le \xi_{ii} \le \pi$$

3. LEM-Earth Tracking Station Communication Capability.

a. Earth Stations. Earth tracking stations will continually communicate with the LEM vehicle. Each ground tracker is specified by a geodetic longitude λ, geodetic latitude ϕ_g and elevation above the reference spheroid, H. Station coordinates resolved to the mean equinox of date (E-frame) are (reference 2):

$$X_{E/G_i} = (R_E C_i + H_i)\cos\phi_i \cos(GHA + \lambda_i)$$

$$Y_{E/G_i} = (R_E C_i + H_i)\cos\phi_i \sin(GHA + \lambda_i) \qquad \text{(H-20)}$$

$$Z_{E/G_i} = (R_E S_i + H_i)\sin\phi_i$$

Earth constant C_i corresponds to the radius of curvature in the prime vertical plane. Parameter GHA (E-10) represents Greenwich Sidereal time.

It was recommended earlier, Subsection III-B-5, that a modified two-body solution be used to compute LEM-CSM motion during independent LMS operations. On a short term basis, the two-body assumption has a trivial effect on communication capability between each ground tracker and the LEM. The communication capability is affected by how often a particular tracker can sight the LEM. Naturally, a difference in this phase relation must exist when two-body motion is compared to n-body motion, because, the LEM mean motion is altered and the nodal regression rate is eliminated. As mentioned earlier, mean motion changes can be compensated for by adjusting the CSM initial state vector (primarily altitude) to account for secular differences between Kepler and n-body motion. In addition, a nodal regression rate correction can also be made, if desired, to modify the siderial GHA such that, to the first order, a proper LEM-ground station phase relation exists. This nodal correction would be implemented whenever an independent LMS Earth training exercise was initiated. Earth nodal regression rate corrections are neglected during independent LMS lunar mission exercises.

The regression rate correction is made in equation (H-20) by altering the sine and cosine arguments to read $GHA + \lambda_i - \dot{\Omega} t$ instead of $GHA + \lambda_i$. Rate $\dot{\Omega}$ is defined by equation (H-22).

b. LEM-Ground Station Visibility - Lunar Phase. The LEM communicates with each ground station by means of an S-band antenna. Ideally, this antenna is directed toward the Earth's center. As shown in Figure 12b, communication may be possible if a clear line-of-sight ($\bar{r}_{G_{i/L}}$) exists between the i^{th} tracker and the LEM, provided the LEM is within the tracker's elevation constraint ($\delta_{i_{limit}}$). A clear line-of-sight is based on distance R_i*, measured from the Moon's center normal to $\bar{r}_{G_{i/L}}$, and angles σ_{E_i} and σ_{E_i}* which are defined in the same sense as angles σ_C and σ_C* given in Figure 12a. Thus:

$$R_i^* = \frac{r_i' \, r_{M/L} \sin \sigma_{E_i}}{r_{G_i/L}} \qquad \text{(H-32)}$$

where:

$$r_{G_i/L} = \left|\bar{r}_{G_i/L}\right| = \left|\bar{r}_{E/M} + \bar{r}_{M/L} - \bar{r}_{E/G_i}\right|$$

$$r_i' = \left|\bar{r}_i'\right| = \left|\bar{r}_{E/M} - \bar{r}_{E/G_i}\right| \qquad \text{(H-33)}$$

$$\cos \sigma_{E_i} = - \frac{\bar{r}_i' \cdot \bar{r}_{M/L}}{\left|\bar{r}_i'\right| \left|\bar{r}_{M/L}\right|} \; ; \quad 0 \le \sigma_{E_i} \le \pi \qquad \text{(H-31)}$$

and:

$$\cos \sigma_{E_i}^* = \frac{R_M}{\left|\bar{r}_i'\right|} \; ; \quad 0 \le \sigma_{E_i}^* \le \frac{\pi}{2} \qquad \text{(H-32)}$$

The tracker elevation angle, δ_i, is defined by the tracker local horizon and the tracker-LEM line-of-sight. Since direction $\hat{r}_{E/G_i}$ represents the local vertical of each ground tracker, it follows that:

$$\cos\left(\frac{\pi}{2} - \delta_i\right) = \sin \delta_i = \frac{\bar{r}_{E/G_i} \cdot \bar{r}_{G_i/L}}{\left|\bar{r}_{E/G_i}\right| \left|\bar{r}_{G_i/L}\right|} \qquad \text{(h-3)}$$

But from (H-33);

$$\sin \delta_i = \frac{\bar{r}_{E/G_i} \cdot (\bar{r}_{E/M} + \bar{r}_{M/L})}{\left|\bar{r}_{E/G_i}\right| \left|\bar{r}_{G_i/L}\right|} - \frac{\left|\bar{r}_{E/G_i}\right|}{\left|\bar{r}_{G_i/L}\right|} \qquad \text{(H-31)}$$

Associated with each ground tracker is a minumum elevation angle $\delta_{i_{limit}}$, below which communication is non-existant. The reason for this constraint is due to unacceptable noise levels whenever the radar dish is pointed near the horizon, and the existence of terrestrial obstructions such as mountains. Accordingly, $\delta_{i\,limit}$ would be a function of tracker azimuth angle. It is recommended, however, that a maximum value of $\delta_{i\,limit}$ be selected and used for all azimuth angles. This results in a gross simplification because there is no requirement to compute the azimuth angle or program the function $\delta_{i_{limit}}$ versus azimuth angle for each ground tracker.

For the lunar mission mode, the foregoing information is resolved into the following compact LEM-Earth visibility logic (see H-30):

i. Communication is not possible if the tracker elevation constraint is not satisfied ($\sin \delta_i < \sin \delta_{i\,limit}$) because either the station is on the back side of the Earth or an unacceptable noise level exists.

ii. Communication is not possible if the tracker elevation constraint is satisfied ($\sin \delta_i \leq \sin \delta_{i\,limit}$) but $R_i^* < R_M$ and $\sigma_{E_i} > \sigma_{E_i}^*$. This condition corresponds to the LEM located on the back side of the Moon.

iii. Communication may be possible whenever $\sin \delta_i \geq \sin \delta_{i\,limit}$ and $R_i^* \geq R_M$ or $R_i^* < R_M$ but $\sigma_{E_i} \leq \sigma_{E_i}^*$.

c. <u>S-Band Antenna Orientation - Lunar Phase</u>. Whenever the visibility requirements are satisfied, a final test must be made to determine whether or not the LEM can communicate with the Earth. This test demands that the S-band antenna be pointed in a desired direction and remain within allowable gimbal limits.

Ideally, the antenna should be pointed toward the Earth's center (lunar mission). This direction is:

$$\bar{r}_M = -(\bar{r}_{M/L} + \bar{r}_{E/M}) \qquad (H-43)$$

Resolving equations H-43 into body coordinates gives the direction required for S-band pointing:

$$\bar{r}_{B_M} = g_{ij_M}\ \bar{r}_M \qquad \text{(H-45)}$$

Figure 13 presents the S-band gimbal geometry. This geometry corresponds to the rendezvous radar gimbal geometry (Figure 8) discussed earlier. Thus, rendezvous radar equations f-3, f-4 and f-5 define the relationships between S-band coordinates and body coordinates provided E_{LS} and A_{LS} are replaced by θ_c and ϕ_c, respectively. The desired S-band gimbal angles, for communication, are therefore:

$$\tan\theta_c = \frac{X_{B_M}}{Z_{B_M}} \qquad \text{(H-40)}$$

$$\tan\phi_c = \frac{-Y_{B_M}}{X_{B_M}\sin\theta_c + Z_{B_M}\cos\theta_c} \qquad \text{(H-42)}$$

Angles θ_c and ϕ_c are inputted to the Communication Math Model and compared to the allowable S-band gimbal angles. If θ_c and ϕ_c lie within allowable limits, then communication is possible; otherwise, the LEM orientation must be altered before communication can commence.

d. <u>LEM-Ground Station Visibility - Earth Phase</u> - The only visibility requirement for Earth mission exercises is that the LEM lie within acceptable tracker elevation limits. On this basis:

$$\cos\left(\frac{\pi}{2} - \delta_i\right) = \sin\delta_i = \frac{\bar{r}_{E/G_i} \cdot \bar{r}_{G_i/L}}{|\bar{r}_{E/G_i}|\ |\bar{r}_{G_i/L}|} \qquad \text{(h-4)}$$

But:

$$\bar{r}_{G_i/L} = \bar{r}_{E/L} - \bar{r}_{E/G_i} \qquad \text{(h-5)}$$

Consequently:

$$\sin\delta_i = \frac{\bar{r}_{E/G_i} \cdot \bar{r}_{E/L}}{|\bar{r}_{E/G_i}|\ |\bar{r}_{G_i/L}|} - \frac{|\bar{r}_{E/G_i}|}{|\bar{r}_{G_i/L}|} \qquad \text{(H-35)}$$

Visibility is assured when $\sin \delta_i \geq \sin \delta_{i\,limit}$ (H-34).

e. Conical Log Antenna Orientations. Two conical log spiral-fixed antennas are used as an emergency backup for the S-band steerable antenna when in lunar orbit and for Earth communications when in Earth orbit. The signal-to-noise ratio is dependent on the angle ξ_i' measured between the antenna direction $\hat{\ell}_i'$ and the line-of-sight direction (see sketch).

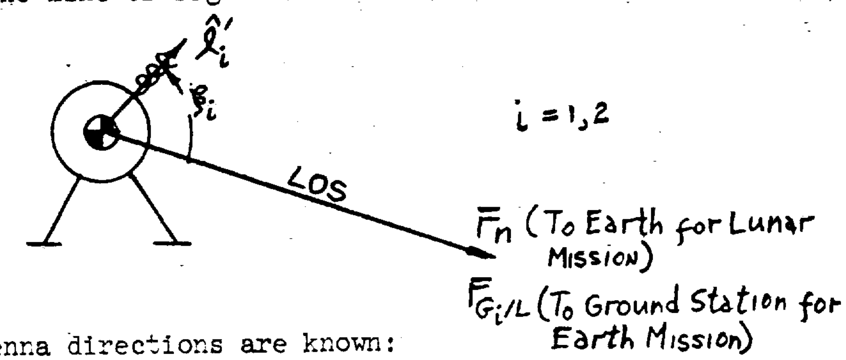

The body fixed antenna directions are known:

$$\hat{\ell}_i' = \ell_1' \hat{\imath}_B + \ell_2' \hat{\jmath}_B + \ell_3' \hat{K}_B \qquad \text{(H-51)}$$

$$i = 1,2$$

Resolving these directions into M or E-frame coordinates gives:

$$\hat{\ell}_{n_i}' = g_{ij_n}^T \hat{\ell}_i' \qquad \text{(H-52)}$$

If the spiral antennas are used for communication during an emergency situation while in lunar orbit, then the angle required to determine the signal-to-noise level is:

$$\cos \xi_i' = \frac{\bar{r}_M \cdot \hat{\ell}_i'}{|\bar{r}_M|} \qquad \text{(H-46)}$$

$$0 \leq \xi_i' \leq \pi$$

During all Earth Mission phases compute ξ_i' as follows:

$$\cos \xi_i' = \frac{\bar{r}_E \cdot \hat{\ell}_i'}{|\bar{r}_E|} \qquad \text{(H-47)}$$

$$0 \leq \xi_i' \leq \pi$$

where:

$$\bar{r}_E = \bar{r}_{E/G_i} - \bar{r}_{E/L} \qquad \text{(H-44)}$$

4. Conclusions.

a. Alter the rotation rate of the Earth to compensate for LEM-ground tracker phasing during independent LMS Earth mission modes. This increment in Earth rate corresponds to the CSM nodal regression rate.

b. Ground tracker elevation constraints are assumed constant rather than a function of tracker azimuth angles. The elevation constraint $\delta_{i_{limit}}$ may be conservatively or optimistically selected.

I. Weights and Balance.

1. Purpose. The purpose of Set I is to compute the instantaneous LEM mass, center of gravity, and moments and products of inertia. Subsidiary calculations are made to define reference distances measured from the vehicle CG to specific subsystem centroids.

2. LEM Mass. An attempt is made to simplify the mass breakdown of the LEM vehicle. Mass calculations, equation I-10, are characterized by constant and variable mass groups. Component mass contributions to each group follow.

a. Constant Masses. The total dry mass of the ascent (m_{I}) and descent (m_{II}) stages are invariant initial inputs. These constant masses do not include propellant mass but do include expendables ejected during the ascent or descent phases. During an actual mission, mass is continually expended in the form of vented material, gas leaks, waste management, etc. It is an unnecessary complication to generate the expendable mass profile as a time dependent function. Instead, it is assumed that all expendables are included as a rigid part of the ascent (m_{I}) or descent (m_{II}) stages.

In the event that the CSM propulsion system malfunctions, the LEM propulsion system will be required to initiate the trans-earth maneuver. Since the LEM and CSM must be attached during this emergency condition, the total system mass must reflect the CSM mass, m_c. Mass m_c represents a constant input whenever the vehicles are attached during independent LMS mission modes. Mass m_c, together with component distances α_c, β_c and γ_c, measured from the CSM-CG to the weights and balance reference axes, will be supplied by the AMS during integrated operations.

b. Variable Masses. Variable masses include all propellants only. Main engine ascent (m_{Aj}) and descent (m_{Dj}) fuel and oxidizer masses are supplied by the Main Engine Math Model (I-12). RCS system a and b propellants are computed by the RCS Math Model and inserted as inputs to interface equations (I-11).

3. Instantaneous Center-of-Gravity. The LEM-CG is found by summing the product of all component masses and their local reference arms measured from the 0, 0, 0 origin of the design reference system (I-20). Note that most reference arms are constant inputs that remain invariant during any run. These include the arms corresponding to the dry masses (v_I, v_{II}; $v \rightarrow \alpha, \beta, \gamma$), the RCS propellants ($v_{Rj}$), the ascent propellants (v_{Aj}) and the β_{Dj} and γ_{Dj} components of the descent propellants. Component distances α_{Dj} are computed variables that reflect the combined mass centers of the rigid propellant CG's and the slosh propellant CG's. The slosh proplellant CG is defined by the slosh model pendulum support hinge.

Slosh forces are zero whenever the main engine is inoperative. For this condition the propellants move to the tank periphery and moment arm $\Delta\alpha_{Dj}$ goes to zero (see equation A-48 and Figure 4).

4. Moments and Products of Inertia. Moments and products of inertia may be computed by a direct or indirect method. Direct computations require that each component mass first be located relative to the total vehicle CG ($\overline{v} = v + v_{CG}$) and then transferred to the instantaneous LEM-CG. Component reference distances, $\overline{v}$, are time dependent, since the vehicle CG varies as mass is expended. Thus, the squares and products of each reference distance must be continually computed. These calculations impose large storage requirements on the computer.

Indirect calculations are based on defining moments and products of inertia with respect to the invariant design reference origin and subsequently transferring these inertias to the instantaneous CG. Indirect, rather than direct, calculations are preferred since reference distances, v, required to specify the inertias with respect to the reference origin (I-41, 51), are constant except for v_{Dj}. Even when the transfer terms are included (I-40, 50), the computations required to program the indirect method are less than those required to program the direct method.

Ascent and descent propellants are treated as mass points in all inertia computations. The reason for this assumption follows (reference 36). Fuel-oxidizer slosh forces are considered as a perturbation to the rigid body equations of motion. In the absence of viscosity, these first order fluid pressure forces are directed radially outward from each tank. Hence, there can be no moment induced by the fluid about the effective tank centroid. With regard to the spherical ascent tank, the effective centroid coincides with the geometric center. Small motions exist between the effective, cylindrical descent tank centroid and the geometric centroid (references 6 and 7). On these bases, effective propellant inertias are computed by assuming that all the propellant mass is concentrated at the effective tank centroid which represents the support hinge of the mechanical pendulum analog (see Section III-A-4). Experimental data (reference 36) have indicated that "this approach of calculating rigid body inertias should give substantially more realistic results than would be obtained by assuming that the propellant in each tank frozen and concentrating this frozen mass at its center of gravity."

5. Conclusions.

a. The AMS will supply all CSM weights and balance parameters to the LMS during integrated operations whenever the LEM and CSM are physically attached.

b. Moments and products of inertia will be computed relative to the origin of the fixed weights and balance reference system and subsequently transferred to the vehicle CG.

c. Fuel and oxidizer inertias will be computed based on mass point considerations. The mass point is located at the geometric centroid of the ascent tank and at the composite centroid defined by the slosh and rigid masses for each descent tank.

d. Expendables are included as a rigid mass contribution to m_I and m_{II}.

J. Visual Display Drive Equations.

1. Purpose. The purpose of Set J is to generate drive signals for the External Visual Display Equipment (EVDE). This equipment provides real world visual cues to the astronauts during all lunar and Earth mission modes. Realistic motion may be perceived through each of three windows or three telescope positions.

Optical simulations are generated by four primary hardware subsystems. Briefly, the star field is generated by a Celestial Sphere subsystem. Stars can be occulted by the Moon, or the Earth, or Sun. A Mission Effects Projector (MEP) enables the astronauts to view the lunar or Earth terrain during orbital operations. Detailed landing site viewing is provided by the Landing and Ascent Image Generator. CSM visual sightings are generated by a Rendezvous and Docking Image Generator.

No attempt is made to define the mechanical-optical details of each hardware item since these details are available in numerous Farrand documents. An EVDE hardware summary report is given in reference 37. Equivalent drive signals required to activate each hardware item are derived below.

2. Celestial Sphere.

a. Gimbal Drives. Four Celestial Spheres, one for each window and one for all telescopes, are used to present an infinity star display to the astronauts. Each Celestial Sphere contains 997 stars referenced to the mean ecliptic of 1950, of which 54 stars are used for navigation. Star motion is simulated by positioning the Celestial Sphere relative to the astronauts, or more appropriately, relative to the body-fixed optical axes (Figure 7).

Presented in Figure 14a is a schematic of the Celestial Sphere gimbal assembly. Motion about the outer (a_{pq})† and middle (b_{pq}) gimbal axes are

† Footnote on next page

shown. Inner gimbal motion is mechanized by rotating the Northern and Southern hemispheres relative to a split ring which represents the ecliptic plane. Arbitrary orientations of the star field can, therefore, be achieved by independent gimbal angle inputs a_{pq}, b_{pq} and c_{pq}. For example, let the Celestial Sphere gimbal axes be initially aligned to the window axes Z_{pq}, Y_{pq}, X_{pq}. Rotate through angle a_{pq} about the optical line-of-sight axis Z_{pq}. Follow this by a rotation b_{pq} about the new X'_{pq} axis so formed. Finally, follow this by a rotation c_{pq} about the north ecliptic pole to generate the general transformation between the Celestial Sphere axes and the optical axes (see Figure 14b):

$$\begin{bmatrix} x_{\epsilon pq} \\ y_{\epsilon pq} \\ z_{\epsilon pq} \end{bmatrix} = \begin{bmatrix} \cos a_{pq} \sin c_{pq} + \sin a_{pq} \sin b_{pq} \cos c_{pq} & \sin a_{pq} \sin c_{pq} - \cos a_{pq} \sin b_{pq} \cos c_{pq} & \cos b_{pq} \cos c_{pq} \\ \cos a_{pq} \cos c_{pq} - \sin a_{pq} \sin b_{pq} \sin c_{pq} & \sin a_{pq} \cos c_{pq} + \cos a_{pq} \sin b_{pq} \sin c_{pq} & -\cos b_{pq} \sin c_{pq} \\ -\sin a_{pq} \cos b_{pq} & \cos a_{pq} \cos b_{pq} & \sin b_{pq} \end{bmatrix} \begin{bmatrix} X_{pq} \\ Y_{pq} \\ Z_{pq} \end{bmatrix} \qquad \text{(j-1)}$$

or:

$$\bar{r}_{\epsilon pq} = A_{ij\,pq} \bar{r}_{pq}$$

Effectively, equations (j-1) represent the mechanical transformation between optical and ecliptic axes. This transformation can also be gen-

---

* As mentioned earlier, generalized subscript p refers to window (W) or telescope (T) viewing, while q denotes the viewing mode, either left (l), right (r) or above (a).

erated from computed trajectory data. Recall that equations (D-80) relate the optical axes to the M or E-frame. A single rotation about the equinox $\hat{X}_n$, through the obliquity of the ecliptic, ϵ, is sufficient to reference the optical axes to the ecliptic axes. Thus:

$$\bar{r}_{\epsilon_{pq}} = n_{ij_{pq}} \bar{r}_{pq} \qquad (j\text{-}2)$$

where:

$$n_{ij_{pq}} = \begin{pmatrix} 1 & 0 & 0 \\ 0 & \cos\epsilon & \sin\epsilon \\ 0 & -\sin\epsilon & \cos\epsilon \end{pmatrix} \ell_{ij_{pq}} \qquad (J\text{-}12)$$

But, equation (j-2) is identical to equation (j-1). Hence:

$$A_{ij_{pq}} = n_{ij_{pq}} \qquad (j\text{-}3)$$

Solving for the unknown gimbal angle drive inputs a_{pq}, b_{pq} and c_{pq} in terms of known elements $n_{ij_{pq}}$, gives the required drive inputs shown by equation (J-10).

Equation (J-10) exhibits a singularity when the middle gimbal angle b_{pq} approaches $\pm \frac{\pi}{2}$. This condition is circumvented by the introduction of gimbal lock logic (J-11). Logic (J-11) was derived based on the considerations given in Section III-D-4e.

b. Lunar or Earth Occulters. Mechanical provisions are included to obstruct the star field whenever the Moon or Earth appears in the windows or telescopes during Lunar or Earth Mission modes, respectively. In order to occult the stars, it is required to locate the Moon or Earth relative to the optical axes. This is readily accomplished since the position vector of the central body ($\bar{r}_{B/L}$, G-42) in LEM body coordinates is known. Thus:

$$\bar{r}^{\,n}_{pq} = -h_{ij_{pq}} \bar{r}_{B/L} \qquad (J\text{-}20)$$

Superscript n denotes either the Moon (M) or Earth (E). The negative sign is needed to direct the vector from the body axes origin to the M or E-frame origin.

A disc of varying diameter is used to occult the star field. As shown in Figure 15, the disc moves in a plane normal to the line-of-sight optical axis and has coordinates given by:

$$\rho_{pq} = \frac{d_{pq}}{Z^n_{pq}} \left[(X^n_{pq})^2 + (Y^n_{pq})^2 \right]^{\frac{1}{2}} \qquad \text{(J-23)}$$
$$\tan \theta_{pq} = \frac{Y^n_{pq}}{X^n_{pq}}$$

Parameter d_{pq} represents the scale distance measured from the optical axis origin to the plane of the occulting disc.

The field of view measured in the plane of the disc can be approximated by a circle of maximum radius $\rho_{pq_{max}}$. Whenever ρ_{pq} is greater than this distance, the central body cannot be seen. To ensure, however, that the central body re-enters the window at the correct position, it is proposed that angle θ_{pq} continually be computed. Accordingly, when $\rho_{pq} < \rho_{pq_{max}}$, the disc appears as it should provided the central body is not behind the line-of-sight. To provide for these contingencies, the following logic is introduced (J-24):

i. If $Z^n_{pq} < 0$, then do not compute ρ_{pq}. Instead, let $\rho_{pq} = \rho_{pq_{max}}$.

ii. If $Z^n_{pq} \geq 0$ and if $\rho_{pq} \geq \rho_{pq_{max}}$, then do not compute ρ_{pq}. Instead let $\rho_{pq} = \rho_{pq_{max}}$.

iii. For all other combinations, compute ρ_{pq}. Also, always compute θ_{pq}.

The occulting discs for the upper window and telescope viewing modes are driven by a mechanical device that requires cartesian rather than polar coordinate inputs, thus drive coordinates are specified by:

$$x_{pq} = \rho_{pq} \cos\theta_{pq}$$
$$y_{pq} = \rho_{pq} \sin\theta_{pq} \qquad \text{(J-22)}$$

Occulting logic described above also pertains to equation (J-22).

As the vehicle approaches the central body, the body's apparent diameter increases. This effect is simulated by representing the disc as a variable wrap-up reel containing mylar tape. The disc diameter and rate of wrap-up is proportional to the central angle μ^* (μ max., Figure 10) subtended by the LEM. Hence:

$$\sin\mu^* = \frac{R_n}{r_{n/L}} \quad ; \; 0 \le \mu^* \le \frac{\pi}{2}$$
$$\dot{\mu}^* = -\frac{\dot{r}_{n/L}}{r_{n/L}} \tan\mu^* \qquad \text{(J-21)}$$

A configuration can exist when the LEM is behind the Earth or Moon, wherein both central bodies occult the star field. During lunar mission operations, Earth occultation will be synthesized by physically pasting a configuration of the Earth on the Celestial Sphere. The Earth's position in the star field will be based on the Earth's right ascension and declination relative to the M-frame at problem start. Earth parallax will be given by the mean Earth-Moon distance. Similarly, during Earth training exercises, the Moon is fixed to the Celestial Sphere based on its right ascension and declination relative to the E-frame. Obviously, motion of a pasted Moon or Earth across the star field cannot be simulated. However, this should have no influence on LEM-astronaut training.

c. <u>Solar Occulter</u>. As the Sun enters the field of view, the CRT light intensity is increased. This has the effect of washing-out the star field. The control parameter of interest is angle $\gamma^{\odot}_{pq}$ measured from the optical line-of-sight to the Sun's vector direction. Angle $\gamma_{pq}^{\odot}$ is computed as follows: Define the Sun's position in the optical axes system:

$$\bar{r}_{pq}^{\odot} = l_{ij_{pq_n}} \bar{r}_{n/\odot} \qquad \text{(J-30)}$$

Vector $\bar{r}_{n/\odot}$ denotes the Sun's position relative to the E or M-frame. Vector $\bar{r}_{E/\odot}$ is generated by the Ephemeris (E-30), whereas $\bar{r}_{M/\odot}$ is:

$$\bar{r}_{M/\odot} = \bar{r}_{E/\odot} - \bar{r}_{E/M} \qquad \text{(J-31)}$$

The angle subtended by the Sun is:

$$\cos \gamma_{pq}^{\odot} = \frac{\bar{r}_{pq}^{\odot} \cdot \hat{K}_{pq}}{|\bar{r}_{n/\odot}|} = \frac{z_{pq}^{\odot}}{r_{n/\odot}}$$
$$0 \leq \gamma_{pq}^{\odot} \leq \pi \qquad \text{(J-32)}$$

Normal lighting conditions exist whenever the Sun is outside of the field of view ($\gamma_{pq}^{\odot} > \gamma_{pq_{max}}^{\odot}$) whereas, maximum lighting conditions exist when the Sun is within the field of view (see logic J-33).

3. Mission Effects Projector.

a. Location of LEM with Respect to Film Strip Reference. The MEP provides continual lunar or geographic terrain displays to the astronauts at altitudes above approximately 1200 feet. Pre-selected terrain swaths are recorded on film strips and displayed by a T.V. image generator. Each film strip is scaled for five altitude ranges. As the altitude ($h_{M/L}$; G-30) diminishes or increases beyond prescribed limits, the film strip views are dissolved into the next.

The film strip is positioned with respect to the projection apparatus, based on the location of the vehicle's subsatellite point relative to the film strip centerline (see Figure 16). It is assumed that all film strips represent great circle swaths around the central body. If the nominal training mission orbits are equatorial, then the film centerline will correspond to the nominal orbit trace projected on the central body. For this case, film strip drive coordinates are given by the vehicle's selenographic longitude and latitude (G-12) or geographic longitude and latitude.

If, however, the nominal orbits are inclined to the equator, then the projected orbit trace will not correspond to the film strip centerline. This results because the orbit trace on a rotating central body cannot be represented by a great circle path. For this case, the subsatellite point may be located by angles θ_f and δ_f. This point must fall within the confines of the film strip. Note that (Figure 16):

i. θ_f is measured from the film strip ascending node, along the film strip centerline to the projection of the LEM radius vector onto the film strip plane. For an equatorial orbit θ_f would be measured from the X_S or X_G axis and correspond exactly to $\lambda_{S/L}$ or $\lambda_{G/L}$.

ii. δ_f represents the declination relative to the film strip ℄ plane and is measured positive northward. Whenever equatorial orbits are considered, δ_f reduces to latitude.

Angles θ_f and δ_f, for the general case, are ascertained below.

Let any desired terrain swath (film strip) be specified by a right ascension of the ascending node (Ω_f) and an inclination (i_f). Film strip axes X_f, Y_f and Z_f are related to the reference central body axes as follows:

$$\begin{bmatrix} \hat{i}_f \\ \hat{j}_f \\ \hat{k}_f \end{bmatrix} = \begin{bmatrix} \cos\Omega_f & \sin\Omega_f & 0 \\ -\sin\Omega_f \cos i_f & \cos i_f \cos\Omega_f & \sin i_f \\ \sin\Omega_f \sin i_f & -\sin i_f \cos\Omega_f & \cos i_f \end{bmatrix} \begin{bmatrix} \hat{i}_Q \\ \hat{j}_Q \\ \hat{k}_Q \end{bmatrix}$$

$$Q = S \text{ or } G \qquad \text{(j-4)}$$

Equatorial direct orbits are specified by $\Omega_f = i_f = 0$, while equatorial retrograde orbits (LEM) are specified by $\Omega_f = 0$, $i_f = \pi$. This means that $\hat{r}_f = \hat{r}_Q$.

The LEM radius vector in terms of selenographic (lunar mission) and geographic (Earth mission) coordinates is required. The former is known (A-22); the latter is computed as follows:

$$\begin{bmatrix} X_G \\ Y_G \\ Z_G \end{bmatrix} = \begin{bmatrix} \cos GHA & \sin GHA & 0 \\ -\sin GHA & \cos GHA & 0 \\ 0 & 0 & 1 \end{bmatrix} \begin{bmatrix} X_{E/L} \\ Y_{E/L} \\ Z_{E/L} \end{bmatrix} \qquad \text{(J-49)}$$

It was recommended earlier that relative motion equations, based on two-body CSM motion, be used to compute $\bar{r}_{E/L}$ during independent LMS Earth mission modes. Consequently, nodal regression due to the Earth's oblateness is not accounted for whenever this mode is activated. Accordingly, after a complete circuit around the Earth, the astronaut would view a geographic scene that corresponds to the change in the Earth's angular position only. The real world scene would correspond to a view from a slightly different spatial position due to the orbit plane regression relative to inertial space. This "true scene" can be synthesized (first order only) by altering the Earth's true rotation rate. For example, replace GHA in (J-49 or D-60) by GHA$-\dot{\Omega} t$, where $\dot{\Omega}$ is given by equation (H-22).

Drive angle θ_f depends on the projection of $\bar{r}_{Q/L}$ onto the film strip reference plane. Call this projection $\hat{P}$, where:

$$\hat{P} = \frac{\hat{K}_f \times [\bar{r}_{Q/L} \times \hat{K}_f]}{r_{n/L} \sin \delta_f} \qquad \text{(J-5)}$$

Now:

$$\tan \theta_f = \frac{\cos(\frac{\pi}{2} - \theta_f)}{\cos \theta_f} = \frac{\hat{P} \cdot \hat{J}_f}{\hat{P} \cdot \hat{I}_f} \qquad \text{(J-40)}$$

and:

$$\sin \delta_f = \cos\left(\frac{\pi}{2} - \delta_f\right) = \hat{P} \cdot \hat{K}_f \qquad \text{(J-40)}$$

$$-\frac{\pi}{2} \leq \delta_f \leq \frac{\pi}{2}$$

Equations (J-40) reduce to longitude and latitude whenever equatorial orbits are considered.

b. Angular Drive For MEP Optics. Film strip terrain information is transmitted to a TV vidicon camera through a series of mirrors, lenses and prisms (reference 37). The optical equipment is positioned by three angular drive signals, ψ^*_{pq}, σ^*_{pq} and ϕ^*_{pq}. Physically, these angles relate the optical axes system to a local terrain coordinate system (X_T, Y_T, Z_T), where, as shown in Figure 16:

i. $\hat{i}_T$ is directed along the local radius vector.

ii. $\hat{j}_T$ lies in the local horizon plane and is parallel to the plane formed by the strip centerline.

iii. $\hat{k}_T = \hat{i}_T \times \hat{j}_T$.

Let all MEP drive angles be zero. For this condition the relation between the optical axes $\hat{r}_{pq}$ and the terrain axes $\hat{r}_T$ is:

$$\hat{X}_{pq} = \hat{Z}_T$$

$$\hat{Y}_{pq} = \hat{Y}_T$$

$$\hat{Z}_{pq} = -\hat{X}_T$$

To obtain any arbitrary orientation between $\hat{r}_{pq}$ and $\hat{r}_T$ rotate first about $-\hat{X}_T$ through the azimuth angle ψ^*_{pq}. Note that ψ^*_{pq} is always measured in the LEM local horizon plane. Next, rotate about the new $\hat{Y}'_T$ axis so formed through an elevation angle σ^*_{pq}. Angles ψ^*_{pq} and σ^*_{pq} position the optical line-of-sight axis to the landmark being sighted. Last, rotate about the optical line-of-sight through roll angle ϕ^*_{pq}. The correspondence between $\hat{r}_{pq}$ and $\hat{r}_T$ is:

$$\begin{bmatrix} X_{Pg} \\ Y_{Pg} \\ Z_{Pg} \end{bmatrix} = \begin{bmatrix} \cos\phi^*_{Pg}\sin\sigma^*_{Pg} & \sin\phi^*_{Pg}\cos\psi^*_{Pg} + \cos\phi^*_{Pg}\cos\sigma^*_{Pg}\sin\psi^*_{Pg} & \cos\phi^*_{Pg}\cos\sigma^*_{Pg}\cos\psi^*_{Pg} - \sin\phi^*_{Pg}\sin\psi^*_{Pg} \\ -\sin\phi^*_{Pg}\sin\sigma^*_{Pg} & \cos\phi^*_{Pg}\cos\psi^*_{Pg} - \sin\phi^*_{Pg}\cos\sigma^*_{Pg}\sin\psi^*_{Pg} & -\sin\phi^*_{Pg}\cos\sigma^*_{Pg}\cos\psi^*_{Pg} - \cos\phi^*_{Pg}\sin\psi^*_{Pg} \\ -\cos\sigma^*_{Pg} & \sin\sigma^*_{Pg}\sin\psi^*_{Pg} & \sin\sigma^*_{Pg}\cos\psi^*_{Pg} \end{bmatrix} \begin{bmatrix} X_T \\ Y_T \\ Z_T \end{bmatrix}$$

or:

$$\hat{r}_{Pg} = M(\psi^*_{Pg}, \sigma^*_{Pg}, \phi^*_{Pg})\,\hat{r}_T \qquad \text{(j-6)}$$

The matrix elements given by (j-6) are known from previously generated data. For example, the optical axes orientation relative to the selenographic (lunar mission) or geographic (Earth mission) coordinate system is specified by:

$$\hat{r}_{Pg} = \ell^T_{ij_{Pg}}\ a^T_{jK}\ \hat{r}_S \qquad \text{(lunar)}$$

$$\text{(j-7)}$$

$$\hat{r}_{Pg} = \ell^T_{ij_{Pg}}\ f^T_{JK}\ \hat{r}_G \qquad \text{(terrestrial)}$$

From (j-4), the constant relation between $\hat{r}_Q$ and the film strip axes system is:

$$\hat{r}_f = M(\Omega_f, i_f)\,\hat{r}_Q \qquad \text{(j-4)}$$

Finally, equations (J-40) provide the link between $\hat{r}_T$ and $\hat{r}_f$:

$$\begin{bmatrix} X_T \\ Y_T \\ Z_T \end{bmatrix} = \begin{bmatrix} \cos\theta_f\cos\delta_f & \cos\delta_f\sin\theta_f & \sin\delta_f \\ -\sin\theta_f & \cos\theta_f & 0 \\ -\sin\delta_f\cos\theta_f & -\sin\delta_f\sin\theta_f & \cos\delta_f \end{bmatrix} \begin{bmatrix} X_f \\ Y_f \\ Z_f \end{bmatrix} \qquad \text{(j-8)}$$

or:
$$\hat{r}_T = M(\theta_f, \delta_f)\, \hat{r}_f \qquad (j\text{-}8)$$

Combining equations j-7, j-4, and j-8 gives the desired transformation:

$$\hat{r}_{pq} = \ell_{ij}^T\, a_{jK}'^T\, M_{K\ell}^T(\Omega_f, i_f)\, M_{\ell m}^T(\theta_f, \delta_f)\, \hat{r}_T \qquad (J\text{-}43)$$

or equivalently:

$$\hat{r}_{pq} = \left[M_{m\ell}(\theta_f, \delta_f)\, M_{\ell K}(\Omega_f, i_f)\, a_{Kj}'\, \ell_{ji}\right]^T \hat{r}_T \qquad (J\text{-}43)$$

Whereupon:

$$\hat{r}_{pq} = V_{ij}\, \hat{r}_T \qquad (J\text{-}43)$$

Angles ψ^*_{pq}, σ^*_{pq} and ϕ^*_{pq} can now be found by comparing elements of V_{ij} and $M(\psi^*_{pq}, \sigma^*_{pq}, \phi^*_{pq})$. The solution is similar to the Celestial Sphere drives and is given by equations (J-41).

Equations (J-42) present gimbal lock logic. This logic ensures a true view of the Earth or Moon limb whenever the astronaut sights along the local horizon ($\sigma_{pq} = \frac{\pi}{2}$).

4. Landing and Ascent Image Generator (L/A).

a. Drive Coordinates Y_{LM} and Z_{LM}. A three dimensional lunar surface model is used to simulate the lunar terrain. Each intended landing site is referenced by a known selenographic latitude (ϕ_{LM}) and longitude (λ_{LM}) which forms the origin of a topocentric, two dimensional coordinate frame $\hat{j}_{LM}$, $\hat{k}_{LM}$ (see Figure 17). This coordinate frame corresponds exactly to the Land Mass coordinate frame described earlier (Section III-G-4). Moreover, the drive coordinates required to position the L/A optical head relative to the lunar surface origin are identical to the drive coordinates required to relate the Land Mass optical head to the Land Mass origin. Accordingly, Land Mass drive coordinates Y_{LM} and Z_{LM} (equations G-50 or g-8) are also used to drive the lunar surface table model.

b. Angular Drives for L/A Optics. The MEP optical head is identical to the L/A optical head. Hence, angles ψ^*_{Wq}, σ^*_{Wq} and ϕ^*_{Wq} serve a dual purpose.

A single (L/A) optical head is used to present the landing site image in either the left window (q = l) or the right window (q = r). Switching between windows will depend on either the astronaut's or instructor's discretion.

c. Altitude Drive For L/A Optical Head. An altitude signal must be generated to drive a focusing circuit included in the optical head. It is intended to measure the altitude from the design eye to the lunar surface. A first order parallax correction ($\theta \simeq 0^o$) is given by:

$$h_{DE} = h_{M/L} + (\alpha_{DE} - \alpha_{CG}) \qquad (J\text{-}9)$$

Altitude $h_{M/L}$ is generated (G-30) by differencing two large numbers of equal magnitude ($\approx 6 \times 10^6$ feet). Thus, the least significant bit that can be computed is about .7 feet. Equation (J-9) therefore exhibits the same erratic motion as the Land Mass drive coordinates Y_{LM} and Z_{LM} (Subsection III-G-46). Altitude motion can be smoothed by initializing $h_{M/L}$ when the Landing and Ascent Image Generator become active $\left[h_{DE_0} = h_{M/L_0} + (\alpha_{DE} - \alpha_{CG})\right]$, and then integrating altitude rate to define h_{DE}:

$$h_{DE} = h_{DE_0} + \int \dot{h}_{M/L}\, dt \qquad (J\text{-}53)$$

5. Rendezvous and Docking Simulator.

a. General. Rendezvous and docking simulation displays depend on the distance between vehicles. Whenever the LEM-CSM range exceeds 14,000 feet, CSM motion is depicted by a blinking light whose intensity varies with distance. Between 14,000 and 8,000 feet, the CSM is represented by an illuminated model. During these phases, the rendezvous table carriage (see Figure 18) remains parked at a maximum distance from the $\frac{1}{80}$-scale CSM model. From 8,000 feet to 530 feet, the table carriage is activated. CSM rotational motion is simulated by a two gimbal, $\frac{1}{80}$ scale model. As the relative distance closes to 530 feet, a three gimbal $\frac{1}{20}$ CSM docking model is employed. Switching occurs by the removal of a dissolve mirror and reversing the carriage motion.

Drive signals must be generated to:

i. Position the CSM in the LEM window.

ii. Define the relative orientation of the CSM as seen by the astronauts.

iii. Provide the correct CSM solar illumination during all mission phases.

Each item is discussed below.

b. Reference Table Coordinates. In order to synthesize true vehicle motions, it is mandatory to establish a rendezvous table reference coordinate system. Let this coordinate system be defined by unit directions $\hat{\rho}_1, \hat{\rho}_2, \hat{\rho}_3$ (Figure 18). Let $\hat{\rho}_1$ be normal to the relative distance table and direct $\hat{\rho}_3$ parallel to the carriage motion toward the $\frac{1}{20}$ CSM scale model. Optical compensation ensures that $\hat{\rho}_3$ is properly directed when the $\frac{1}{20}$ scale model becomes active. Neglecting parallax, the true line-of-sight vector $\bar{\rho}_B$ is always directed along $\hat{\rho}_3$. The basic problem is to define the true vehicle motion in table-top coodinates.

c. Optical Head Drives for Left and Right Window Viewing. An optical head is fixed to the movable carriage. This head represents the LEM vehicle and is used to position the CSM in the LEM windows. The optical head consists of a post and trunnion and has two degrees of angular freedom relative to the non-rotating table-top axes. Fixed to the horizontal trunnion are two cameras positioned on either side of the post. These cameras have the same orientation with respect to the post and trunnion as the LEM window axes have with respect to the body axes. Thus, correspondence between the camera axes and the actual LEM vehicle axes, with respect to the relative range vector $\bar{\rho}_B$, is achieved by a rotation about the post ($\hat{\rho}_1$) through angle ϕ_{LS}, followed by a rotation about the new trunnion axis through θ_{LS}. The relation between the LEM body axes and the table axes is therefore:

$$\begin{bmatrix} \rho_{X_B} \\ \rho_{Y_B} \\ \rho_{Z_B} \end{bmatrix} = \begin{bmatrix} \cos\theta_{LS} & \sin\theta_{LS}\sin\phi_{LS} & -\sin\theta_{LS}\cos\phi_{LS} \\ 0 & \cos\phi_{LS} & \sin\phi_{LS} \\ \sin\theta_{LS} & -\cos\theta_{LS}\sin\phi_{LS} & \cos\theta_{LS}\cos\phi_{LS} \end{bmatrix} \begin{bmatrix} \rho_1 \\ \rho_2 \\ \rho_3 \end{bmatrix}$$

or:

$$\bar{\rho}_B = q_{ij}\ \hat{\rho}_{TABLE} \qquad \text{(J-63)}$$

Vector $\bar{\rho}_B$, given by subset equation (F-23), defines the distance measured from LEM CG to CSM CG. Optical parallax corrections may become important as the relative distance diminishes. For this reason, vector $\bar{\rho}_B$ is redefined. Let $\bar{\rho}_B'$ be measured from the camera origin (Figure 18) to the CSM pivot point which is assumed to correspond to a nominal CSM CG. Hence:

$$\bar{\rho}_B' = \bar{\rho}_B - \bar{\rho}_{DE} \quad ; \quad \rho_{LS}' = |\bar{\rho}_B'| \qquad \text{(J-64a)}$$

Drive angles ϕ_{LS} and θ_{LS} are derived from expression (J-63) as follows. First, replace $\bar{\rho}_B$ by $\bar{\rho}_B'$. Since the line-of-sight vector $\bar{\rho}_B'$ must lie along $\hat{\rho}_3$, the components of $\bar{\rho}_B'$ measured in table axes are $\rho_1 = 0$, $\rho_2 = 0$, $\rho_3 = \rho_{LS}'$. Equations (J-63) can therefore be written as:

$$\begin{aligned} \rho_{X_B}' &= -\rho_{LS}'\cos\phi_{LS}\sin\theta_{LS} \\ \rho_{Y_B}' &= \rho_{LS}'\sin\phi_{LS} \\ \rho_{Z_B}' &= \rho_{LS}'\cos\phi_{LS}\cos\theta_{LS} \end{aligned} \qquad \text{(J-10)}$$

Equations (j-10) are manipulated to give:

$$\tan\theta_{LS} = \frac{-\rho'_{X_B}}{\rho'_{Z_B}}$$

$$\tan\phi_{LS} = \frac{\rho'_{Y_B}}{\rho'_{Z_B}\cos\theta_{LS} - \rho'_{X_B}\sin\theta_{LS}} \qquad \text{(J-64)}$$

d. Optical Head Drives for Telescope and Overhead Window Viewing. The Rendezvous and Docking simulator is designed such that the trunnion-fixed right camera generates a CSM image whenever the telescope modes are activated. Similarly, the trunnion-fixed left camera is employed to simulate CSM motion in the overhead window.

Consider telescope viewing. Recall that the right camera is fixed to the optical head or equivalently, the LEM body axes. The problem, therefore, is to define a new body axes (and associated optical head drive angles $\theta_{LS_{Tq}}$ and $\phi_{LS_{Tq}}$) that has the same orientation with respect to the telescope axes as the original body axes has to the right window axes. This is accomplished by rotating about the telescope Y_{Tq} axes through θ'_{Wr}, followed by a rotation ϕ'_{Wr} about the new X'_{Tq} axis, followed by a raster rotation ψ_{Wr} about the new Z''_{Tq} axis. The correspondence between the new body axes and the telescope axes reduces to:

$$\bar{\rho}_{B_{Tq}} = h'_{ij\,wr}\ \bar{r}_{Tq} \qquad \text{(J-72)}$$

If rotations θ'_{Wr}, ϕ'_{Wr} and ψ'_{Wr} were equal to $-\theta_{Wr}$, $-\phi_{Wr}$ and zero, respectively, then frame $\bar{\rho}_{B_{Tq}}$ would bear the same relation to $\bar{r}_{Tq}$ as $\bar{r}_B$ has to $\bar{r}_{Wr}$. Hardware constraints, however, require that the optical axes relative to the CRT be shifted by angles $\theta\epsilon_{Tq}$ and $\phi\epsilon_{Tq}$ when viewing is switched from the right window to the telescope mode. Furthermore, during the switch from window to telescope viewing, a raster rotation or change in scanning is necessary in order that the vidicon cover the complete field of view. These items are compensated for geometrically by defining the elements of $h'_{ij_{Wr}}$ as:

$$\begin{aligned} \phi'_{Wr} &= \phi_{\epsilon_{T\gamma}} - \phi_{Wr} \\ \theta'_{Wr} &= \theta_{\epsilon_{T\gamma}} - \theta_{Wr} \\ \psi'_{Wr} &= \psi_{RAS_{T\gamma}} \end{aligned} \qquad (J\text{-}74)$$

Relative distance components measured in the new body axes must be found. This is accomplished by eliminating $\bar{r}_{Tq}$ in (J-72). As shown previously:

$$\bar{r}_{T\gamma} = h_{ij_{T\gamma}} \bar{\rho}'_B \qquad (D\text{-}70)$$

Hence:

$$\bar{\rho}_{B_{T\gamma}} = h'_{ij_{Wr}} h_{jk_{T\gamma}} \bar{\rho}'_B \qquad (J\text{-}70a)$$

The relative distance vector $\bar{\rho}_{B_{T\gamma}}$ must lie along $\hat{\rho}_3$. Accordingly, optical head drive angles for telescope viewing are derived based on the same reasoning described in Subsection 5c above. The results are:

$$\tan\theta_{LS_{T\gamma}} = \frac{-\rho_{X_{T\gamma}}}{\rho_{Z_{T\gamma}}} \qquad (J\text{-}71a)$$

$$\tan\phi_{LS_{T\gamma}} = \frac{\rho_{Y_{T\gamma}}}{\rho_{Z_{T\gamma}}\cos\theta_{LS_{T\gamma}} - \rho_{X_{T\gamma}}\sin\theta_{LS_{T\gamma}}}$$

Optical head drive angles for overhead window viewing are derived in a similar manner as above. Exceptions are that the right window subscript is replaced by the left window subscript and the telescope axes are replaced by the overhead window axes.

e. <u>Camera Switch Logic</u>. Two cameras are used for three telescopes, two front windows and overhead window viewing modes. Combination of simultaneous telescope, front viewing or overhead window CSM viewing is impossible. No drawback results with regard to telescope viewing since the telescope and window view cones do not intersect. In addition, when the relative distance is less than 530 feet, the telescopes are inoperative; consequently, the CSM cannot overlap the telescope and front window view cones. During docking the CSM can be seen in the overhead and front windows simultaneously. This configuration, however, cannot be simulated.

As the CSM enters a particular view cone, it is proposed to automatically compute the corresponding post and trunnion drive angles. To determine whether the CSM can be seen, approximate the field of view about each optical axis line-of-sight by a cone angle Λ^{*}_{pq}. If the CSM-CG is within this cone angle, then the appropriate post and trunnion drives are activated.

The optical line-of-sight is $\hat{Z}_{pq}$. The CSM position referenced to the design eye is $\bar{\rho}'_B$. Accordingly, the cone angle made by $\hat{Z}_{pq}$ and $\bar{\rho}'_B$ is:

$$\cos\Lambda_{pq} = \frac{\bar{\rho}'_B \cdot \hat{Z}_{pq}}{\rho'_{LS}} \qquad (J\text{-}75)$$

$$0 \leq \Lambda_{pq} \leq \pi$$

Angle Λ_{pq} is compared to allowable angle Λ^{*}_{pq}, in loop (J-73), to ascertain which set of equations (J-71a, or J-71b, or J-64) should be used to compute the post and trunnion drive angles.

f. CSM Orientation. The foregoing subsections define the CSM position in the LEM windows. It is now required to determine the CSM orientation. Two CSM models are used for this purpose (see Figure 18). Consider the three gimbal, $\frac{1}{20}$ scale, CSM docking model. Locate the table-top reference coordinate system at the CSM pivot point (Figure 18). Let all gimbal angles be zero. This forces the CSM body axes $\hat{X}_{B/C}$ to lie along

$\hat{\rho}_3$, $\hat{Y}_{B/C}$ to lie along $\hat{\rho}_2$ and $Z_{B/C}$, to lie along negative $\hat{\rho}_1$. Rotate first about the negative outer gimbal axis $(-\hat{\rho}_1)$ through $(\psi_G)_{CSM}$, then about the middle gimbal axis through $(\theta_G)_{CSM}$, and last about the inner gimbal axis through $(\phi_G)_{CSM}$ to obtain an arbitrary CSM orientation relative to the reference table axes. The table axes are related to the CSM body axes by the following gimbal angle transformation:

$$\begin{bmatrix} \hat{X}_{B/C} \\ \hat{Y}_{B/C} \\ \hat{Z}_{B/C} \end{bmatrix} = \begin{bmatrix} \sin(\theta_G)_{CSM} & \cos(\theta_G)_{CSM}\sin(\phi_G)_{CSM} & \cos(\theta_G)_{CSM}\cos(\psi_G)_{CSM} \\ -\sin(\phi_G)_{CSM}\cos(\theta_G)_{CSM} & \cos(\phi_G)_{CSM}\cos(\psi_G)_{CSM} + \sin(\psi_G)_{CSM}\sin(\theta_G)_{CSM}\sin(\phi_G)_{CSM} & \cos(\psi_G)_{CSM}\sin(\theta_G)_{CSM}\sin(\phi_G)_{CSM} - \sin(\psi_G)_{CSM}\cos(\phi_G)_{CSM} \\ -\cos(\phi_G)_{CSM}\cos(\theta_G)_{CSM} & -\sin(\phi_G)_{CSM}\cos(\psi_G)_{CSM} + \sin(\psi_G)_{CSM}\sin(\theta_G)_{CSM}\cos(\phi_G)_{CSM} & \sin(\theta_G)_{CSM}\cos(\phi_G)_{CSM}\cos(\psi_G)_{CSM} + \sin(\phi_G)_{CSM}\sin(\psi_G)_{CSM} \end{bmatrix} \begin{bmatrix} \hat{\rho}_1 \\ \hat{\rho}_2 \\ \hat{\rho}_3 \end{bmatrix} \qquad \text{(J-11)}$$

As before, another transformation must be found that relates $\hat{r}_{B/C}$ to $\hat{\rho}_{TABLE}$ based on known, real world, variables.

Matrix operator (J-63; q_{ij}) relates the LEM body axes to the table axes. The LEM body axes relative to the inertial reference axes are known (J-40). Combining gives:

$$\hat{r}_n = \left[g_{ij}^T \, q_{jK} \right] \hat{\rho}_{TABLE} \qquad \text{(J-12)}$$

The CSM is oriented to the same coordinate reference as the LEM. CSM ordered rotations are specified by ψ_c about Z_n followed by θ_c about Y_n', followed by ϕ_c about X_n'' (reference 38). During integrated operation the angles (ψ_c, θ_c, ϕ_c) or the corresponding direction cosine elements are supplied by the AMS. During independent operation the instructor will control the CSM attitude (J-62a). In any event:

$$\hat{r}_{B/C} = (g_{ij})_c \, \hat{r}_n \qquad \text{(J-62)}$$

Combining (J-62) and (J-12) gives:

$$\hat{r}_{B/C} = \left[(g_{iK})_c\, g^T_{K\ell}\, q_{\ell j}\right] \hat{\rho}_{TABLE} \qquad (J\text{-}61)$$

or:

$$\hat{r}_{B/C} = P_{ij}\ \hat{\rho}_{TABLE} \qquad (J\text{-}61)$$

Gimbal angles $(\psi_G)_{CSM}$, $(\theta_G)_{CSM}$ and $(\phi_G)_{CSM}$ are found by comparing known elements of matrix P_{ij} with matrix elements of (J-11). The final result is given in (J-60).

Matrix P_{ij} must be modified whenever the telescope or overhead window viewing mode is activated. This modification is required because matrix q_{ij} (J-63) relates the ficticious body axes $\bar{\rho}_{BT\gamma}$ or $\bar{\rho}_{BWa}$ to the table axes. For telescope viewing, the LEM body axes are reintroduced as follows:

$$\hat{\rho}_{BT\gamma} = \gamma_{ij}\ \hat{\rho}_{TABLE} \qquad (J\text{-}63)$$

But:

$$\hat{\rho}_{BT\gamma} = (h'_{ijwr})(h_{jKT\gamma})\ \hat{r}_{B/L} \qquad (J\text{-}70a)$$

Therefore:

$$\hat{r}_{B/L} = (h_{ijT\gamma})^T (h'_{jKwr})^T \gamma_{K\ell}\ \hat{\rho}_{TABLE} \qquad (J\text{-}13)$$

Matrix operator P_{ij} (J-61) is found by substituting (J-13) and (I-40) into (J-62). This gives:

$$P_{ij} = (g_{iK})_c (g_{K\ell})^T (h_{\ell m T\gamma})^T (h'_{mnWr})^T (\gamma_{nj}) \qquad (J\text{-}61)$$

for the telescope, and:

$$P_{ij} = (g_{iK})_c (g_{K\ell})^T (h_{\ell m Wa})^T (h'_{mnW\ell})^T (\gamma_{nj}) \qquad (J\text{-}61)$$

for the overhead window.

When the relative distance exceeds 530 feet, the two gimbal, $\frac{1}{80}$ CSM scale model is employed. For this regime the inner gimbal angle $(\phi_G)_{CSM}$ is not computed.

g. CSM Solar Illumination. The solar illumination sub-assembly for both CSM models consists of fixed banks of lights arranged in rings and surrounding each model (see Figures 18 and 19). CSM solar illumination is simulated by selective switching of the light bank quadrants. The lighting array is fixed to the table. Each bank of lights extends over an angle range given by $\gamma_n^{\odot} - \gamma_{n-1}^{\odot}$ measured in the $\hat{\rho}_1 - \hat{\rho}_2$ table reference plane (see Figure 19). The problem of light selection, therefore, reduces to ascertaining the Sun's direction in table coordinates.

The Sun's coordinates measured relative to the Earth or Moon are computed in the Ephemeris subsection. The orientation of the CSM is also known relative to the M or E-frame. Consequently, the Sun's coordinates in CSM body axes are:

$$\hat{r}_{B/C}^{\odot} = g_{ij_C} \, \hat{r}_{n/\odot} \qquad \text{(J-85)}$$

But, matrix P_{ij} (J-61) relates the CSM body frame to the table-top frame. Accordingly, the Sun's direction relative to the table is:

$$\hat{\rho}^{\odot} = P_{ij}^{T} \, \hat{r}_{B/C}^{\odot} \qquad \text{(J-84)}$$

Angles $\sigma^{\odot}$ and $\gamma^{\odot}$ are used to control the lights. Angle $\sigma^{\odot}$ defines the central angle between the Sun's direction and $\hat{\rho}_3$ while $\gamma^{\odot}$ locates the Sun's projection in the plane of the lamps (see Figure 19). Hence:

$$\cos\sigma^{\odot} = \hat{\rho}_3 \cdot \hat{\rho}^{\odot} = \rho_3^{\odot} \qquad \text{(J-82)}$$

$$0 \le \sigma^{\odot} \le \pi$$

and:

$$\tan\gamma^{\odot} = \frac{\rho_2^{\odot}}{\rho_1^{\odot}} \qquad \text{(J-83)}$$

Refer to Figure 19. When the Sun lies in region A ($\sigma^{\odot} \le \sigma_{MIN}^{\odot}$), the LEM, CSM and Sun are nearly aligned. The CSM as seen from the LEM is not illuminated. All lamps are turned off. When the Sun lies in region B ($\sigma^{\odot} \ge \pi - \sigma_{MAX}^{\odot}$), the CSM as seen from the LEM is fully illuminated. All lamps are turned on. When the Sun lies in region C $(\pi-\sigma'^{\odot} \leq \sigma^{\odot} < \pi-\sigma^{\odot}_{MAX})$, the CSM is almost fully illuminated; therefore, more than one bank of lamps should be lit. For the remaining region only one lamp is lit. It remains to define which lamp should be lit.

Each lamp segment extends over an angle range $\Delta\gamma^{\odot}$. There are n such equal lamp segments, hence, $n\Delta\gamma^{\odot} = 2\pi$. Angle $\gamma^{\odot}$ relates the Sun's position to the lamp segments. For example, for each $\gamma^{\odot}$ computed, a test must be performed to determine a value of n that satisfies the inequality:

$$(n-1)\Delta\gamma^{\odot} \leq \gamma^{\odot} < n\Delta\gamma^{\odot} \qquad \text{(J-81)}$$

$$n = 1, 2 \ldots . n_{max.}$$

Lamp selection logic is defined in (J-80).

h. <u>CSM or LEM in Shadow</u>. If the CSM lies in the Moon (lunar mission) or Earth shadow (Earth mission), then all lamps are turned off. A shadow cylinder is generated by assuming the Sun is at infinity (see sketch). The CSM is in sunlight whenever the CSM radius vector, projected on a

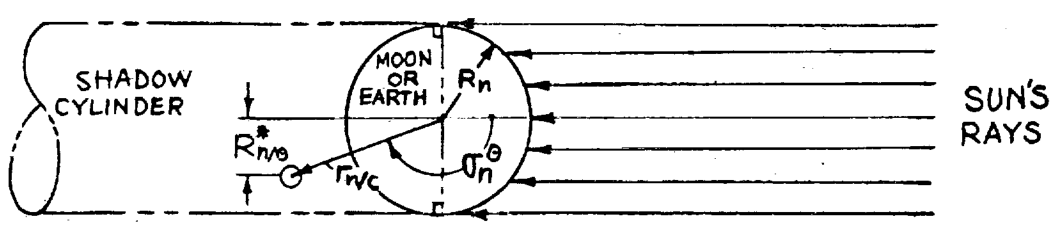

plane normal to the Sun's direction ($R^*_{n/\odot}$), is greater than the central body radius (R_n). In equation form this gives:

$$R^*_{n/\odot} = r_{n/c} \sin \sigma_n^{\odot}$$

where:

$$\cos \sigma_n^{\odot} = \frac{\bar{r}_{n/\odot} \cdot \bar{r}_{n/c}}{r_{n/\odot}\, r_{n/c}} \qquad \text{(J-87)}$$

$$0 \leq \sigma_n^{\odot} \leq \pi$$

As shown in the sketch, if $R^*_{n/\odot} < R_n$ but $0 \leq \sigma_n^{\odot} \leq \frac{\pi}{2}$, the CSM is illuminated (see Logic J-86).

6. Conclusions.

Conclusions and recommendations are inappropriate for this Subsection since all drive equations were based on hardware dictates. The visual display hardware design has not been finalized. As a result, the foregoing drive equations are subject to change. All future changes will be documented and issued as an addendum to this report.

IV. References

1. GAEC: "Design Control Specification For LEM Mission Simulator," LSP-440-43100A, 16 January 1964.

2. Beck, H.D.: "IMCC and AMS Mathematical Model, Compatibility Requirements," NASA, MSC, 8 November 1963.

3. Tross, C.: "Lunar Vehicle Orbit Determination," ARS Journal, April 1962.

4. Pinkham, G.; Sobierajski, F.: "Astrodynamics of Lunar Satellites: Part II - Lunar Orbit Stability," Grumman Research Report RE-170, November 1964.

5. Pulgrano, L.; Howe, E.: "Analysis of the Interaction of Propellant Sloshing in the LEM Ascent Stage with Attitude Control System, Including the Effects of Vertical Slosh Forces," LMO-500-230, 8 December 1964.

6. Pulgrano, L.; Howe, R.: "Mechanical Model Representations for LEM Ascent and Descent Stage Propellant Sloshing," LMO-500-168, 8 April 1964.

7. Pulgrano, L.: "A Mathematical Representation of Main Propellant Sloshing For Use In the Full Mission Enhineering Simulator," LMO-500-169, 31 March 1964.

8. Kelly, C.P.: "Summary Report - Math Models of the Dynamics of the Propulsion System, Propellant Sloshing, and Flight Control System for the LEM Mission Simulator," LED-500-6, 30 June 1965.

9. Pantason, P.: "Simulation of Ascent Stage FITH (Fire-In-The-Hole) Force and Moment Staging Forces," AVO #LAV-500-87, March 1965.

10. Shapiro, M.: "LMS Math Model - First Progress Report," LMO-500-185, 5 May 1964.

11. Billik, B.: "Survey of Current Literature on Satellite Lifetimes," ARS Journal 32, pages 1641-1650, 1962.

12. Battin, R. H.: "Astronautical Guidance," McGraw-Hill Publishing Company, 1964.

13. Grumman Aircraft Engineering Corporation: LEM Mission Simulator Math Model, LED-440-3, February 1965.

14. Kozai, Y.: "The Motion of a Close Earth Satellite," The Astronomical Journal, November 1959.

15. Westerman, H. R.: "Secular Effects of Atmospheric Drag on Satellites," The Astronomical Journal, August 1963.

16. Sterne, T. E.: "An Introduction to Celestial Mechanics," Interscience Publishers, Inc., 1960.

17. Shapiro, M.: "LMS Math Model - Relative Equations of Motion and Perturbative Influences - Fourth Progress Report," LMO-500-239, 8 January 1965.

18. Baker, R. L. M. Jr.; Makemson, M. W.: "An Introduction to Astrodynamics," Academic Press, 1960.

19. Rosser, J. B.; Newton, R. R.; Gross, G. L.: "Mathematical Theory of Rocket Flight," McGraw-Hill Book Company, 1947.

20. Davis, L.; Follin, W.; Blitzer, L.: "Exterior Ballistics of Rockets," Van Nostrand, 1958.

21. Aeder, R.: "LEM Mass Property Report," LED-49-17, 1 February 1965, Title unclassified, report confidential.

22. Pantason, P.: "LEM Staging Dynamics For Abort During the Lunar Powered Descent Phase," LMO-500-213, 30 January 1965.

23. Greene, J. P.: "The Use of Quaternions in FMES," LMO-510-248, 21 August 1964.

24. Greene, J. P.: "Quaternions," LMO-570-260, 12 October 1964.

25. Shapiro, M.: "LMS Math Model - Notes on Attitude Simulation Utilizing Either Quaternion Rate Equations or Direction Cosine Rate Equations-Third Progress Report," LMO-500-207, 1 August 1964.

26. Robinson, A. C.: "On the Use of Quaternions in Simulation of Rigid-Body Motion," WADC Technical Report 58-17, December 1958.

27. Goldstein, H.: "Classical Mechanics," Addison-Wesley Publishing Company, 1959.

28. Eichler, J.: "A Method to Force Orthogonality of the Quaternion-Derived Attitude Matrix," LMO-500-216, 5 October 1964.

29. "Explanatory Supplement to the Astronomical Ephemeris and the American Ephemeris and Nautical Almanac," Her Majesty's Stationery Office, 1961.

30. Hutchinson, R. C.: "Inertial Orientation of the Moon," MIT-IL-R-335, October 1962.

31. Linderifelser, W. A.: "Definition of Coincidence of LEM Vehicle Axes and Inertial Reference Frame At Lunar Landing Site," LMO-300-99, 27 March 1964.

32. Sears, N. E.; Trageser, M. B.; Woodbury, R. B.: "Primary G & N System Lunar Orbit Operations," MIT R-446, Volume I of II, April 1964.

33. Peabody, P. R.; Scott, J. F.; Orozco, E. G.: "Users' Descriptions of JPL Ephemeris Tapes," TR No. 32-580, March 2, 1964.

34. "The American Ephemeris and Nautical Almanac - 1966," U. S. Government Printing Office.

35. Green, J.: "GAEC Recommended Changes to LSP-370-2A," LMO-370-168, 22 April 1964.

36. Pulgrano, L.: "An Alternate Mathematical Representation of Propellant Sloshing For Use in the LEM Simulators," LMO-500-198, 9 July 1964.

37. Project 545-556: "LEM-EVDE Design Report," Farrand Optical Company, 8 January 1965.

38. Woycechowsky, B. J.: "Apollo Mission Simulator - Equations of Motion," General Precision ER-448, 15 June 1963.

39. Howe, R. E.: "Planar Analysis of Propellant Sloshing Interactions With the LEM Descent Stage Flight Control System," LMO-500-256, 15 March 1965.

40. Higgens, R. F.: "Contract NAS 9-1100, LEM Mission Simulators, Math Model Meeting Minutes," MSC-CF332-L13-15-65-414, 8 May 1965.

41. Shapiro, M.: "LMS Simulator - PNGS Equations and IMU and AOT Subsystem Equations," To be published.

Symbol	Definition	Units	Range (Estimated)	Remarks
a_o	Semi-major axis of CSM orbit.	ft.	5.7×10^6 to 7.0×10^6 20.9×10^6 to 24.5×10^6	Lunar orbit Earth orbit
a_{pq}, b_{pq}, c_{pq}	Celestial sphere gimbal angle drives.	deg.	0 to 360	Input to EVDE
a_{ij}	Transformation matrix from inertial M-Frame to selenographic S-Frame.	----	± 1	All direction cosine elements can vary from -1 to +1
a_{ij}^*	Constant transformation matrix from inertial M-frame to selenographic S-Frame computed at some epoch t*.	----	± 1	Constant, once t* is specified
a_k, b_k, c_k k=1,2,3,4	Direction cosines between X_B, Y_B, Z_B body axis and landing radar beam directions	----	± 1	
A,B,C	Lunar inertia constants: $\frac{I_C - I_A}{I_C}$, $\frac{I_C - I_B}{I_C}$, $\frac{M I_C}{2M_m}$	----	619.36×10^{-6} 202.70×10^{-6} 2.8159948×10^{27}	Input constants
A_{TL}, A_{LS}	Rendezvous radar azimuth gimbal angle to tracking-line or line-of-sight	deg.	0 to 360	A_{TL} - Input from RRMM A_{LS} - Input to RRMM
A_x/v, A_y/v, A_z/v	Aerodynamic drag perturbation components (LEM or CSM)	ft./sec^2	$\pm 6 \times 10^{-5}$	
A_{Aw_i}, E_{Aw_i} w = 1 or c	LEM or CSM VHF antenna direction cosines with respect to LEM or CSM body axes	deg		Input constant

Symbol	Definition	Units	Range (Estimated)	Remarks
c_{ij_n}	Transformation matrix from inertial M or E-frame to ideal IMU R-frame	--	± 1	Constant matrix
c_{1ni}, c_{2ni}, c_{3ni}	CSM VHF antenna direction cosines with respect to n-frame	--	± 1	Supplied by AMS during integrated mode
d_{pq}	Distance of Earth or Moon viewing screen from window or telescope	ft	0 to 20	Input constant
d	Mean solar days from Jan. 1.0 1950 to date	days	$(6 \text{ to } 9) \times 10^3$	Not required if included in JPL tapes
D_{Si} $i=1,2,3$	Landing radar doppler velocity signals	ft/sec	0 to 500	Input to LRMM
D^*	Integer mean solar days from beginning of launch year to problem start	days	0 - 365	Input constant
D_1, D_2	Fixed distance between CSM and LEM. This parameter is used to switch the computation from inertial coordinates to relative coordinates or vice versa.	ft.		Input constants
D_{Y_K}, D_{Z_K}	Jet damping force along body axis.	lbs	± 4	

Symbol	Definition	Units	Range (Estimated)	Remarks
e^2	Earth flattening equivalent	--	.006693219	Input constant
e_1; e_2; e_3; e_4	Quaternions	--	± 1	
$(E-E_o)$	Change in CSM eccentric anomaly	rad.	0 to 2π	Iterate for this parameter
$E_{TL,LS}$	Rendezvous radar elevation gimbal angle to tracking line or line-of-sight	deg.	0 to 360	E_{TL} - Input from RRMM E_{LS} - Input from RRMM
f"	Earth flattening parameter	--	$\frac{1}{298.30}$	Input constant
$(F_X$; F_Y; $F_Z)_B$	Total external force components along LEM body axes	lbs	$\pm 12 \times 10^3$	
g_{ij_n}	Transformation matrix from inertial E or M-frame to LEM body B-frame	--	± 1	
$(g_{ij})_c$	Transformation matrix from M or E-frame to CSM body frame	--	± 1	Supplied by AMS during integrated mode
g_E	Mean Earth surface gravity	ft/sec^2	32.1740	Input constant
g	Mean longitude of the sun	deg	0 to 360	Required for physical libration
GHA	Greenwich hour angle	deg	0 to 360	
H_i	Altitude of i^{th} earth tracking station above reference spheroid	ft	0 to 2000	Input constant
$h_{ij_{pq}}$	Transformation matrix from LEM body axis to window or telescope axes	--	± 1	Constant matrix

Symbol	Definition	Units	Range (Estimated)	Remarks
$h_{M/L}$	Altitude of LEM CG above lunar surface	ft	0 to 6 x 10^5	Lunar altitude measured with respect to reference spherical surface
$h_{M/LR}$	Altitude of LEM landing radar above lunar surface	ft	0 to 6 x 10^5	
h_{DE}	Altitude of design eye reference point above lunar surface	ft	0 to 3 x 10^4	Input to Landing And Ascent Image Generator
h	Altitude above spheroidal surface	ft	6 x 10^5 to 3 x 10^6	Earth orbits
H	Hours (UT) from Greenwich midnight to problem start	hrs	0 to 24	
$H_{n/C}$	Total CSM angular momentum	ft2/sec	30 x 10^9	
H_x; H_y; H_z	Component CSM angular momentum	ft^2/sec	30 x 10^9	
i_f	Inclination of MEP film strip relative to lunar equator	deg	150 to 180	Input constant
I	Hayn's inclination constant of lunar equator to ecliptic	deg	1.535	Input constant
$(I_{sp})_K$	Specific impulse (Main engine)	sec	300	Input constant for jet damping
I_x; I_y; I_z	Moments of inertia with respect to body B-axes	slug-ft^2	2000 to 22,000	Does not include CSM
I_{xy}; I_{yz}; I_{zx}	Products of inertia with respect to B-body axes	slug-ft	-100 to 700	

Symbol	Definition	Units	Range (Estimated)	Remarks
JD	Julian Date	days	(2.4 to 2.5) x 10^6	
J_2	Oblateness Constant	--	1.62345 x 10^{-3}	Input constant
l_{1n_i}, l_{2n_i} l_{3n_i}	LEM-VHF antenna direction cosines with respect to n-frame	--	± 1	
l_1, l_2	Distance from fixed RCS reference point to RCS jets	ft	4 to 6	Input constant
$l_{ij_{pq}}$	Transformation matrix from LEM window or telescope axis to M or E frame.	--	± 1	
L_{ij}	Physical lunar libration matrix	--	± 1	
L_B; M_B; N_B	Total LEM body torques in X_B, Y_B, Z_B directions, about the instantaneous CG	ft-lbs	$\pm$40,000	
$L_{\bar{R}}$; $M_{\bar{R}}$; $N_{\bar{R}}$	Reaction control torques about RCS fixed reference points	ft-lbs	$\pm$3000	
L_R; M_R; N_R	Reaction control torques about instantaneous CG	ft-lbs	$\pm$4000	
L_K; M_K; N_K	Main engine (ascent or descent torques about instantaneous CG)	ft-lbs	$\pm$10,000	
L_{S_K}; M_{S_K}; N_{S_K}	Fuel slosh torques about instantaneous CG	ft-lbs	$\pm$3000	

Symbol	Definition	Units	Range (Estimated)	Remarks
M_{D_K}; N_{D_K}	Jet damping torques about instantaneous CG	ft-lbs	± 10	
M^*, N^*	Stage separation torque about instantaneous CG	ft-lbs	$\pm 12{,}000$	
m_{K_e}	Expendables ejected during ascent or descent	slugs	1	Delete
$\dot{m}_K$	Main engine propellant flow rate	slug/sec	1	Required for jet damping
m_{Kj}	Sum of rigid and solid mass	slugs		Main engine Math Model
m_{R_1}	Total RCS propellant mass remaining (system a or b; 1 = a, 1 = b)	slugs	10	Input from RCS Math Model
m_L	Instantaneous total LEM mass	slugs	1000	
m_I	Total dry mass of ascent stage	slugs	200	Input constant
m_{II}	Total dry mass of descent stage	slugs	150	Input constant
m_{sKj}	Main engine fuel or oxidizer slosh mass in j^{th} tank	slugs		See A-46a, A-47a
m_{rDj}	Descent engine fuel or oxidizer rigid mass in j^{th} tank	slugs		See A-46a, A-47a
n_{ij}	Transformation matrix from LEM window or telescope axes to mean ecliptic axes of date	--	± 1	
N	Leap year integer correction for computing Julian date	days	4-6	

Symbol	Definition	Units	Range (Estimated)	Remarks
P_{ij}	Transformation from rendezvous and docking display axes ($\hat{\rho}$) to CSM body axes	--	± 1	
p_B; q_B; r_B	LEM body rates about X_B, Y_B, Z_B axes, respectively, relative to an inertial system	rad/sec	± 1.0	
p_X; p_Y; p_Z	Lunar triaxiality acceleration components	ft/sec^2		
Q_{ij}	Transformation from rendezvous and docking display axes ($\hat{\rho}$) to LEM body axes	--	± 1	
$r_{n/V}$ n = M or E V = L or C	Distance between LEM or CSM CG and Moon or Earth	ft	6×10^6 $2[illegible] \times 10^6$	
$r'_{B/L}$	Distance measured from LEM landing radar to Moon center	ft	6×10^6	
$r_{E,Gi}$	Distance from Earth center to i^{th} ground tracking station	ft	21×10^6	
$r_{Ei}/r_{Gi,L}$	Distance from i^{th} ground tracking station to LEM	ft	12×10^6 13×10^8	Earth orbit Lunar orbit
r'_i	Distance from i^{th} ground tracking station to center of moon	ft	13×10^8	
R_{K_T}	Ascent or descent tank radius	ft	$R_{A_T} = 2.0-$ $R_{D_T} = 2.12$	Input constant
$R\,A_T$	Right ascension of Earth take off site at launch	deg	0 to 360	Input constant

Symbol	Definition	Units	Range (Estimated)	Remarks
$(RA)_{\odot}$	Right ascension of Sun measured at problem start	deg	0 to 360	
R_M	Mean radius of moon	ft	5.702395×10^6	Input constant
R_E	Mean equatorial radius of earth	ft	20.92573818×10^6	Input constant
R_k $k = 1,2,3,4$	Slant range along each landing radar beam from LEM to lunar surface	ft	0 to 7.5×10^5	Input to LRMM
R_{LM}	Design lunar radius based on Land Mass Simulator datum reference	ft	5.7×10^6	Input constant. The value depends on the intended landing or take-off site.
$\bar{S}_x$; $\bar{S}_y$; $\bar{S}_z$	Component fuel and oxidizer slosh force in LEM body coordinates	lbs	400	
S_x^*	Stage separation force	lbs	$(3 \text{ to } 7) \times 10^3$	
S_V	Reference Area	ft^2		Input constant
t	Problem time	sec	--	
t*	Time measured from problem start which specifies the position of the IMU vertical X_R direction (landing site at landing or take-off at take-off)	sec		Input constant

Symbol	Definition	Units	Range (Estimated)	Remarks
T_o	Julian centuries measured from Jan. 1.0 1950 to problem start	J. cent's		Required for JPL Tapes
T^*	Julian centuries measured from Jan. 1.0 1950 to t*.	J. cent's		
T_u $u = 1,2\ldots 16$	RCS thrust	lbs	0 to 100	Input from RCSMM
T_K	Main engine thrust (ascent or descent).	lbs	0 to 3,500 0 to 10,500	Input from MEMM
$T_{X_{BR}}$; $T_{Y_{BR}}$; $T_{Z_{BR}}$	RCS thrust components along body axes	lbs	0 to 400	Input from RCSMM
$T_{X_{BK}}$; $T_{Y_{BK}}$; $T_{Z_{BK}}$	Main engine thrust components along body axes	lbs	11,000	Input from MEMM
$V_{R/V}$	Velocity of LEM or CSM relative to atmosphere	ft/sec	25×10^3	
$\ddot{\overline{V}}_s$; $\ddot{\overline{W}}_s$	Component slosh acceleration parameter in tank Y, Z coordinates	ft/sec^2	± 5	
$\ddot{V}_s$; $\ddot{W}_s$	Component slosh acceleration parameter in Y_B, Z_B body coordinates	ft/sec^2	± 5	
$V_{n/c}$	CSM velocity in inertial M- or E-frame	ft/sec	6,000 25,000	

Symbol	Definition	Units	Range (Estimated)	Remarks
X_{LM}, Y_{LM}	Displacement of subsatellite point with respect to origin of Landing Table Model or Landing Mass Simulator	ft		Input to EVDE and Land Mass Simulator
$X_{pq}^{M,}$, $Y_{pq}^{M,}$	Coordinates of Moon or Sun in window or telescope axes	ft	6×10^6 60×10^{10}	
$X_{n/L}$; $Y_{n/L}$ $Z_{n/L}$	LEM position coordinates in inertial M- or E-frame	ft	6×10^6 24×10^6	
$X_{B/L}$; $Y_{B/L}$ $Z_{B/L}$	LEM position coordinates measured in body frame	ft	6×10^6 24×10^6	
$X_{n/c}$; $Y_{n/c}$ $Z_{n/c}$	CSM position coordinates in inertial M- or E-frame	ft	6×10^6 24×10^6	
$\dot{X}_{B/S}$; $\dot{Y}_{B/S}$ $\dot{Z}_{B/S}$	Component velocities along LEM body axes with respect to lunar surface	ft/sec	5×10^3	
$\dot{X}_{M/S}$; $\dot{Y}_{M/S}$ $\dot{Z}_{M/S}$	Component velocities of lunar surface measured in M-frame	ft/sec	15	
$X_{S/V}$; $Y_{S/V}$ $Z_{S/V}$	LEM or CSM coordinates in selenographic S-frame	ft	6×10^6	
$X_{E/M}$; $Y_{E/M}$ $Z_{E/M}$	Position of Moon in E-frame	ft	15×10^8	Input from JPL Tapes
$X_{E/\odot}$; $Y_{E/\odot}$ $Z_{E/\odot}$	Position of Sun in E-frame	ft	60×10^{10}	Input from JPL Tapes
$\dot{X}_{R/n}$; $\dot{Y}_{R/n}$ $\dot{Z}_{R/n}$	Velocity components of vehicle relative to atmosphere	ft/sec	25×10^3	

Symbol	Definition	Units	Range (Estimated)	Remarks
$X_{E/Gi}$; $Y_{E/Gi}$ $Z_{E/Gi}$	Position of i^{th} ground tracking station in E-frame	ft	21×10^6	
X_x; X_y; X_z	Elements of precession matrix	--	± 1	Included in JPL tapes
Y	Launch year	--	1969 to 1975	Input constant
α_j $j = 1,2$	Position of LEM landing radar plate relative to LEM body axes	deg		Input constants
$\bar{\alpha}, \bar{\beta}, \bar{\gamma}$	Distance from LEM CG to local CG of any particular item along X_B, Y_B, Z_B directions, respectively.	ft	± 20	
$\alpha_{CG}, \beta_{CG}, \gamma_{CG}$	Distance from fixed body reference axis to instantaneous LEM CG	ft	± 20	
α, β, γ	Distance from fixed body reference axis to local CG of any particular item	ft	± 20	
$\Delta\alpha_{D_j}$	Distance from center of j^{th} descent tank to CG of remaining oxidizer or fuel	ft		
$\Delta\gamma$	Angle range of lamp segment representing solar illumination	deg		Input constant
$\gamma^{\odot}$	Angle made by the projection of the Sun in the $\hat{\rho}_1$ $\hat{\rho}_2$ rendezvous display plane with direction $\hat{\rho}_1$	deg	0 to 360	

Symbol	Definition	Units	Range (Estimated)	Remarks
$\gamma_{pq}^{\odot}$	Angle between Sun direction and optical axis line of sight direction	deg	0 to 180	
Γ'	Mean longitude of the lunar perigee	deg	0 to 360	
δ_K	Declination of landing or take-off site	deg	$\pm 20^\circ$	Input constant
δ_f	Angular displacement of sub-satellite relative to MEP film strip centerline	deg	$\pm 20^\circ$	
δ_i	Radar elevation angle of the i^{th} earth ground tracking station	deg	0 to 360	
$\delta_{i\,MIN}$	Minimum radar elevation angle of the i^{th} earth ground tracking station required for communications	deg	0 to 20	Input constant
$\delta_{\theta K}, \delta_{\psi K}$	Main engine gimbal angles	deg	0 to 10	Input from SCMM
ϵ	Obliquity of the ecliptic	deg	23	
ϵ^*	Tolerance parameter	deg	.1	Input constant
ζ_{ii}	LEM-CSM polarization angle measured in a plane normal to the line-of-sight vector	deg	0 to 180	Input to CRMM
θ_f	Position of LEM subsatellite point relative to ascending node of MEP film strip	deg	0 to 360	

Symbol	Definition	Units	Range (Estimated)	Remarks
θ_c, ϕ_c	Earth communication antenna gimbal angles	deg	0 to 360	Input to Communication math model
θ_{ok} k=1,2,3,4	The angle between each landing radar beam direction and the local vertical formed by the intersection of each beam direction with the lunar surface	deg	0 to 90	Input to LRMM
θ_{LS}, ϕ_{LS}	Orientation of LEM line of sight relative to rendezvous display axes (LEM camera angle drives)	deg	0 to 360	Input to EVDE
θ, ϕ, ψ	LEM Euler angles (ordered rotations given by θ, then ψ then ϕ)	deg	0 to 360	
θ_c, ϕ_c, ψ_c	CSM Euler angles (ordered rotations given by ψ_c, then θ_c, then ϕ_c)	deg	0 to 360	Supplied by AMS or instructor
$(\theta_G)_{CSM}$; $(\phi_G)_{CSM}$; $(\psi_G)_{CSM}$	1/20 or 1/80 scale CSM CSM docking model gimbal angle rotations	deg	0 to 360	Input to EVDE
θ_{pq}, ϕ_{pq} ψ_{pq}	Orientation of window or telescope axis relative to LEM body axes	deg		Input constants
λ_i	Longitude of ith earth ground tracking station	deg	0 to 360	Input constant
λ_{LM}	Selenographic longitude which locates the origin of the landing table or land mass simulator	deg	0 to 360	Input constant
λ_{SV}	Selenographic longitude of either LEM or CSM	deg	0 to 360	

Symbol	Definition	Units	Range (Estimated)	Remarks
λ_{SK}	Selenographic longitude of either the landing site or take-off site	deg	0 to 360	Input constant
Λ_i i=1,2,3	Angle between landing radar beams	deg		Input constants
$\Delta\Lambda_i$	Angular error between landing radar beams	deg		Input constants
μ_k k=1,2,3,4	Angle between slant range vector and local vertical	deg	0 to 90	
μ_n	Central force gravitational constant of Moon or Earth	$\frac{ft^3}{sec^2}$	$1.73139972 \times 10^{14}$ $1.40765391 \times 10^{16}$	Input constants
μ^*	Semi angle of moon subtended by the LEM vehicle	deg	0 to 90	
ξ_{V_i}	LEM or CSM VHF antenna angles with respect to the line-of-sight vector	deg	0 to 180	Input to Communication math model
ξ'_i	LEM spiral antenna angles with respect to line-of-sight vector	deg	0 to 180	Input to Communication math model
ξ_K	Damping ratio of descent engine or ascent engine fuel or oxidizer	--		Input constant
ξ_k k=1,2,3,4	Angle between landing radar beams	deg		Input constant
$\Delta\xi_k$	Angular error in direction of landing radar beams	deg		Input constant

Symbol	Definition	Units	Range (Estimated)	Remarks
ρ_{LS}	Line-of-sight distance between LEM-CG and CSM-CG	ft	24×10^5	
ρ'_{LS}	Line-of-sight distance measured from design eye to CSM-CG	ft	24×10^5	
ρ_X, ρ_Y, ρ_Z	Component relative distances of CSM WRT LEM measured in E-or M-frame directions	ft	$\pm 24 \times 10^5$	
$\rho_{X_B}, \rho_{Y_B}, \rho_{Z_B}$	Component relative distances of CSM WRT LEM measured in body B-frame directions	ft	$\pm 24 \times 10^5$	
$\rho_{pq_{max}}$	Maximum viewing distance measured in the plane of the occulting disc from the optical line-of-sight	ft		Input constants
ρ_V	Atmospheric density	slugs/ ft^3		Table look-up
$\hat{\rho}_1, \hat{\rho}_2, \hat{\rho}_3$	Rendezvous and docking model reference axes			
$\rho_1^{\odot}, \rho_2^{\odot}, \rho_3^{\odot}$	Coordinates of sun in $\hat{\rho}_1, \hat{\rho}_2, \hat{\rho}_3$ reference frame	--	± 1	
σ_c	Central angle between LEM-moon radius vector and CSM-moon radius vector	deg	0 to 180	
σ_{Ei}	Central angle measured at moon between the LEM-moon radius vector, and the moon i^{th} earth station radius vector	deg	0 to 180	

Symbol	Definition	Units	Range (Estimated)	Remarks
$\sigma^{\odot}$	Angle between $\hat{\rho}_3$ axis and sun's direction	deg	0 to 180	
$\sigma^{\odot}_{min,max}$	Fixed angles measured between $\hat{\rho}_3$ and the sun's direction	deg		Input constants
$\sigma^{\odot}_{M,E}$	Angle between either $r_{M/C}$ or $r_{E/C}$ and sun's direction	deg	0 to 180	
σ^{*}_{pq}	Angle between window or t telescope optical axis and LEM local vertical	deg	0 to 180	Input to EVDE
ϕ_{LM}	Selenographic latitude which locates the origin of the landing table or land mass origin	deg		Input constant
$\phi_{S/V}$	Selenographic latitude of either the LEM or CSM vehicle	deg	0 to ± 90	
ϕ_{SK}	Selenographic latitude of either the lunar landing site or take off site	deg	$\pm 90°$	Input constant
ϕ_i $i = 1,2,3...$	Geodetic latitude of i^{th} earth ground tracking station	deg	$\pm 90°$	Input constant
ϕ_k	Angular displacement of the tank coordinate system about the X_B LEM axis	deg	0 to 360	
ϕ^{*}_{pq}	Angle which measures roll about optical line-of-sight	deg	0 to 360	Input to EVDE
ψ^{*}_{pq}	Angle measured between the projection of window or telescope optical axes on the lunar surface and the direction of the MEP film strip center line	deg	0 to 360	Input to EVDE

Symbol	Definition	Units	Range (Estimated)	Remarks
Ω	Longitude of lunar orbit ascending node	deg	0 to 360	
$\dot{\Omega}$	Nodal regression rate of CSM (Earth orbit)	deg/ sec	6×10^{-5}	
Ω_f	Right ascension of ascending node of MEP film strip center line measured in selenographic or geographic coordinates	deg	0 to 360	Input constant
$\omega_{x_s}; \omega_{y_s}; \omega_{z_s}$	Total angular velocity of the moon in selenographic coordinates	rad/ sec	3×10^{-6}	
$\omega_{LS_{ob}}$	Total CSM line-of-sight angular velocity about out-board axis	rad/ sec		Input to RRMM
$\omega_{LS_{ib}}$	Total CSM line-of-sight angular velocity about inboard axis	rad/ sec		Input to RRMM
$\omega_{B_{ob,ib}}$	LEM body angular rate about outboard axis or inboard axis	rad/ sec	$\pm .05$	
ω_E	Earth rotation rate	deg/ sec	4×10^{-3}	
ω_{TL}	LEM body angular rate about tracking line	rad/ sec		Input to RRMM
ω_n	Natural frequency (fuel slosh)	rad/ sec		See A-46a, A-47a
☾	Mean longitude of moon measured in ecliptic from mean equinox of date to the mean ascending mode of the lunar orbit, and then along the orbit	deg	0 to 360	

SUBSCRIPTS

Subscript Symbol	Definition
a	RCS system a.
A	Ascent engine.
b	RCS system b.
B	LEM body axes B-frame.
C	CSM, also communications antenna.
CG	Center of gravity.
D	Descent engine
DE	Design eye.
e	Expendables.
E	Earth, also geocentric mean equinox reference system
f	MEP film strip or landing table display.
G	Earth ground station, also Earth fixed references.
H	Local horizon, local vertical reference system.
ib	Inboard axis.
K	Either A (Ascent Engine) or D (Descent Engine).
l	RCS system a or b.
L	LEM
LR	Landing radar antenna.
LS	Line-of-sight.
LM	Land Mass Simulator.
M	Moon; also selenocentric mean equinox reference system.
N	Nozzle
n	Either E-frame or M-frame
O	Initial condition.

SUBSCRIPTS (Cont'd)

Subscript Symbol	Definition
ob	Outboard axis.
r	Roll about tracking line; also denotes rigid portion of fuel or oxidizer mass.
p	Window (W) or telescope (T).
q	Right (r), left (l) or center (c) window or telescope.
R	RCS jets, also IMU reference system, also relative.
$\bar{R}$	Reference point of RCS jets.
RR	Rendezvous radar.
S	Selenographic reference system; also refers to fuel slosh.
T	Table-top axes (Land Mass Simulator)
V	Vehicle, either L (LEM) or C (CSM).
X; Y; Z	With respect to X, Y, Z directions
I	With respect to dry weight of LEM vehicle ascent stage.
II	With respect to dry weight of LEM vehicle descent stage.
$\odot$	Sun

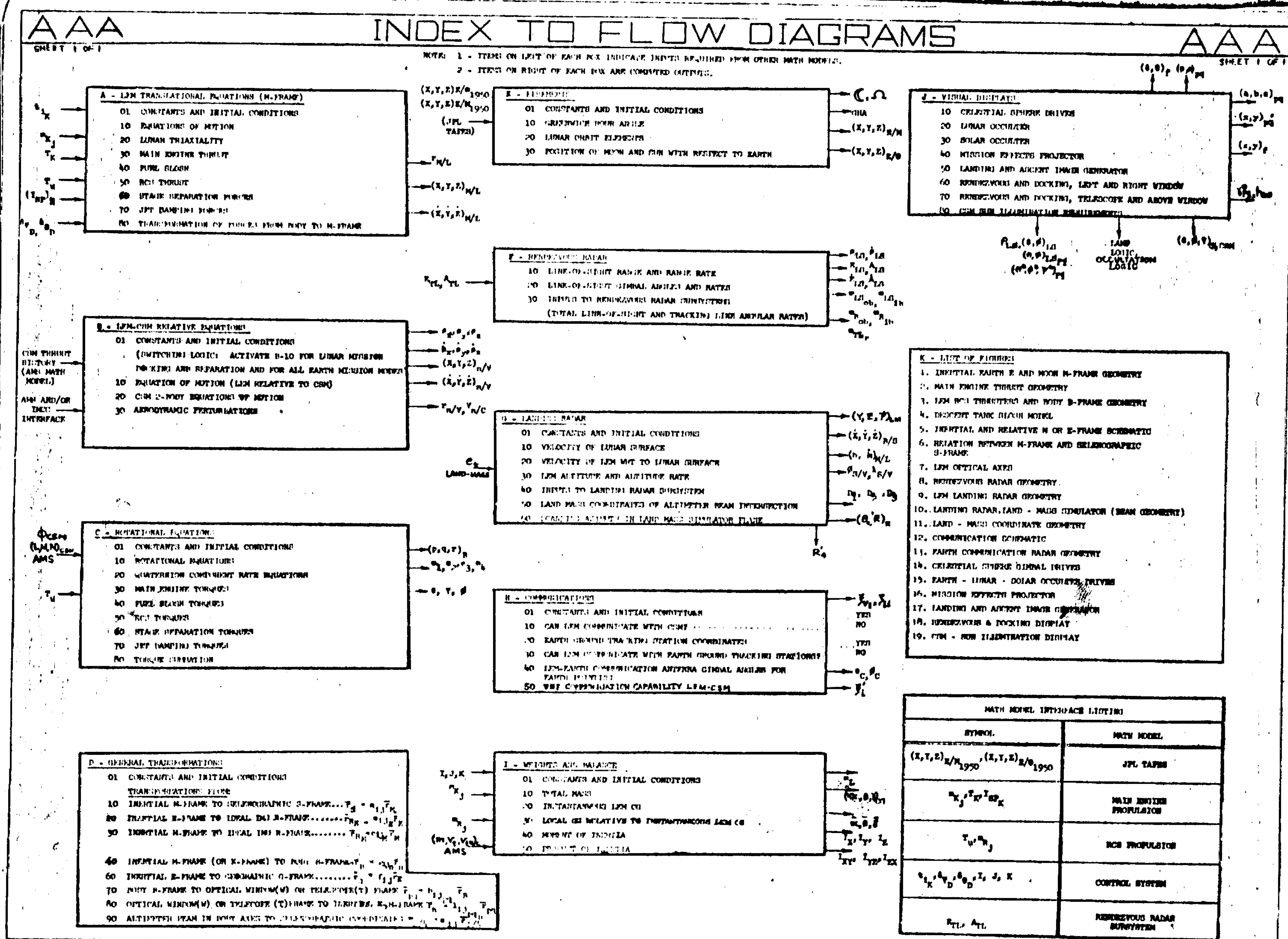

MATH MODEL INTERFACE LISTING

SYMBOL	MATH MODEL
$(X,Y,Z)_{E/M_{1950}}, (X,Y,Z)_{E/\theta_{1950}}$	JPL TAPES
$\alpha_{K_J}, T_K, T_{SP_K}$	MAIN ENGINE PROPULSION
T_U, α_{R_J}	RCS PROPULSION
$\theta_{I_K}, \theta_{Y_D}, \theta_{P_D}, I, J, K$	CONTROL SYSTEM
R_{TL}, A_{TL}	RENDEZVOUS RADAR SUBSYSTEM

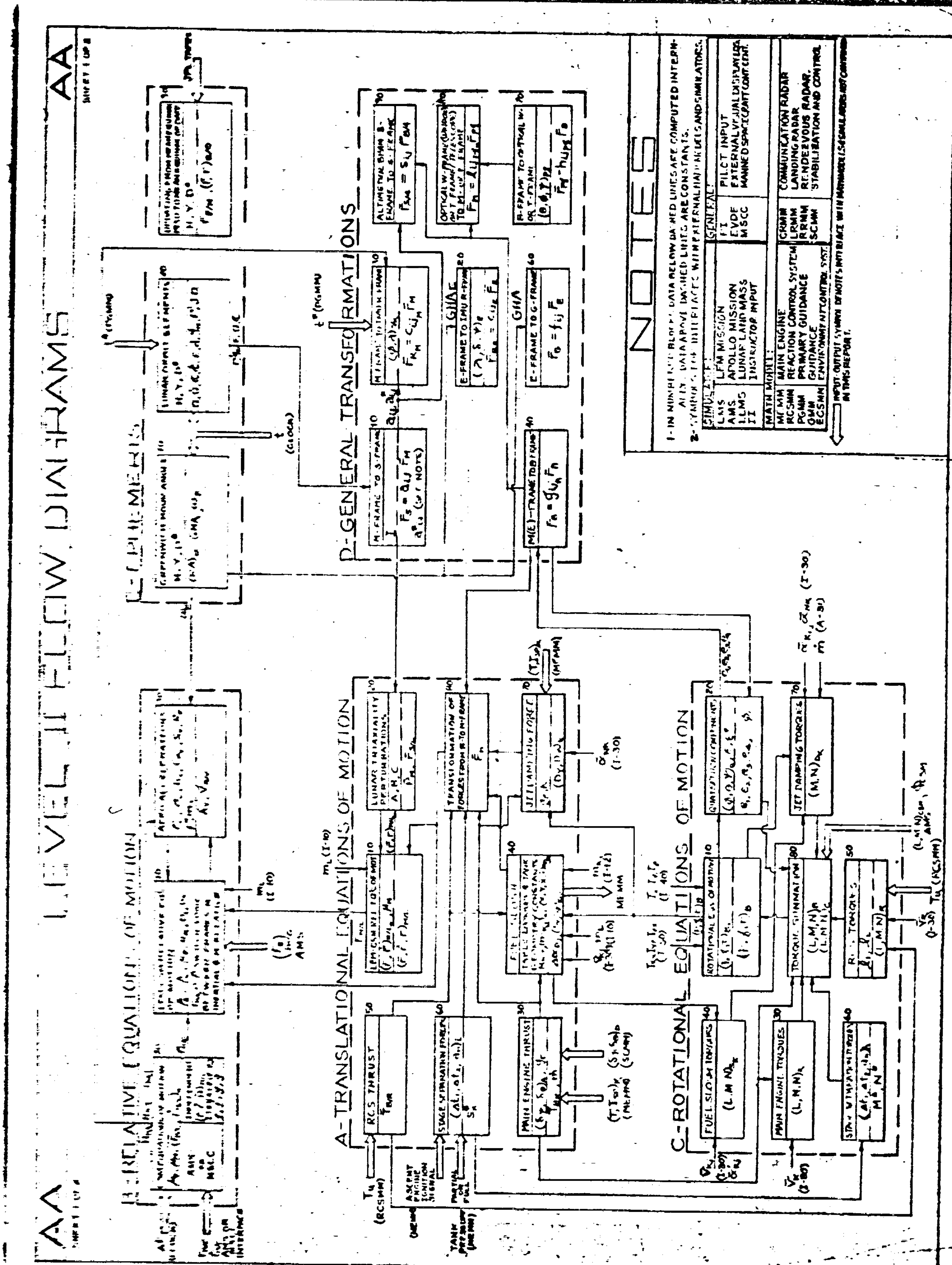
AA
LEVEL II FLOW DIAGRAMS
B-RELATIVE EQUATIONS OF MOTION
A-TRANSLATIONAL EQUATIONS OF MOTION
C-ROTATIONAL EQUATIONS OF MOTION
D-GENERAL TRANSFORMATIONS
NOTES
RCS THRUST
MAIN ENGINE THRUST
JET DAMPING TORQUES
GRUMMAN AIRCRAFT ENGINEERING CORPORATION

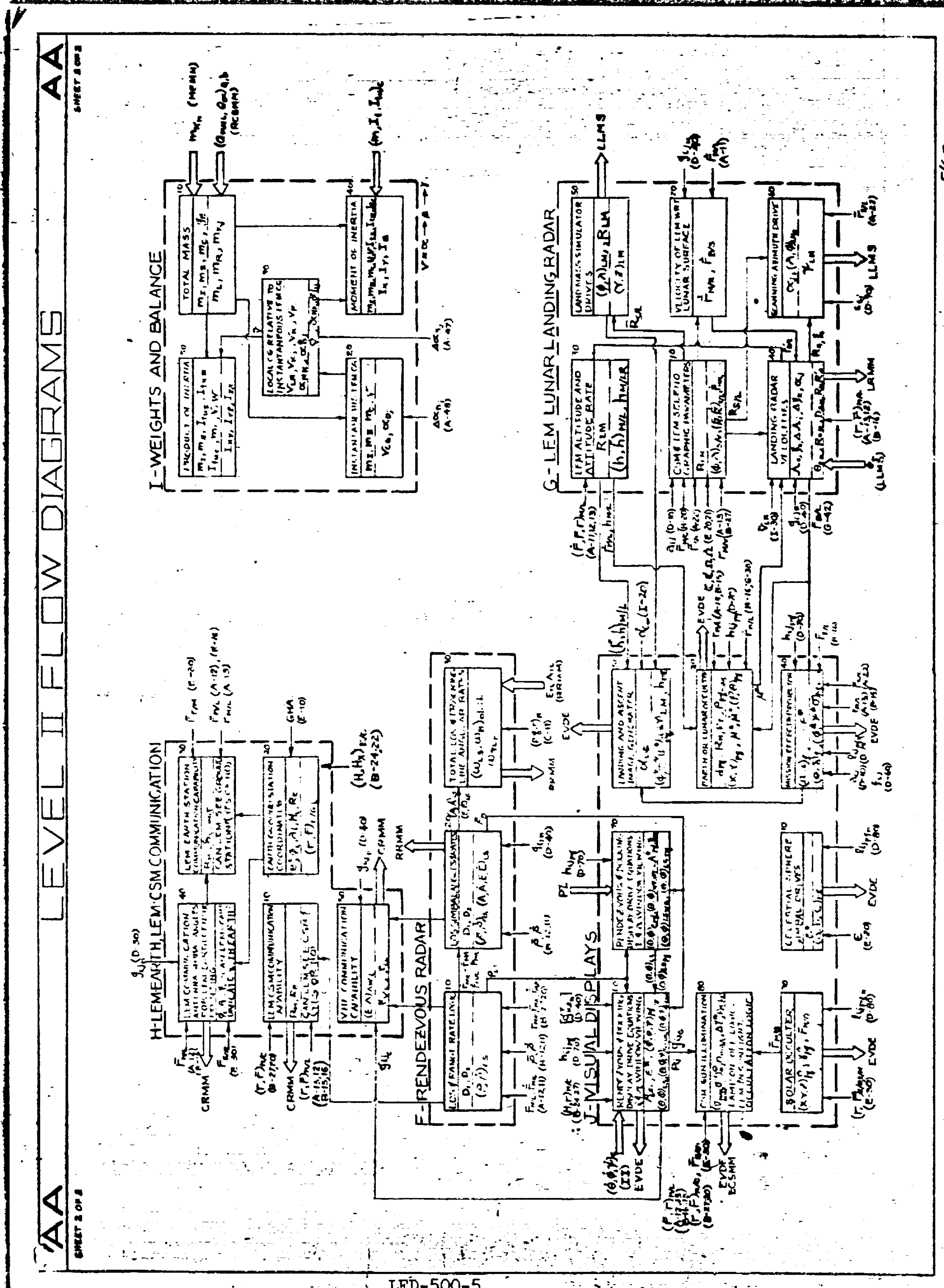
LEVEL II FLOW DIAGRAMS
AA
I-WEIGHTS AND BALANCE
G-LEM LUNAR LANDING RADAR
H-LEM-EARTH, LEM-CSM COMMUNICATION
F-RENDEZVOUS RADAR
J-VISUAL DISPLAYS
5/65

A- TRANSLATIONAL EQUATIONS, M-FRAME — A

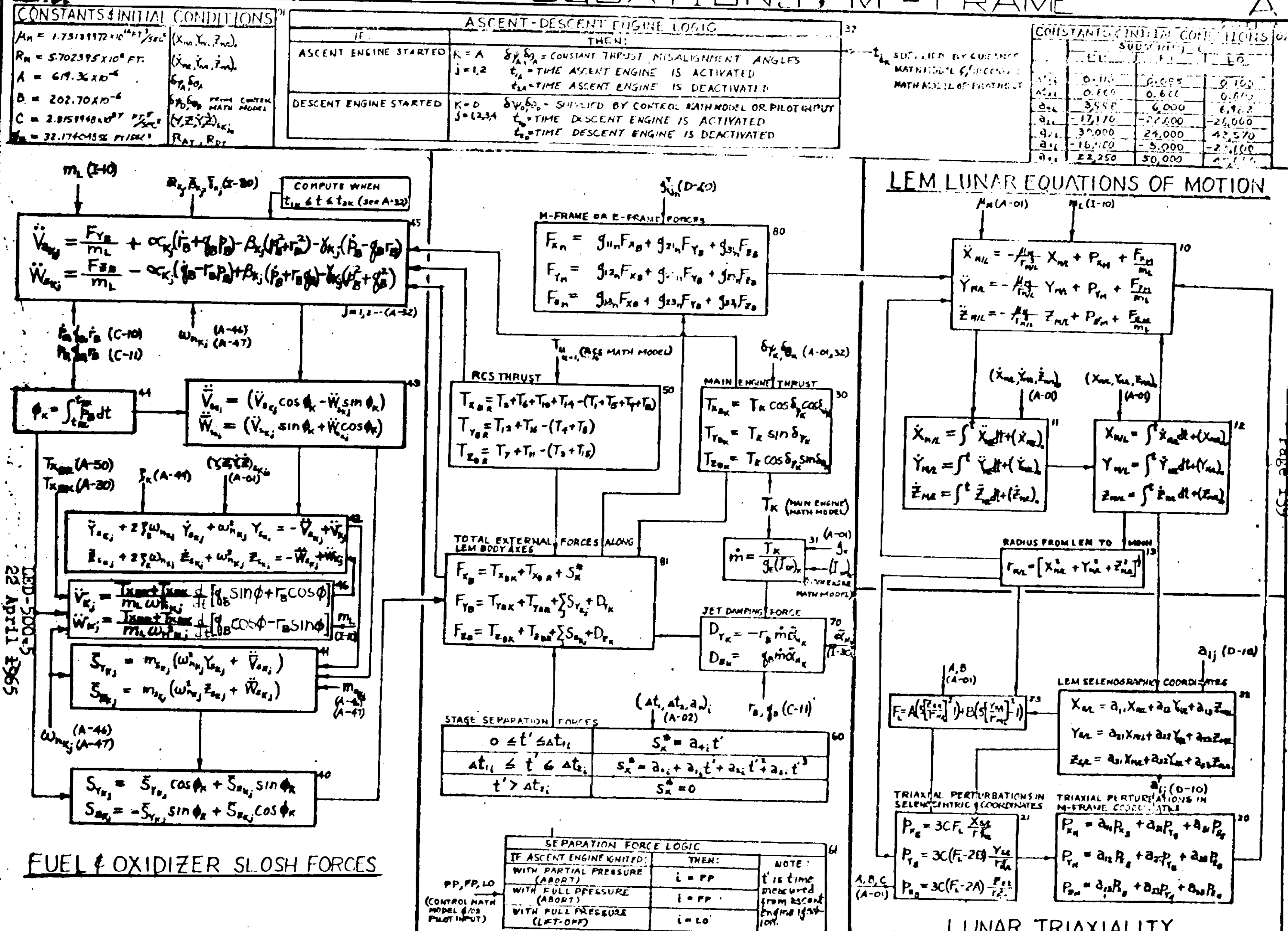

LONGITUDINAL EQUATIONS, M-FRAME

A

CONSTANTS AND INITIAL CONDITIONS (03)

$A_A = 0.025$	$A_D = 0.1$	W_{1D}	W_{1A}	a_{1D}	a_{1A}	h_{1D}	h_{1A}
$B_A = 0.175$	$B_D = 0.25$	W_{2D}	W_{2A}	a_{2D}	a_{2A}	h_{2D}	h_{2A}
$C_A = 1.0$	$C_D = 1.38$	W_{3D}	W_{3A}	a_{3D}	a_{3A}	h_{3D}	h_{3A}
$D_A = 2.8$	$D_D = 4.0$		W_{4A}		a_{4A}		h_{4A}

FUEL SLOSH FUNCTIONS (ASCENT TANKS) (46a)

$j = 1, 2$

Inputs: m_{Aj} (I-12), $(m_{Aj})_0$ (I-01)

$\left[\frac{m_{Aj}}{(m_{Aj})_0}\right]$	$\left[\frac{m_{sAj}}{(m_{Aj})_0}\right]$	M_{Aj}	$H_{j_A} = \frac{h_{jA}}{2R_{AT}}$	E_A
0	0	1.00	0	1.000
.1	.08	1.06	.200	1.000
.2	.16	1.10	.285	.982
.3	.22	1.14	.362	.962
.4	.27	1.18	.435	.919
.5	.30	1.22	.500	.881
.6	.31	1.27	.570	.850
.7	.30	1.33	.640	.800
.8	.27	1.43	.715	.751
.9	.19	1.64	.805	.686
1.0	0	2.30	1.000	.471

FUEL SLOSH FUNCTIONS (DESCENT TANKS) (47a)

$j = 1, 2, 3, 4$

Inputs: m_{Dj} (I-12), $(m_{Dj})_0$ (I-01)

$\left[\frac{m_{Dj}}{(m_{Dj})_0}\right]$	$\left[\frac{m_{sDj}}{(m_{Dj})_0}\right]$	$\left[\frac{\Delta\alpha_{Rj}}{2R_{DT}}\right]$	$\left[\frac{\Delta\alpha_{sj}}{2R_{DT}}\right]$	M_{Dj}	$H_{j_D} = \frac{h_{jD}}{2R_{DT}}$	E_D
0	0	-.19	-.19	1.00	0	1.000
.1	.08	-.19	-.19	1.09	.250	1.000
.2	.15	-.19	-.19	1.16	.370	.975
.3	.18	-.18	-.18	1.23	.480	.962
.4	.20	-.17	-.16	1.29	.584	.919
.5	.21	-.15	-.12	1.33	.690	.878
.6	.21	-.14	-.06	1.35	.793	.843
.7	.21	-.12	+.03	1.38	.900	.790
.8	.21	-.11	.12	1.44	1.010	.747
.9	.16	-.08	.17	1.56	1.130	.673
1.0	0	0	.19	2.50	1.380	.471

FUEL SLOSH PARAMETERS (ASCENT TANK) (46)

$$m_{sAj} = \left[\frac{m_{sAj}}{(m_{Aj})_0}\right](m_{Aj})_0$$

$$\omega_{nAj} = M_{Aj}\sqrt{\frac{T_{xBA}/m_L}{R_{AT}}}$$

Inputs: $(m_{Aj})_0$ (I-01), T_{xBA} (A-30), m_L (I-10), R_{AT} (A-01)

FUEL SLOSH PARAMETERS (DESCENT TANK) (47)

$$m_{sDj} = \left[\frac{m_{sDj}}{(m_{Dj})_0}\right](m_{Dj})_0 \qquad m_{rDj} = m_{Dj} - m_{sDj}$$

$$\Delta\alpha_{sj} = \left[\frac{\Delta\alpha_{sj}}{2R_{DT}}\right]2R_{DT} \qquad \Delta\alpha_{Rj} = \left[\frac{\Delta\alpha_{Rj}}{2R_{DT}}\right]2R_{DT}$$

$$\omega_{nDj} = M_{Dj}\sqrt{\frac{T_{xBD}/m_L}{R_{DT}}}$$

Inputs: $(m_{Dj})_0$ (I-01), T_{xBD} (A-30), R_{DT} (A-01), m_L (I-10)

(49e)

$$h_{j_K} = 2R_{KT}H_{j_K}$$

Input: R_{KT} (A-01)

(48)

$$\Delta\alpha_{Dj} = \frac{\Delta\alpha_{sj}\cdot m_{sDj} + \Delta\alpha_{Rj}\cdot m_{rDj}}{m_{Dj}}$$

Inputs: m_{sDj}, m_{rDj}, $\Delta\alpha_{Rj}$, $\Delta\alpha_{sj}$, m_{Dj} (I-12)

(49c)

$$\alpha_{\beta K} = \frac{W_{\beta K}}{a_{\beta K}}\left(2 - \frac{W_{\beta K}}{a_{\beta K}}\right)$$

Inputs: $W_{\beta K}$ (A-03), $a_{\beta K}$ (A-03)

DAMPING RATIO (49)

Inputs: (A,B,C,D)$_K$ (A-03), $a_{\beta K}$ (A-03), R_{KT} (A-01), $h_{\beta K}$ (A-03)

$0 \le H_{j_K} \le A_K$	$\zeta_K = 0.1$
$A_K < H_{j_K} < B_K$	$\zeta_K = 0.1\, e^{-10[H_{j_K} - A_K]}$
$B_K \le H_{j_K} \le C_K$	$\zeta_{j_K} = \frac{D_K\sqrt{\beta_{j_K}}}{e^{10H_{j_K}}}\sum_{\beta=1}^{3,4} e^{-\frac{5h_{\beta K}}{R_{KT}}}\sqrt{\frac{\alpha_{\beta K}^3}{a_{\beta K}}}$

$\beta = 1, 2, 3$ in ascent engine
$\beta = 1, 2, 3, 4$ ascent engine

(49a)

$$\zeta_{j_K} = a_{j_K}(E_K)\Gamma_{P_{jK}}$$

Inputs: E_A, E_D (A-46a, 47a), a_{j_K}

(49b)

$$\Gamma_{P_{jK}} = \tan^{-1}\left[\frac{m_L\omega_{nKj}^2(Y_{sKj}^2 + Z_{sKj}^2)}{T_{xBK} + I_{xxK}}\right]$$

Inputs: T_{xBK} (A-30), T_{xBR} (A-50), m_L (I-10), ω_{nKj} (A 46, 47), Y_{sKj}, Z_{sKj} (A 4..)

(49d)

IF:	THEN:
$0.88 \le H_{j_D} \le 1.38$	$a_{j_D} = R_{DT}\sqrt{1 - 4(H_{j_D} - 0.88)^2}$
$0.5 \le H_{j_D} \le 0.88$	$a_{j_D} = R_{DT}$
$0 \le H_{j_D} \le 0.5$	$a_{j_K} = 2R_{KT}\sqrt{H_{j_K}(1 - H_{j_K})}$
$0 \le H_{j_A} \le 1$	

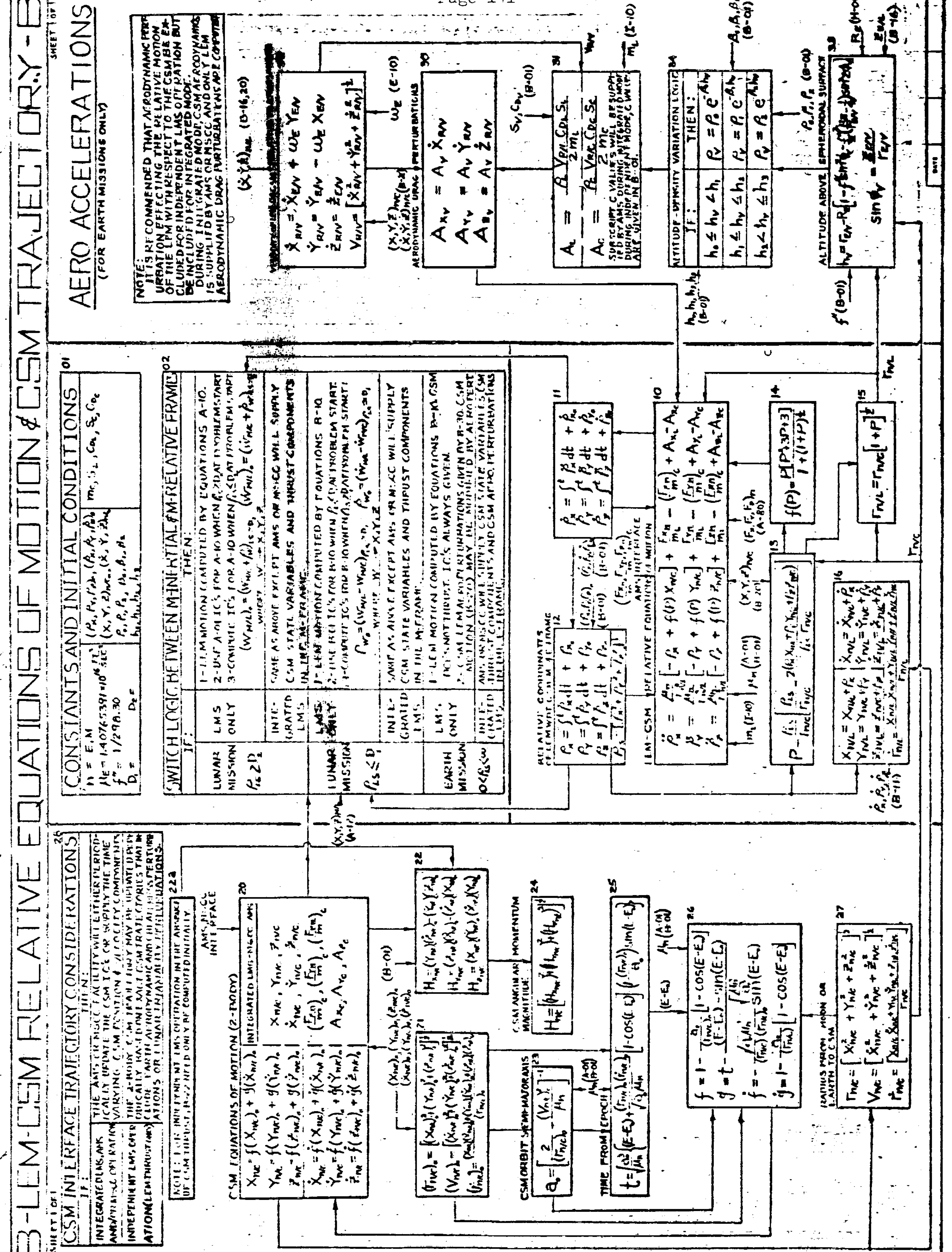
B-LEM-CSM RELATIVE EQUATIONS OF MOTION & CSM TRAJECTORY-B
CSM INTERFACE TRAJECTORY CONSIDERATIONS
CONSTANTS AND INITIAL CONDITIONS
SWITCH LOGIC BETWEEN M-INERTIAL & M-RELATIVE FRAME
AERO ACCELERATIONS
(FOR EARTH MISSIONS ONLY)
CSM EQUATIONS OF MOTION (2-BODY)
CSM ORBIT SEMI-MAJOR AXIS
CSM ANGULAR MOMENTUM MAGNITUDE
TIME FROM EPOCH
ALTITUDE-DENSITY VARIATION LOGIC
ALTITUDE ABOVE SPHEROIDAL SURFACE

ROTATIONAL EQUATIONS OF MOTION

CONSTANTS & INITIAL CONDITIONS (01)

p_{B_o}	DEG/SEC	θ_o	DEG	$\ell_1 = 5.0$ FT	ϕ_{CSM}		
q_{B_o}	DEG/SEC	ϕ_o	DEG	$\ell_2 = 5.5$ FT			
r_{B_o}	DEG/SEC	ψ_o	DEG	$\epsilon^* = .1$ DEG			
$R = 57.2957795$ DEG/RAD				$\epsilon = 10^{-3}$			

CONSTANTS AND INITIAL CONDITIONS (02)

M^*	SUBSCRIPT i: PP	FP	LO
t_{1_i}			
Δt_{1_i}			
Δt_{2_i}			
a_{0_i}			
a_{1_i}			
a_{2_i}			
a_{3_i}			
a_{4_i}			

CONSTANTS AND INITIAL CONDITIONS (03)

N^*	SUBSCRIPT i: PP	FP	LO
t_{1_i}			
Δt_{1_i}			
Δt_{2_i}			
a_{0_i}			
a_{1_i}			
a_{2_i}			
a_{3_i}			
a_{4_i}			

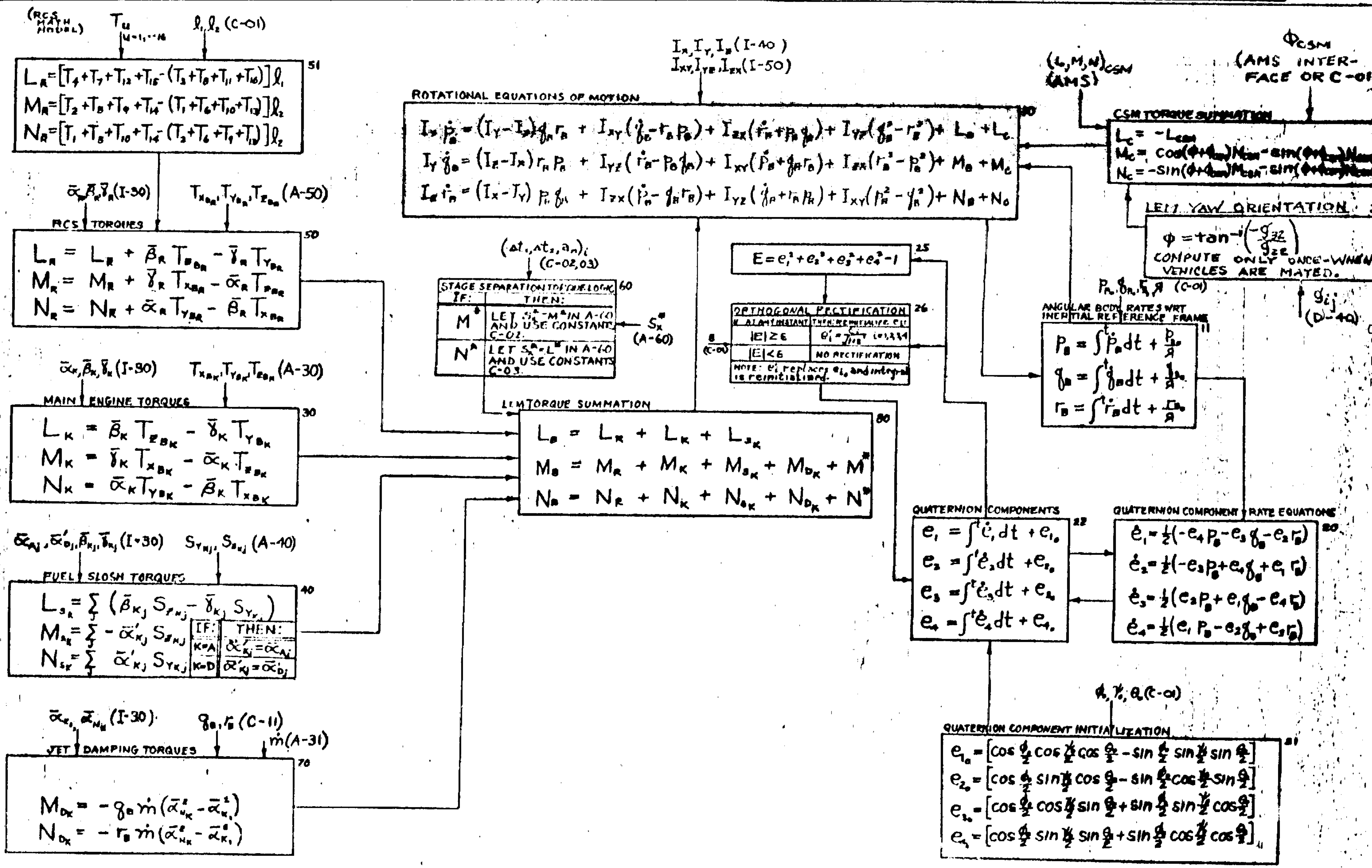

D- GENERAL TRANSFORMATIONS D

SHEET 1 OF 2

10 — TRANSFORM FROM INERTIAL M-FRAME TO SELENOGRAPHIC S-FRAME

$$\bar{F}_S = a_{ij}\,\bar{F}_M$$

$$a_{ij} = L_{i\ell}\,a_{\ell\ell}\,a_{\ell m}\,a_{mn}\,a_{nj}$$

Inputs: $a_{\ell m}$, a_{nj}, a_{mn}, $a_{\ell\ell}$

11 — PHYSICAL LIBRATION MATRIX $L_{i\ell}$

$L_{11} = L_{22} = L_{33} = 1$

$L_{12} = -L_{21} = L_Z$

$L_{13} = -L_{31} = -L_Y$

$L_{23} = -L_{32} = L_X$

12

$L_X = \left[34.42\cos(\Gamma' - \Omega) - 5.33\cos(\mathbb{C} - \Omega)\right]10^{-5}$

$L_Y = \left[70.30\sin(\Gamma' - \Omega) - 5.33\sin(\mathbb{C} - \Omega)\right]10^{-5}$

$L_Z = \left[8.73\sin 2(\Gamma' - \Omega) - 5.82\sin(\mathbb{C} - \Gamma') + 2R\varepsilon\sin g_0\right]10^{-5}$

$\Gamma', \Omega, \mathbb{C}, g_0$ (E-20)

13 — $a_{k\ell(\mathbb{C}-\Omega)}$

$a_{11} = a_{22} = -\cos(\mathbb{C} - \Omega)$

$a_{12} = -a_{21} = -\sin(\mathbb{C} - \Omega)$

$a_{13} = a_{31} = a_{23} = a_{32} = 0$

$a_{33} = 1$

14 — $a_{mn(\Omega)}$

$a_{11} = a_{22} = \cos\Omega$

$a_{12} = -a_{21} = \sin\Omega$

$a_{13} = a_{31} = a_{23} = a_{32} = 0$

$a_{33} = 1$

I (E-01)

15 — $a_{\ell m(I)}$

ELEMENTS ARE CONSTANT

$a_{11} = 1$

$a_{12} = a_{13} = a_{21} = a_{31} = 0$

$a_{22} = a_{33} = \cos I$

$a_{23} = -a_{32} = -\sin I$

ϵ (E-20)

16 — $a_{nj(\epsilon)}$

ELEMENTS CAN BE CONSIDERED CONSTANT

$a_{11} = 1$

$a_{12} = a_{13} = a_{21} = a_{31} = 0$

$a_{22} = a_{33} = \cos\epsilon$

$a_{23} = -a_{32} = \sin\epsilon$

01 — INITIAL CONDITIONS AND CONSTANTS

ϕ_G $\quad \lambda_E, \delta_E, \gamma_E$

ϕ_{S_A} $\quad \phi_{S_D}$

λ_{S_A} $\quad \lambda_{S_D}$

t^* sec

$K = A$ or D

20 — TRANSFORM FROM INERTIAL E-FRAME TO IDEAL IMU R-FRAME (USED FOR EARTH TRAINING MISSIONS ONLY)

$$\bar{F}_{R_E} = C_{ij_E}\,\bar{F}_E$$

δ_E, γ_E (D-01)

$C_{11_E} = \cos RA_E \cos\delta_E$	$C_{21_E} = C_{32_E}C_{13_E} - C_{33_E}C_{12_E}$
$C_{12_E} = \sin RA_E \cos\delta_E$	$C_{22_E} = C_{33_E}C_{11_E} - C_{31_E}C_{13_E}$
$C_{13_E} = \sin\delta_E$	$C_{23_E} = C_{31_E}C_{12_E} - C_{32_E}C_{11_E}$

$C_{31_E} = -\cos RA_E \sin\delta_E \cos\gamma_E - \sin RA_E \sin\gamma_E$

$C_{32_E} = -\sin RA_E \sin\delta_E \cos\gamma_E + \cos RA_E \sin\gamma_E$

$C_{33_E} = \cos\delta_E \cos\gamma_E$

λ_E (D-01), GHA_E (E-10)

21

$RA_E = GHA_E + \lambda_E$

GHA_E IS SPECIFIED BY UNIVERSAL TIME AT PROBLEM START AND IS HELD CONSTANT DURING A RUN.

35

$b'_{21} = \dfrac{H_{XNIC}}{H_{NIC}} \qquad b'_{22} = \dfrac{H_{YNIC}}{H_{NIC}} \qquad b'_{23} = \dfrac{H_{ZNIC}}{H_{NIC}}$

ELEMENTS b'_{ij} ARE CONSTANT; THEY ARE BASED ON THE CURRENT VALUE OF THE CSM ANGULAR MOMENTUM COMPONENTS AT TIME OF PLATFORM ALIGN.

$(H_X, H_Y, H_Z, H)_{NIC}$ (B-22,24)

b'_{ij}

30 — TRANSFORM FROM INERTIAL M-FRAME TO IDEAL IMU R-FRAME

$$\bar{F}_{R_M} = C_{ij_M}\,\bar{F}_M$$

$C_{21_M} = C_{32_M}C_{13_M} - C_{33_M}C_{12_M}$

$C_{22_M} = C_{33_M}C_{11_M} - C_{31_M}C_{13_M}$

$C_{23_M} = C_{31_M}C_{12_M} - C_{32_M}C_{11_M}$

$C_{31_M} = \left[b'_{22}C_{13_M} - b'_{23}C_{12_M}\right]\dfrac{1}{H'}$

$C_{32_M} = \left[b'_{23}C_{11_M} - b'_{21}C_{13_M}\right]\dfrac{1}{H'}$

$C_{33_M} = \left[b'_{21}C_{12_M} - b'_{22}C_{11_M}\right]\dfrac{1}{H'}$

31

$$H' = \left[(b'_{22}C_{13_M} - b'_{23}C_{12_M})^2 + (b'_{23}C_{11_M} - b'_{21}C_{13_M})^2 + (b'_{21}C_{12_M} - b'_{22}C_{11_M})^2\right]^{\frac{1}{2}}$$

40 — TRANSFORM FROM INERTIAL M OR E-FRAME TO LEM BODY AXIS B-FRAME

$$\bar{F}_B = g_{ij_n}\,\bar{F}_n$$

e_1, e_2, e_3, e_4 (C-22)

$g_{11} = e_1^2 - e_2^2 - e_3^2 + e_4^2$

$g_{12} = 2(e_1e_2 + e_3e_4)$

$g_{13} = 2(e_1e_4 - e_1e_3)$

$g_{21} = 2(e_3e_4 - e_1e_2)$

$g_{22} = e_1^2 - e_2^2 + e_3^2 - e_4^2$

$g_{23} = 2(e_2e_3 + e_4e_1)$

$g_{31} = 2(e_1e_3 + e_2e_4)$

$g_{32} = 2(e_2e_3 - e_1e_4)$

$g_{33} = e_1^2 + e_2^2 - e_3^2 - e_4^2$

32

NOTE: THE ELEMENTS OF a^*_{ij} ARE CONSTANT. THESE ELEMENTS ARE DEFINED (SEE E-20) AT SOME EPOCH TIME t^*. t^* DENOTES THE NOMINAL TIME FROM PROBLEM START TO EITHER:

(1) TOUCHDOWN AT SOME LANDING SITE DESIGNATED BY A SELENOGRAPHIC LATITUDE ϕ_{S_D} AND LONGITUDE λ_{S_D}.

(2) ASCENT FROM SOME TAKE-OFF SITE DESIGNATED BY ϕ_{S_A} AND λ_{S_A}.

$C_{11_M} = a^*_{11}X_{S_K} + a^*_{21}Y_{S_K} + a^*_{31}Z_{S_K}$

$C_{12_M} = a^*_{12}X_{S_K} + a^*_{22}Y_{S_K} + a^*_{32}Z_{S_K}$

$C_{13_M} = a^*_{13}X_{S_K} + a^*_{23}Y_{S_K} + a^*_{33}Z_{S_K}$

a^{T*}_{ij} (D-10)

33

$X_{S_K} = \cos\phi_{S_K}\cos\lambda_{S_K}$

$Y_{S_K} = \cos\phi_{S_K}\sin\lambda_{S_K}$

$Z_{S_K} = \sin\phi_{S_K}$

$\phi_{S_K}, \lambda_{S_K}$ (D-01)

34 — K LOGIC

IF:	THEN:
IMU R-FRAME ESTABLISHED DURING DESCENT	$K = D$
IMU R-FRAME ESTABLISHED DURING ASCENT	$K = A$

K (D-01)

SHEET 1 OF 2

80

TRANSFORM FROM OPTICAL WINDOW W- OR TELESCOPE T- FRAME TO INERTIAL M- FRAME OR E-FRAME

$h_{ij\rho\gamma}$ (D-70)

g_{ij_n} (D-40)

$$\bar{F}_n = l_{ij\rho\gamma_n} \bar{F}_{\rho\gamma}$$

$$\begin{bmatrix} l_{11\rho\gamma} & l_{12\rho\gamma} & l_{13\rho\gamma} \\ l_{21\rho\gamma} & l_{22\rho\gamma} & l_{23\rho\gamma} \\ l_{31\rho\gamma} & l_{32\rho\gamma} & l_{33\rho\gamma} \end{bmatrix}_n = \begin{bmatrix} g_{11} & g_{21} & g_{31} \\ g_{12} & g_{22} & g_{32} \\ g_{13} & g_{23} & g_{33} \end{bmatrix}_n \begin{bmatrix} h_{11\rho\gamma} & h_{21\rho\gamma} & h_{31\rho\gamma} \\ h_{12\rho\gamma} & h_{22\rho\gamma} & h_{32\rho\gamma} \\ h_{13\rho\gamma} & h_{23\rho\gamma} & h_{33\rho\gamma} \end{bmatrix}$$

60

TRANSFORM FROM INERTIAL E-FRAME TO GEOGRAPHIC G-FRAME

GHA (E-10)

$$\bar{F}_G = f_{ij} \bar{F}_E$$

$f_{11} = f_{22} = \cos GHA$ $\qquad f_{13} = f_{23} = f_{31} = f_{32} = 0$

$f_{12} = -f_{21} = \sin GHA$ $\qquad f_{33} = 1$

90

TRANSFORM FROM ALTIMETER BEAM IN BODY AXES TO ALTIMETER BEAM IN SELENOGRAPHIC COORDINATES

g_{ij_n} (D-40)

a_{ij} (D-10)

$$\bar{F}_{SA} = s_{ij} \bar{F}_{BA}$$

$$\begin{bmatrix} s_{11} & s_{13} \\ s_{21} & s_{23} \\ s_{31} & s_{33} \end{bmatrix} = \begin{bmatrix} a_{11} & a_{12} & a_{13} \\ a_{21} & a_{22} & a_{23} \\ a_{31} & a_{32} & a_{33} \end{bmatrix} \begin{bmatrix} g_{11} & g_{31} \\ g_{12} & g_{32} \\ g_{13} & g_{33} \end{bmatrix}_M$$

TRANSFORM FROM THE LEM BODY B-FRAME TO OPTICAL WINDOW W-FRAME OR TELESCOPE T-FRAME

70

$(\phi,\theta,\psi)_{\rho\gamma}$ (J-01)

$$\bar{F}_{\rho\gamma} = h_{ij\rho\gamma} \bar{F}_B$$

$h_{11\rho\gamma} = \cos\psi_{\rho\gamma} \cos\theta_{\rho\gamma}$

$h_{12\rho\gamma} = \cos\psi_{\rho\gamma} \sin\theta_{\rho\gamma} \sin\phi_{\rho\gamma} + \sin\psi_{\rho\gamma} \cos\phi_{\rho\gamma}$

$h_{13\rho\gamma} = -\cos\psi_{\rho\gamma} \sin\theta_{\rho\gamma} \cos\phi_{\rho\gamma} + \sin\psi_{\rho\gamma} \sin\phi_{\rho\gamma}$

$h_{21\rho\gamma} = -\sin\psi_{\rho\gamma} \cos\theta_{\rho\gamma}$

$h_{22\rho\gamma} = -\sin\psi_{\rho\gamma} \sin\theta_{\rho\gamma} \sin\phi_{\rho\gamma} + \cos\psi_{\rho\gamma} \cos\phi_{\rho\gamma}$

$h_{23\rho\gamma} = \sin\psi_{\rho\gamma} \sin\theta_{\rho\gamma} \cos\phi_{\rho\gamma} + \cos\psi_{\rho\gamma} \sin\phi_{\rho\gamma}$

$h_{31\rho\gamma} = \sin\theta_{\rho\gamma}$

$h_{32\rho\gamma} = -\cos\theta_{\rho\gamma} \sin\phi_{\rho\gamma}$

$h_{33\rho\gamma} = \cos\theta_{\rho\gamma} \cos\phi_{\rho\gamma}$

71

NOTES

$$\bar{F}_{\rho\gamma} = h_{ij\rho\gamma} \bar{F}_B$$

SUBSCRIPTS:

$\gamma = l, r, a$

- l DENOTES LEFT
- r DENOTES RIGHT
- a DENOTES ABOVE

$\rho = W, T$

- W DENOTES WINDOW
- T DENOTES TELESCOPE

WINDOW MATRICES l, r, a WILL BE COMPUTED CONCURRENTLY. AT ANY ONE TIME EITHER THE $l, r,$ or, a TELESCOPE MATRIX WILL BE COMPUTED. ANGULAR INPUTS PERTAINING TO THE WINDOW AND TELESCOPE OPTICAL AXES $(\phi,\theta,\psi)_{\rho\gamma}$ ARE GIVEN IN J-01.

01 CONSTANTS AND INITIAL CONDITIONS

- Y — LAUNCH YEAR
- D^* — INTEGER DAYS FROM BEGINNING OF LAUNCH YEAR (GREENWICH MIDNIGHT DECEMBER 31) TO PROBLEM START.
- H — HOURS (U.T.) FROM GREENWICH MIDNIGHT TO PROBLEM START.
- I — HAYN'S CONSTANT - 1.535°

N = INTEGER VALUE OF $\frac{(Y-1953)}{4} + 1$

$d_0 = 365(Y-1950) + N + D^* + \frac{11}{24}$

$T_0 = d_0/36{,}525$

$T^* = T_0 + \frac{t^*/24(3{,}600)}{36{,}525}$

t^* (D-01)

02 JPL EPHEMERIS TAPE OUTPUT
(SEE JPL TR 32-580)
(MEAN EQUINOX JAN 1.0, 1950)

$(X_{E/M})_{50}$ $(Y_{E/M})_{50}$ $(Z_{E/M})_{50}$

$(X_{E/\odot})_{50}$ $(Y_{E/\odot})_{50}$ $(Z_{E/\odot})_{50}$

J.D. (E-22)

EARTH RADII

10 GREENWICH HOUR ANGLE

T_0, H

$(RA)_\odot = 280.081147 + 36000.769305\,T_0 + 0.0003871\,T_0^2$

$GHA = ((RA)_\odot + 180 + 15H + \omega_e t)(\text{MOD } 360°)$

$\omega_e = \frac{360}{86164.09974 + 0.0016\,4T_0}$

31

T_0

$X_x = 1 - 0.29696\times10^{-3}\,T_0^2 - 0.13\times10^{-6}\,T_0^3$

$Y_x = -X_Y = -0.2234941\times10^{-1}\,T_0 - 0.676\times10^{-5}\,T_0^2 + 0.221\times10^{-5}\,T_0^3$

$Z_x = -X_z = -0.971690\times10^{-2}\,T_0 + 0.207\times10^{-5}\,T_0^2 + 0.96\times10^{-6}\,T_0^3$

$Y_Y = 1 - 0.24975\times10^{-3}\,T_0^2 - 0.15\times10^{-6}\,T_0^3$

$Y_z = Z_Y = -0.10858\times10^{-3}\,T_0^2$

$Z_z = 1 - 0.4721\times10^{-4}\,T_0^2$

LUNAR ORBIT ELEMENTS

20

$\Omega = 12.1127902 - 0.0529539\,d + 0.20795\times10^{-2}\,T_0 + 0.2081\times10^{-2}\,T_0^2$

$\mathbb{C} = 64.37545167 + 13.17639653\,d - 0.1131575\times10^{-2}\,T_0 - 0.11302\times10^{-2}\,T_0^2$

$\epsilon = 23.445787 - 0.0130138\,T_0 - 0.8855\times10^{-6}\,T_0^2$

$\Gamma' = 208.8439877 + 0.1114040\,8d - 0.010334\,T_0 - 0.010343\,T_0^2$

$= 358.009067 + 0.9856005\,d$

MATRIX COMPUTE $\Omega, \mathbb{C}, \epsilon$ AT FIXED TIME T^*

T_0, T^*

UPDATING FROM MEAN EQUINOX JAN 1.0 1950 TO MEAN EQUINOX OF DATE

30

$X_{E/M} = X_x(X_{E/M})_{50} + Y_x(Y_{E/M})_{50} + Z_x(Z_{E/M})_{50}$

$Y_{E/M} = X_Y(X_{E/M})_{50} + Y_Y(Y_{E/M})_{50} + Z_Y(Z_{E/M})_{50}$

$Z_{E/M} = X_z(X_{E/M})_{50} + Y_z(Y_{E/M})_{50} + Z_z(Z_{E/M})_{50}$

$X_{E/\odot} = X_x(X_{E/\odot})_{50} + Y_x(Y_{E/\odot})_{50} + Z_x(Z_{E/\odot})_{50}$

$Y_{E/\odot} = X_Y(X_{E/\odot})_{50} + Y_Y(Y_{E/\odot})_{50} + Z_Y(Z_{E/\odot})_{50}$

$Z_{E/\odot} = X_z(X_{E/\odot})_{50} + Y_z(Y_{E/\odot})_{50} + Z_z(Z_{E/\odot})_{50}$

$r_{E/\odot} = \left[(X_{E/\odot})^2 + (Y_{E/\odot})^2 + (Z_{E/\odot})^2\right]^{\frac{1}{2}}$

21

$\ldots 696984\times10^{-7} + 0.63012538\times10^{-18}\,d$

$\ldots 1706\times10^{-5} - 0.3422086\times10^{-18}\,d$

d

d, d^*

22

$d = d_0 + t/24(3600)$

$d^* = d_0 + t^*/24(3600)$

$J.D. = 2{,}433{,}282.5 + d$

d_0

t^* (D-01)

RENDEZVOUS RADAR

F

SHEET 1 OF 1

LINE-OF-SIGHT RANGE AND RANGE RATE LOGIC (10)

IF:	THEN:
LUNAR MISSION (n=M) AND $\rho_{LS} > D_2$	$\rho_{LS} = +\sqrt{\rho_{XM}^2 + \rho_{YM}^2 + \rho_{ZM}^2}$; $\dot{\rho}_{LS} = \frac{\rho_{XM}\dot{\rho}_{XM} + \rho_{YM}\dot{\rho}_{YM} + \rho_{ZM}\dot{\rho}_{ZM}}{\rho_{LS}}$
LUNAR MISSION (n=M) AND $\rho_{LS} \leq D_1$ OR EARTH MISSION (n=E)	ρ_{LS} FROM (B-12) ; $\dot{\rho}_{LS} = \frac{\rho_X\dot{\rho}_X + \rho_Y\dot{\rho}_Y + \rho_Z\dot{\rho}_Z}{\rho_{LS}}$

$D_{1,2}$ (B-01)

ρ_X, ρ_Y, ρ_Z (B-12) $\quad \dot{\rho}_X, \dot{\rho}_Y, \dot{\rho}_Z$ (B-11)

$(X, Y, Z)_{M/L}$ (A-12) $\quad (X, Y, Z)_{M/C}$ (B-20)

(12)

$$\rho_{XM} = X_{M/C} - X_{M/L}$$
$$\rho_{YM} = Y_{M/C} - Y_{M/L}$$
$$\rho_{ZM} = Z_{M/C} - Z_{M/L}$$

CSM COORDINATES WRT LEM MEASURED IN M-FRAME

$(\dot{X}, \dot{Y}, \dot{Z})_{M/L}$ (A-11) $\quad (\dot{X}, \dot{Y}, \dot{Z})_{M/C}$ (B-20)

(11)

$$\dot{\rho}_{XM} = \dot{X}_{M/C} - \dot{X}_{M/L}$$
$$\dot{\rho}_{YM} = \dot{Y}_{M/C} - \dot{Y}_{M/L}$$
$$\dot{\rho}_{ZM} = \dot{Z}_{M/C} - \dot{Z}_{M/L}$$

INERTIAL M-FRAME VELOCITIES OF CSM WRT LEM

RELATIVE DISTANCES AND INERTIAL VELOCITIES OF CSM WRT LEM IN M- OR E-FRAME COORDINATES

ρ^* AND $\dot{\rho}^*$ LOGIC (25)

IF:	THEN:
LUNAR MISSION (n=M) AND $\rho_{LS} > D_2$	$\rho_X^* = \rho_{XM}$; $\dot{\rho}_X^* = \dot{\rho}_{XM}$ $\rho_Y^* = \rho_{YM}$; $\dot{\rho}_Y^* = \dot{\rho}_{YM}$ $\rho_Z^* = \rho_{ZM}$; $\dot{\rho}_Z^* = \dot{\rho}_{ZM}$
LUNAR MISSION (n=M) AND $\rho_{LS} \leq D_1$ OR EARTH MISSION (n=E)	$\rho_X^* = -\rho_X$; $\dot{\rho}_X^* = -\dot{\rho}_X$ $\rho_Y^* = -\rho_Y$; $\dot{\rho}_Y^* = -\dot{\rho}_Y$ $\rho_Z^* = -\rho_Z$; $\dot{\rho}_Z^* = -\dot{\rho}_Z$

$D_{1,2}$ (B-01) $\quad \rho_{LS}$

(ρ_X, ρ_Y, ρ_Z) (B-12) $\quad (\dot{\rho}_X, \dot{\rho}_Y, \dot{\rho}_Z)$ (B-11)

TOTAL LINE-OF-SIGHT AND TRACKING LINE ANGULAR RATES

(30)

$\dot{E}_{LS}$, E_{LS}

$$\omega_{LS_{ab}} = \dot{A}_{LS} + p_B \cos E_{LS} - r_B \sin E_{LS}$$
$$\omega_{LS_{ib}} = \dot{E}_{LS} \cos A_{LS} + p_B \sin A_{LS} \sin E_{LS} + q_B \cos A_{LS} + r_B \sin A_{LS} \cos E_{LS}$$

p_B, q_B, r_B (C-11) $\quad E_{TL}, A_{TL}$ (RENDEZVOUS RADAR SUB-SYSTEM MATH MODEL)

(31)

$$\omega_{B_{ab}} = p_B \cos E_{TL} - r_B \sin E_{TL}$$
$$\omega_{B_{ib}} = p_B \sin A_{TL} \sin E_{TL} + q_B \cos A_{TL} + r_B \sin A_{TL} \cos E_{TL}$$
$$\omega_{TL_r} = p_B \cos A_{TL} \sin E_{TL} - q_B \sin A_{TL} + r_B \cos A_{TL} \cos E_{TL}$$

LEM BODY ANGULAR RATES MEASURED ALONG TRACKING-LINE AXES

A_{LS}, $\dot{A}_{LS}$

LINE-OF-SIGHT GIMBAL ANGLES AND RATES

(20)

$$E_{LS} = \tan^{-1}\left[\frac{\rho_{XB}}{\rho_{ZB}}\right]$$
$$\dot{E}_{LS} = \frac{\cos^2 E_{LS}}{\rho_{ZB}}\left[\dot{\rho}_{XB} - \dot{\rho}_{ZB} \tan E_{LS}\right]$$

$\dot{E}_{LS}$, E_{LS}

(22)

IF:	THEN: SET
$\rho_{Y_B} = 0$	$\dot{A}_{LS} = 0$
$\rho_{Z_B} = 0$	$\dot{E}_{LS} = 0$
$\rho_{Z_B} = \rho_{X_B} = 0$	$E_{LS} = 0$

E_{LS}, $\dot{E}_{LS}$ $\quad \dot{A}_{LS}$ $\quad \rho_{X_B}, \rho_{Y_B}, \rho_{Z_B}$

(21)

$$A_{LS} = \tan^{-1}\left[\frac{-\rho_{YB}}{\rho_{XB}\sin E_{LS} + \rho_{ZB}\cos E_{LS}}\right]$$
$$\dot{A}_{LS} = \frac{\sin^2 A_{LS}}{\rho_{YB}^2}\left[\left[\sin E_{LS}\left[\rho_{YB}\dot{\rho}_{XB} - \rho_{XB}\dot{\rho}_{YB}\right] + \cos E_{LS}\left[\rho_{YB}\dot{\rho}_{ZB} - \rho_{ZB}\dot{\rho}_{YB}\right]\right]\right]$$

CSM COORDINATES WRT LEM MEASURED IN LEM B-FRAME (23)

$\rho_X^*, \rho_Y^*, \rho_Z^*$

$$\rho_{XB} = g_{11n}\rho_X^* + g_{12n}\rho_Y^* + g_{13n}\rho_Z^*$$
$$\rho_{YB} = g_{21n}\rho_X^* + g_{22n}\rho_Y^* + g_{23n}\rho_Z^*$$
$$\rho_{ZB} = g_{31n}\rho_X^* + g_{32n}\rho_Y^* + g_{33n}\rho_Z^*$$

g_{ijn} (D-40)

RELATIVE VELOCITY OF CSM WRT LEM MEASURED IN LEM B-FRAME (24)

$\dot{\rho}_X^*, \dot{\rho}_Y^*, \dot{\rho}_Z^*$

$$\dot{\rho}_{XB} = g_{11n}\dot{\rho}_X^* + g_{12n}\dot{\rho}_Y^* + g_{13n}\dot{\rho}_Z^*$$
$$\dot{\rho}_{YB} = g_{21n}\dot{\rho}_X^* + g_{22n}\dot{\rho}_Y^* + g_{23n}\dot{\rho}_Z^*$$
$$\dot{\rho}_{ZB} = g_{31n}\dot{\rho}_X^* + g_{32n}\dot{\rho}_Y^* + g_{33n}\dot{\rho}_Z^*$$

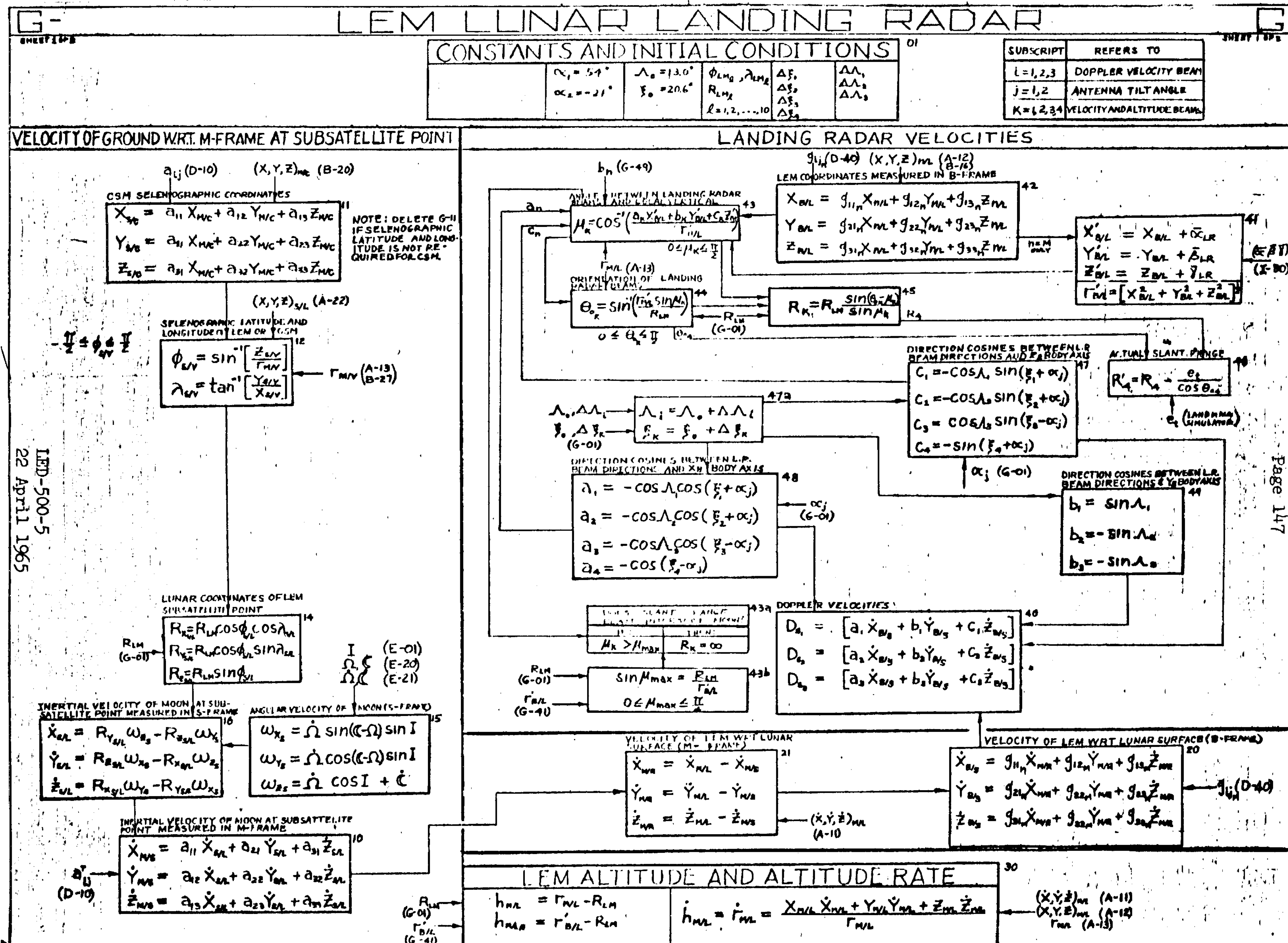

G-
LEM LUNAR LANDING RADAR
G
CONSTANTS AND INITIAL CONDITIONS
01
SUBSCRIPT
REFERS TO
i = 1,2,3
DOPPLER VELOCITY BEAM
j = 1,2
ANTENNA TILT ANGLE
K = 1,2,3,4
VELOCITY AND ALTITUDE BEAMS
VELOCITY OF GROUND W.R.T. M-FRAME AT SUBSATELLITE POINT
CSM SELENOGRAPHIC COORDINATES
11
NOTE: DELETE G-11 IF SELENOGRAPHIC LATITUDE AND LONGITUDE IS NOT REQUIRED FOR CSM.
SELENOGRAPHIC LATITUDE AND LONGITUDE OF LEM OR CSM
12
LUNAR COORDINATES OF LEM SUBSATELLITE POINT
14
INERTIAL VELOCITY OF MOON AT SUBSATELLITE POINT MEASURED IN S-FRAME
16
ANGULAR VELOCITY OF MOON (S-FRAME)
15
INERTIAL VELOCITY OF MOON AT SUBSATELLITE POINT MEASURED IN M-FRAME
10
LANDING RADAR VELOCITIES
LEM COORDINATES MEASURED IN B-FRAME
42
ANGLE BETWEEN LANDING RADAR BEAM AND LOCAL VERTICAL
43
ORIENTATION OF LANDING RADAR BEAM
44
45
41
DIRECTION COSINES BETWEEN L.R. BEAM DIRECTIONS AND Z_B BODY AXIS
47
ACTUAL SLANT RANGE
46
47a
DIRECTION COSINES BETWEEN L.R. BEAM DIRECTIONS AND X_B BODY AXIS
48
DIRECTION COSINES BETWEEN L.R. BEAM DIRECTIONS & Y_B BODY AXIS
44
43a
43b
DOPPLER VELOCITIES
40
VELOCITY OF LEM WRT LUNAR SURFACE (M-FRAME)
21
VELOCITY OF LEM WRT LUNAR SURFACE (B-FRAME)
20
LEM ALTITUDE AND ALTITUDE RATE
30

G- SHEET 2 OF 2

LEM LUNAR LANDING RADAR

G SHEET 2 OF 2

LAND MASS SIMULATOR COORDINATE DRIVES

FIXED SELENOGRAPHIC COORDINATES OF FILM TRANSPORT ORIGIN (51)

$$R_{X_{LM}} = R_{LM} \cos\phi_{LM} \cos\lambda_{LM}$$
$$R_{Y_{LM}} = R_{LM} \cos\phi_{LM} \sin\lambda_{LM}$$
$$R_{Z_{LM}} = R_{LM} \sin\phi_{LM}$$

Inputs: R_{LM} (G-01); ϕ_{LM}, λ_{LM} (G-01)

INITIAL POSITION OF SUBSATELLITE PT. WRT LAND MASS ORIGIN (52)

$$\Delta X_{s_0} = R_{X_{SL_0}} - R_{X_{LM}}$$
$$\Delta Y_{s_0} = R_{Y_{SL_0}} - R_{Y_{LM}}$$
$$\Delta Z_{s_0} = R_{Z_{SL_0}} - R_{Z_{LM}}$$

INITIALIZE $(R_X, R_Y, R_Z)_{SL}$ WHEN LAND MASS SIMULATOR IS ACTIVATED. AT LIFT-OFF $\Delta X_s = \Delta Y_s = \Delta Z_s = 0$ SINCE $R_{SL_0} = R_{LM}$

Input: $(R_X, R_Y, R_Z)_{SL}$ (G-14)

SELENOGRAPHIC COORDINATES OF SUBSATELLITE POINT RELATIVE TO LAND MASS ORIGIN (53)

$$\Delta X_s = \Delta X_{s_0} - \int (a_{11}\dot{X}_{NR} + a_{12}\dot{Y}_{NR} + a_{13}\dot{Z}_{NR})\,dt$$
$$\Delta Y_s = \Delta Y_{s_0} - \int (a_{21}\dot{X}_{NR} + a_{22}\dot{Y}_{NR} + a_{23}\dot{Z}_{NR})\,dt$$
$$\Delta Z_s = \Delta Z_{s_0} - \int (a_{31}\dot{X}_{NR} + a_{32}\dot{Y}_{NR} + a_{33}\dot{Z}_{NR})\,dt$$

Inputs: a_{ij} (D-10); $(\dot{X}, \dot{Y}, \dot{Z})_{NR}$ (G-21)

LEM SUBSATELLITE POINT MEASURED IN LAND MASS COORDINATES (50)

$$Y_{LM} = \sin\lambda_{LM}\,\Delta X_s + \cos\lambda_{LM}\,\Delta Y_s$$
$$Z_{LM} = -\sin\phi_{LM}\left[\cos\lambda_{LM}\,\Delta X_s + \sin\lambda_{LM}\,\Delta Y_s\right] + \cos\phi_{LM}\,\Delta Z_s$$

Input: ϕ_{LM}, λ_{LM} (G-01)

LAND MASS SIMULATOR AZIMUTH DRIVE

COORDINATES OF VECTOR FROM LEM TO INTERSECTION OF ALTIMETER BEAM WITH LUNAR ELLIPSOID, IN BODY AXES (61)

$$X_{B/4} = -R_4 \cos(\xi_4 + \alpha_j)$$
$$Z_{B/4} = -R_4 \sin(\xi_4 + \alpha_j)$$

Inputs: R_4 (G-45); ξ_4, α_j (G-47a,01)

ALTIMETER BEAM COORDINATE TRANSFORMATION FROM BODY AXES TO SELENOCENTRIC COORDINATES (62)

$$X_{S/4} = S_{11} X_{B/4} + S_{13} Z_{B/4}$$
$$Y_{S/4} = S_{21} X_{B/4} + S_{23} Z_{B/4}$$
$$Z_{S/4} = S_{31} X_{B/4} + S_{33} Z_{B/4}$$

Input: S_{ij} (D-90)

SELENOGRAPHIC VECTOR FROM SUBSATELLITE POINT TO INTERSECTION OF ALTIMETER BEAM WITH LUNAR SURFACE (63)

$$\Delta X_{S/4} = X_{S/L} + X_{S/4} - R_{X_{SL}}$$
$$\Delta Y_{S/4} = Y_{S/L} + Y_{S/4} - R_{Y_{SL}}$$
$$\Delta Z_{S/4} = Z_{S/L} + Z_{S/4} - R_{Z_{SL}}$$

Inputs: $(X, Y, Z)_{S/L}$ (A-28); (R_X, R_Y, R_Z) (G-14)

COMPONENTS OF SUBSATELLITE POINT-TO-BEAM INTERSECTION POINT VECTOR IN LAND MASS COORDINATES (64)

$$\Delta Y_4 = -\sin\lambda_{LM}\,\Delta X_{S/4} + \cos\lambda_{LM}\,\Delta Y_{S/4}$$
$$\Delta Z_4 = -\sin\phi_{LM}(\cos\lambda_{LM}\,\Delta X_{S/4} + \sin\lambda_{LM}\,\Delta Y_{S/4}) + \cos\phi_{LM}\,\Delta Z_{S/4}$$

Input: ϕ_{LM}, λ_{LM} (G-01)

SCANNING AZIMUTH IN FILM TRANSPORT COORDINATES (60)

$$\gamma_{LM} = \tan^{-1}\left(\frac{\Delta Y_4}{\Delta Z_4}\right)$$

LOGIC FOR SCANNING AZIMUTH ANGLE (65)

IF:	THEN: SET
$\gamma_{LM} = \tan^{-1}\left(\frac{0}{0}\right)$	$\gamma_{LM} = 0$

LEM-CSM COMMUNICATION CAPABILITY

10

IF:		THEN LEM-CSM COMMUNICATION:
$R_c^* \geq R_n$		POSSIBLE ($B_{115}=1$)
$R_c^* < R_n$	$\sigma_c \leq \sigma_c^*$	POSSIBLE ($B_{115}=1$)
	$\sigma_c > \sigma_c^*$	NOT POSSIBLE ($B_{115}=0$)

R_M, R_e (A-01)(H-01)

11

$$R_c^* = \frac{r_{M/C}\, r_{M/L} \sin\sigma_c}{r_{L/S}}$$

$$\sigma_c^* = \cos^{-1}\left(\frac{R_M}{r_{M/C}}\right)$$

$0 \leq \sigma_c^* \leq \frac{\pi}{2}$

R_e (F-10)

$(X,Y,Z,r)_{M/C}$ (A-20,27) $(X,Y,Z,r)_{M/L}$ (A-12,13)(B-16,15)

LEM-CSM CENTRAL ANGLE 12

$$\sigma_c = \cos^{-1}\left[\frac{X_{M/L} X_{M/C} + Y_{M/L} Y_{M/C} + Z_{M/L} Z_{M/C}}{r_{M/L}\, r_{M/C}}\right]$$

$0 \leq \sigma_c \leq \pi$

LEM-EARTH STATION COMMUNICATION CAPABILITY

LEM IN LUNAR ORBIT COMMUNICATING WITH EARTH STATION 30

IF:		THEN LEM-EARTH STATION COMMUNICATION:
$\sin\delta_{i_M} < \sin\delta_{i_{LIMIT}}$		NOT POSSIBLE ($B_{112}=0$)
$\sin\delta_{i_M} \geq \sin\delta_{i_{LIMIT}}$	$R_i^* \geq R_M$	POSSIBLE ($B_{112}=1$)
	$R_i^* < R_M$, $\sigma_{E_i} \leq \sigma_{E_i}^*$	POSSIBLE ($B_{112}=1$)
	$R_i^* < R_M$, $\sigma_{E_i} > \sigma_{E_i}^*$	NOT POSSIBLE ($B_{112}=0$) (LEM IS BACK SIDE OF MOON)

R_M (A-01) $\delta_{i_{LIMIT}}$ (H-01) $\sin\delta_{i_M}$ σ_{E_i} R_i^* $\sigma_{E_i}^*$

TRACKING STATION ELEVATION ANGLE (δ_i) AND OCCULTATION ANGLE (σ_{E_i}) 31

$$\sin\delta_{i_M} = -\left[\frac{X_M X_{E/G_i} + Y_M Y_{E/G_i} + Z_M Z_{E/G_i}}{r_{E/G_i}\, r_{G_i/L}} + \frac{r_{E/G_i}}{r_{G_i/L}}\right]$$

$$\sigma_{E_i} = \cos^{-1}\left[\frac{(X_{E/G_i}-X_{E/M})X_{M/L} + (Y_{E/G_i}-Y_{E/M})Y_{M/L} + (Z_{E/G_i}-Z_{E/M})Z_{M/L}}{r_i'\, r_{M/L}}\right]$$

$0 \leq \sigma_{E_i} \leq \pi$

$(X,Y,Z)_{E/M}$ (E-30) $(X,Y,Z)_{M/L}$ (A-12) $r_{M/L}$ (A-13) r_i' $r_{G_i/L}$

32

$$R_i^* = \frac{r_i'\, r_{M/L} \sin\sigma_{E_i}}{r_{G_i/L}}\ ;\quad \sigma_{E_i}^* = \cos^{-1}\left(\frac{R_M}{r_i'}\right)$$

$0 \leq \sigma_{E_i}^* \leq \frac{\pi}{2}$

$(X,Y,Z)_{E/M}$ (E-30) $r_{M/L}$ (A-13) R_M (A-01)

33

$$r_{G_i/L} = \left[(X_M + X_{E/G_i})^2 + (Y_M + Y_{E/G_i})^2 + (Z_M + Z_{E/G_i})^2\right]^{\frac{1}{2}}$$

$$r_i' = \left[(X_{E/M} - X_{E/G_i})^2 + (Y_{E/M} - Y_{E/G_i})^2 + (Z_{E/M} - Z_{E/G_i})^2\right]^{\frac{1}{2}}$$

INITIAL CONDITIONS AND CONSTANTS

01

$K = 1, 2, 3$

$i = 1, 2, \dots n$ (i DENOTES THE NUMBER OF EARTH iTH TRACKING STATION)

ϕ_i	$A_{A_{L_1}}$	$A_{A_{C_1}}$	$A_{A_{E_1}'}$
λ_i	$A_{A_{L_2}}$	$A_{A_{C_2}}$	$A_{A_{E_2}'}$
H_i	$E_{A_{L_1}}$	$E_{A_{C_1}}$	$E_{A_{E_1}'}$
$\delta_{i_{LIMIT}}$	$E_{A_{L_2}}$	$E_{A_{C_2}}$	$E_{A_{E_2}'}$

$R_e = 20.92573818 \times 10^6$ FT.

$e^2 = 0.0066934219$; $J_2 = 1.62345 \times 10^{-3}$

LEM IN EARTH ORBIT COMMUNICATING WITH EARTH STATION 34

IF:	THEN LEM-EARTH STATION COMMUNICATION:
$\sin\delta_{i_E} \geq \sin\delta_{i_{LIMIT}}$	POSSIBLE
$\sin\delta_{i_E} < \sin\delta_{i_{LIMIT}}$	NOT POSSIBLE

35

$$\sin\delta_{i_E} = -\left[\frac{X_{E/G_i} X_{E_i} + Y_{E/G_i} Y_{E_i} + Z_{E/G_i} Z_{E_i}}{r_{E/G_i}\, r_{E_i}}\right]$$

$(X,Y,Z)_{E/L}$ (B-16) $(X,Y,Z)_{E/G_i}$ (H-20)

EARTH GROUND TRACKING STATION COORDINATES

EARTH ROTATION RATE CORRECTION DURING INDEPENDENT LHS MODE 22

DURING INDEPENDENT LHS EARTH OPERATION REPLACE $GHA + \lambda_i$ IN H-20 WITH $GHA + \lambda_i - \dot{\Omega}t$

WHERE:

$$\dot{\Omega} = \frac{-J_2\, \bar{n}\, Y_e}{\left[\frac{a_e}{R_e}(1-e_e^2)\right]^2} \cos i_e$$

$$\cos i_e = \frac{H_{Ze/L}}{H_{e/L}}\ ;\quad a_e = \left[1 - \frac{H_{e/L}^2}{a_e \mu_e}\right]^{\frac{1}{2}}$$

$$\bar{n} = \sqrt{\frac{\mu_e}{a_e^3}}\left[1 + \frac{J_2}{\left[\frac{a_e}{R_e}(1-e_e^2)\right]^2}\left(1 - \frac{3}{2}\sin^2 i_e\right)\sqrt{1-e_e^2}\right]$$

a_e (H-21)

$(H,H_z)_{e/L}$ (H-24,20) μ_e (B-01) J_2, R_e (H-01) Ω (C-01)

COORDINATES OF GROUND TRACKING STATION MEASURED IN E-FRAME 20

$$X_{E/G_i} = (R_e C_i + H_i)\cos\phi_i \cos(GHA + \lambda_i)$$

$$Y_{E/G_i} = (R_e C_i + H_i)\cos\phi_i \sin(GHA + \lambda_i)$$

$$Z_{E/G_i} = (R_e S_i + H_i)\sin\phi_i$$

$$r_{E/G_i} = \left[X_{E/G_i}^2 + Y_{E/G_i}^2 + Z_{E/G_i}^2\right]^{\frac{1}{2}}$$

21

$$C_i = \left[1 - e^2 \sin^2\phi_i\right]^{-\frac{1}{2}}$$

$$S_i = (1-e^2)C_i$$

GHA (E-10) e^2, ϕ_i (H-01) $R_e, H_i, \lambda_i, \phi_i$ (H-01)

S-BAND STEERABLE AND OMNI (LOG SPIRAL) ANTENNA ANGLES FOR EARTH COMMUNICATION

COORDINATES OF LEM WRT EARTH IN LEM B-FRAME (LUNAR OR EARTH ORBIT) 45

$$X_{B_M} = g_{11_M} X_M + g_{12_M} Y_M + g_{13_M} Z_M$$

$$Y_{B_M} = g_{21_M} X_M + g_{22_M} Y_M + g_{23_M} Z_M$$

$$Z_{B_M} = g_{31_M} X_M + g_{32_M} Y_M + g_{33_M} Z_M$$

g_{ijM} (D-40)

LUNAR ORBIT: COORDINATES OF LEM WRT EARTH IN INERTIAL M-FRAME (EARTH-CENTER POINTING) 43

$$X_M = -(X_{M/L} + X_{E/M})$$

$$Y_M = -(Y_{M/L} + Y_{E/M})$$

$$Z_M = -(Z_{M/L} + Z_{E/M})$$

$$r_M = \left[X_M^2 + Y_M^2 + Z_M^2\right]^{\frac{1}{2}}$$

$(X,Y,Z)_{M/L}$ (A-12) $(X,Y,Z)_{E/M}$ (E-30)

EARTH ORBIT: COORDINATES OF LEM WRT EARTH IN INERTIAL E-FRAME (iTH TRACKING STATION POINTING) 44

$$X_{E_i} = X_{E/G_i} - X_{E/L}$$

$$Y_{E_i} = Y_{E/G_i} - Y_{E/L}$$

$$Z_{E_i} = Z_{E/G_i} - Z_{E/L}$$

$$r_{E_i} = \left[X_{E_i}^2 + Y_{E_i}^2 + Z_{E_i}^2\right]^{\frac{1}{2}}$$

$(X,Y,Z)_{E/G_i}$ (H-20) $(X,Y,Z)_{E/L}$ (B-16)

COMMUNICATION ANTENNA ANGLE (ELEVATION) 40

$$\theta_c = \tan^{-1}\left[\frac{X_{B_M}}{Z_{B_M}}\right]$$

41

IF:	THEN: SET
$X_{B_M} = Z_{B_M} = 0$	$\theta_c = 0$

COMMUNICATION ANTENNA ANGLE (AZIMUTH) 42

$$\phi_c = \tan^{-1}\left[\frac{-Y_{B_M}}{X_{B_M}\sin\theta_c + Z_{B_M}\cos\theta_c}\right]$$

LEM SPIRAL ANTENNA ALIGNMENT ANGLE FOR EARTH COMMUNICATION IN EARTH ORBIT 47

$$\cos\gamma_j' = \frac{X_{E_i}\ell_{1E_j} + Y_{E_i}\ell_{2E_j} + Z_{E_i}\ell_{3E_j}}{r_{E_i}}$$

LEM SPIRAL ANTENNA ALIGNMENT ANGLE FOR EARTH COMMUNICATION IN LUNAR ORBIT 46

$$\cos\gamma_j' = \frac{X_M \ell_{1M_j} + Y_M \ell_{2M_j} + Z_M \ell_{3M_j}}{r_M}$$

COMPUTE DURING ENGAGE ... CONDITION ONLY WHEN S-BAND STEERABLE IS INOPERATIVE.

j = ANTENNA 1, 2

$L_{M_{ij}} = \ell_{E_{ij}}$ (H-02)

LEM-EARTH, LEM-CSM COMMUNICATION REQS. DURING LUNAR & EARTH OPERATIONS

SHEET 2 OF 2

VHF COMMUNICATION CAPABILITY

NOTE: ACTIVATE LOOP ONLY WHEN LEM-CSM COMMUNICATION IS POSSIBLE (PER H-10).
i = ANTENNA 1, 2.

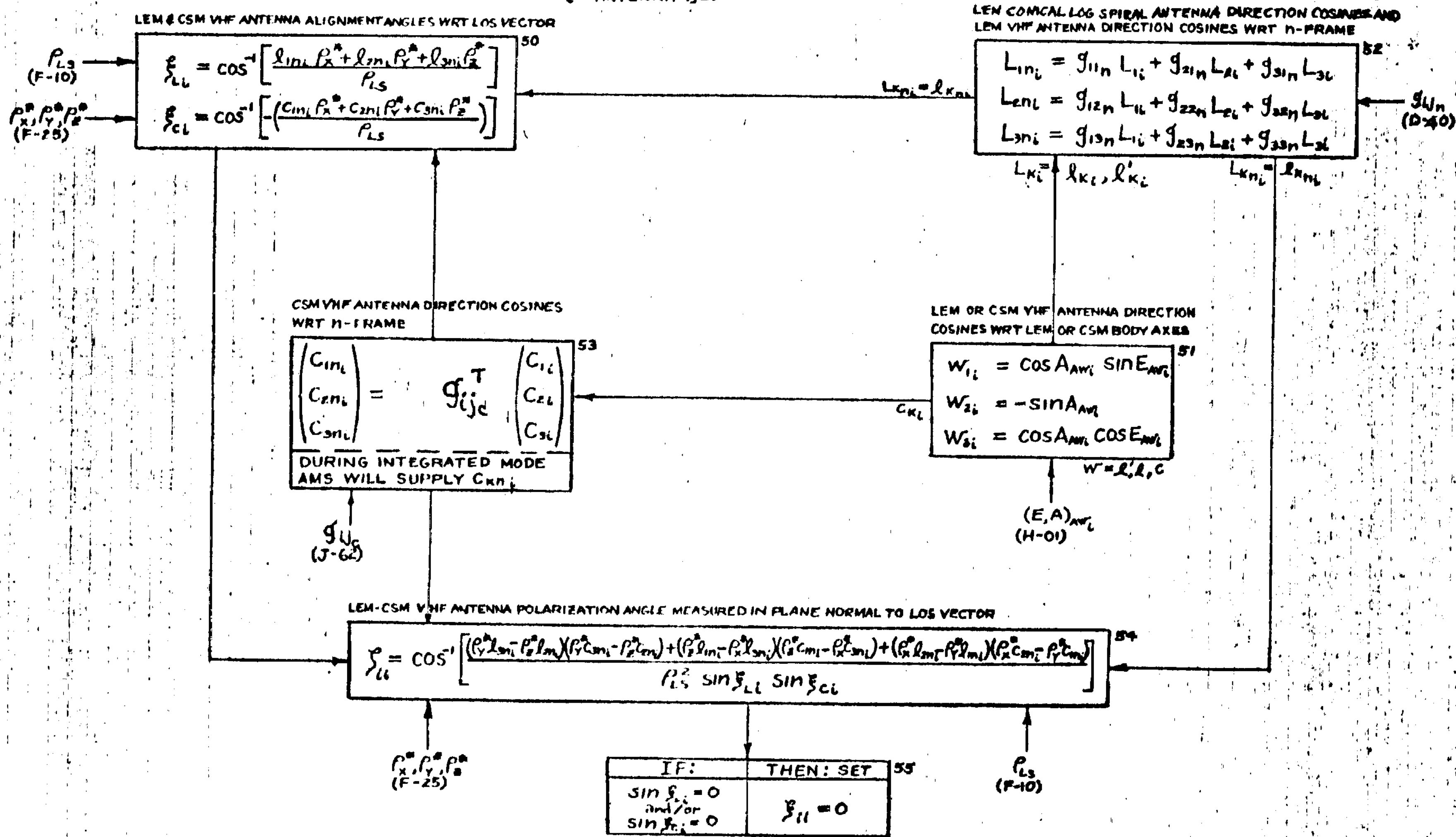

SHEET 2 OF 2

WEIGHTS AND BALANCE

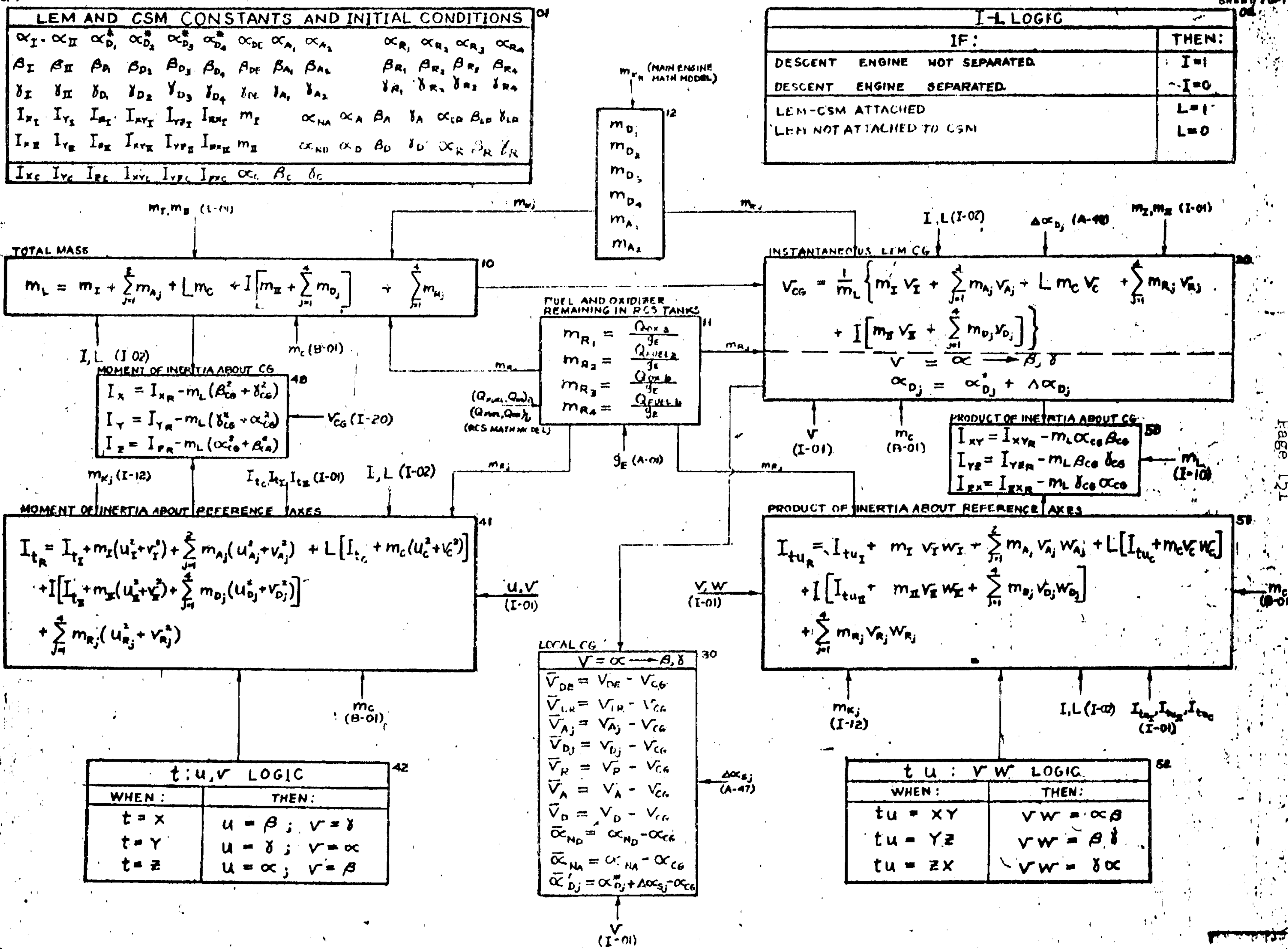

VISUAL DISPLAY DRIVES

SHEET 1 OF 4

CELESTIAL SPHERE DRIVES

CELESTIAL SPHERE GIMBAL ANGLES (10)

$$a_{P\gamma} = \tan^{-1}\left[\frac{-n_{31P\gamma}}{n_{32P\gamma}}\right] \; ; \; b_{P\gamma} = \tan^{-1}\left[\frac{n_{33}}{-n_{31}\sin a_{P\gamma} + n_{32}\cos a_{P\gamma}}\right]$$

$$c_{P\gamma} = \tan^{-1}\left[\frac{n_{11}\sin a_{P\gamma} + n_{12}\cos a_{P\gamma}}{n_{21}\sin a_{P\gamma} + n_{22}\cos a_{P\gamma}}\right]$$

GIMBAL LOCK LOGIC (11)

IF:	THEN:
$\frac{\pi}{2} - \epsilon^{*} \le b_{P\gamma} \le \frac{\pi}{2}$	$a_{P\gamma}$ = CONSTANT DEFINED WHEN $b_{P\gamma} = \frac{\pi}{2} - \epsilon^{*}$
$-\frac{\pi}{2} \le b_{P\gamma} \le -\frac{\pi}{2} + \epsilon^{*}$	$a_{P\gamma}$ = CONSTANT DEFINED WHEN $b_{P\gamma} = -\frac{\pi}{2} + \epsilon^{*}$

ϵ^{*} (C-01)

TRANSFORMATION FROM WINDOW AXES TO MEAN ECLIPTIC AXES OF DATE (12)

$$n_{11P\gamma} = l_{11P\gamma_n}$$
$$n_{12P\gamma} = l_{13P\gamma_n}$$
$$n_{21P\gamma} = l_{21P\gamma_n}\cos\epsilon + l_{31P\gamma_n}\sin\epsilon$$
$$n_{22P\gamma} = l_{22P\gamma_n}\cos\epsilon + l_{32P\gamma_n}\sin\epsilon$$
$$n_{31P\gamma} = -l_{21P\gamma_n}\sin\epsilon + l_{31P\gamma_n}\cos\epsilon$$
$$n_{32P\gamma} = -l_{22P\gamma_n}\sin\epsilon + l_{32P\gamma_n}\cos\epsilon$$
$$n_{33P\gamma} = -l_{23P\gamma_n}\sin\epsilon + l_{33P\gamma_n}\cos\epsilon$$

ϵ (F-20); $l_{ijP\gamma_n}$ (D-80)

SOLAR OCCULTER

$(X,Y,Z)_{E/O}$ (E-30)

POSITION OF SUN IN WINDOW OR TELESCOPE AXES (30)

$l_{ijP\gamma_n}$ (D-80)

$$X^{o}_{P\gamma} = l_{11P\gamma_n} X_{N/O} + l_{21P\gamma_n} Y_{N/O} + l_{31P\gamma_n} Z_{N/O}$$
$$Y^{o}_{P\gamma} = l_{12P\gamma_n} X_{N/O} + l_{22P\gamma_n} Y_{N/O} + l_{32P\gamma_n} Z_{N/O}$$
$$Z^{o}_{P\gamma} = l_{13P\gamma_n} X_{N/O} + l_{23P\gamma_n} Y_{N/O} + l_{33P\gamma_n} Z_{N/O}$$

POSITION OF SUN RELATIVE TO MOON M-FRAME (31)

$(X,Y,Z)_{E/L}$ (E-30); $(X,Y,Z)_{E/M}$ (E-30)

$$X_{M/O} = X_{E/O} - X_{E/M}$$
$$Y_{M/O} = Y_{E/O} - Y_{E/M}$$
$$Z_{M/O} = Z_{E/O} - Z_{E/M}$$
$$r_{M/O} = \left[(X_{M/O})^2 + (Y_{M/O})^2 + (Z_{M/O})^2\right]^{\frac{1}{2}}$$

STAR-FIELD WASHOUT DUE TO DIRECT SUNLIGHT (32)

$r_{E/O}$ (E-30)

$$\cos \gamma^{o}_{P\gamma} = \frac{Z^{o}_{P\gamma}}{r_{N/O}}$$
$$0 \le \gamma^{o}_{P\gamma} \le \pi$$

(33)

IF:	THEN:
$\gamma^{o}_{P\gamma} < \gamma^{o}_{P\gamma max}$	SUN IS IN WINDOW. INCREASE STAR-FIELD ILLUMINATION
$\gamma^{o}_{P\gamma} \ge \gamma^{o}_{P\gamma max}$	NORMAL STAR-FIELD ILLUMINATION

CONSTANTS AND INITIAL CONDITIONS (01)

$\gamma = l, r, \text{ or } a$; $P = W \text{ or } T$; $n = M \text{ or } E$

$\theta_{ETg}, \theta_{EWa}$	$\phi_{WL} = +$
ϕ_{ETg}, ϕ_{EWa}	$\theta_{WL} = -$
γ_{PRSMg}	$\psi_{WL} = 0$
γ_{MAWa}	$\phi_{WR} = -$
$\Lambda^{*}_{P\gamma}$	$\theta_{WR} = -$
ρ_{LS}	$\psi_{WR} = 0$
	$\phi_{WA} = 0$
	$\theta_{WA} = +$
	$\psi_{WA} = 0$
$\rho_{P\gamma max}$	$\phi_{TL} = +$
$d_{P\gamma}$	$\theta_{TL} = +$
	$\psi_{TL} = -$
	$\phi_{TR} = -$
	$\theta_{TR} = +$
$n_{max}, \Delta\gamma^{o}$	$\psi_{TR} = +$
$\sigma^{o}_{min}, \sigma^{o}_{max}$	$\phi_{TA} = 0$
$\gamma^{o}_{P\gamma max}, \sigma^{-o}$	$\theta_{TA} = +$
	$\psi_{TA} = 0$

EARTH OR LUNAR OCCULTER

POSITION OF EARTH OR MOON IN WINDOW OR TELESCOPE AXES COORDINATES (20)

$(X,Y,Z)_{n/L}$ (C-40); $h_{ijP\gamma}$ (D-70)

$$X^{n}_{P\gamma} = -\left[h_{11P\gamma} X_{n/L} + h_{12P\gamma} Y_{n/L} + h_{13P\gamma} Z_{n/L}\right]$$
$$Y^{n}_{P\gamma} = -\left[h_{21P\gamma} X_{n/L} + h_{22P\gamma} Y_{n/L} + h_{23P\gamma} Z_{n/L}\right]$$
$$Z^{n}_{P\gamma} = -\left[h_{31P\gamma} X_{n/L} + h_{32P\gamma} Y_{n/L} + h_{33P\gamma} Z_{n/L}\right]$$

SEMI-ANGLE OF MOON OR EARTH SUBTENDED BY LEM (21)

$r_{M/L}$ (C-30); $r_{n/L}$ (B-16); $\dot{r}_{M/L}$ (A-15); $\dot{r}_{n/L}$ (B-15)

$$\sin\mu^{*} = \frac{R_n}{r_{n/L}} \; ; \; 0 \le \mu^{*} \le \frac{\pi}{2}$$
$$\dot{\mu}^{*} = -\frac{\dot{r}_{n/L}}{r_{n/L}} \tan\mu^{*}$$

R_M (A-01); R_E (H-01); $\rho_{P\gamma max}$ (J-01)

MOON OR EARTH SCALED COORDINATES IN ABOVE WINDOW AND TELESCOPES (22)

$$x_{P\gamma} = \rho_{P\gamma} \cos\theta_{P\gamma}$$
$$y_{P\gamma} = \rho_{P\gamma} \sin\theta_{P\gamma}$$

MOON OR EARTH SCALED COORDINATES IN LEFT OR RIGHT WINDOW (23)

$$\rho_{P\gamma} = \frac{d_{P\gamma}}{Z^{n}_{P\gamma}}\left[(X^{n}_{P\gamma})^2 + (Y^{n}_{P\gamma})^2\right]^{\frac{1}{2}}$$
$$\theta_{P\gamma} = \tan^{-1}\left[\frac{Y^{n}_{P\gamma}}{X^{n}_{P\gamma}}\right]$$

$d_{P\gamma}$ (J-01)

OCCULTER LOGIC (24)

IF:	THEN:
$Z_{P\gamma} < 0$	$\rho_{P\gamma} = \rho_{P\gamma max}$
$Z_{P\gamma} \ge 0$, $\rho_{P\gamma} \ge \rho_{P\gamma max}$	$\rho_{P\gamma} = \rho_{P\gamma max}$
$X_{P\gamma} = Y_{P\gamma} = 0$	$\theta_{P\gamma} = 0$

MISSION EFFECTS PROJECTOR

DECLINATION AND RIGHT ASCENSION OF LEM RELATIVE TO FILM STRIP CENTERLINE (40)

$$\delta_f = \sin^{-1}\left[\frac{X_{QL}\sin i_f \sin\Omega_f - Y_{QL}\sin i_f \cos\Omega_f + Z_{QL}\cos i_f}{r_{n/L}}\right]$$
$$-\frac{\pi}{2} \le \delta_f \le \frac{\pi}{2}$$
$$\theta_f = \tan^{-1}\left[\frac{-X_{QL}\cos i_f \sin\Omega_f + Y_{QL}\cos i_f \cos\Omega_f + Z_{QL}\sin i_f}{X_{QL}\cos\Omega_f + Y_{QL}\sin\Omega_f}\right]$$

$r_{M/L}$ (A-12); $r_{E/L}$ (B-12); $(X,Y,Z)_{M/L}$ (A-22); Ω_f, i_f (J-01)

(40a)

IF:	THEN:
n = E (EARTH OPERATION)	Q = G (GEOGRAPHIC)
n = M (MOON OPERATION)	Q = S (SELENOGRAPHIC)

(49)

$$X_{GL} = f_{11} X_{EL} + f_{12} Y_{EL} + f_{13} Z_{EL}$$
$$Y_{GL} = f_{21} X_{EL} + f_{22} Y_{EL} + f_{23} Z_{EL}$$
$$Z_{GL} = f_{31} X_{EL} + f_{32} Y_{EL} + f_{33} Z_{EL}$$

f_{ij} (D-60); $(X,Y,Z)_{EL}$ (B-16)

SHEET 1 OF 4

VISUAL DISPLAY DRIVES

SHEET 2 OF 4

MISSION EFFECTS PROJECTOR (CONTINUED)

44

IF:	THEN:
n = E (EARTH OPERATION)	$a'_{ij} = f_{ij}$
n = M (LUNAR OPERATION)	$a'_{ij} = a_{ij}$

f_{ij} (D-60)

a_{ij} (D-10)

45

$$M_{gh} = \begin{bmatrix} \cos\delta_f \cos\theta_f & \cos\delta_f \sin\theta_f & \sin\delta_f \\ -\sin\theta_f & \cos\theta_f & 0 \\ -\sin\delta_f \cos\theta_f & -\sin\delta_f \sin\theta_f & \cos\delta_f \end{bmatrix}$$

δ_f, θ_f (J-40)

43 TRANSFORMATION MATRIX FROM TERRAIN FRAME TO OPTICAL AXES FRAME

$$V_{gk} = \left[M_{gh} M_{hi} a'_{ij} \ell_{ik_{pf_n}} \right]^T$$

$\ell_{ik_{pf_n}}$ (D-80)

46

$$M_{hi} = \begin{bmatrix} \cos\Omega_f & \sin\Omega_f & 0 \\ -\sin\Omega_f \cos i_f & \cos\Omega_f \cos i_f & \sin i_f \\ \sin\Omega_f \sin i_f & -\cos\Omega_f \sin i_f & \cos i_f \end{bmatrix}$$

Ω_f, i_f (J-01)

41 MEP OPTICAL HEAD DRIVES

$$\gamma^*_{pf} = \tan^{-1}\left[\frac{V_{32}}{V_{33}}\right]$$

$$\sigma^*_{pf} = \tan^{-1}\left[\frac{V_{32} \sin\gamma + V_{33} \cos\gamma}{-V_{31}}\right]$$

$$\phi^*_{pf} = \tan^{-1}\left[\frac{V_{12} \cos\gamma - V_{13} \sin\gamma}{V_{22} \cos\gamma - V_{23} \sin\gamma}\right]$$

42 GIMBAL LOCK LOGIC

IF:	THEN:
$\frac{\pi}{2} - \epsilon^* \leq \sigma^*_{pf} \leq \frac{\pi}{2}$	γ^*_{pf} = CONSTANT DEFINED WHEN $\sigma^*_{pf} = \frac{\pi}{2} - \epsilon^*$
$-\frac{\pi}{2} \leq \sigma^*_{pf} \leq -\frac{\pi}{2} + \epsilon^*$	γ^*_{pf} = CONSTANT DEFINED WHEN $\sigma^*_{pf} = -\frac{\pi}{2} + \epsilon^*$

ϵ^* (C-01)

LANDING AND ASCENT IMAGE GENERATOR

50 L/A OPTICAL HEAD DRIVES

LANDING AND ASCENT OPTICAL HEAD DRIVES ARE IDENTICAL TO J-41($\gamma^*_{pf}, \sigma^*_{pf}, \phi^*_{pf}$). AN IMAGE CAN BE GENERATED EITHER IN THE LEFT OR RIGHT WINDOW ($\gamma^*_{wg}, \sigma^*_{wg}, \phi^*_{wg}$; $g = \ell$ or r). CAMERA SWITCHING WILL BE DONE BY THE ASTRONAUT OR INSTUCTOR.

53 ALTITUDE REQUIRED TO FOCUS OPTICAL HEAD

$$h_{DE} = h_{DE_0} + \int \dot{h}_{ML}\, dt$$

$\dot{h}_{ML}$ (G-30)

52

$$h_{DE_0} = h_{ML_0} + (\alpha_{DE} - \alpha_{CG})$$

INITIALIZE h_{ML} WHEN LANDING AND ASCENT IMAGE GENERATOR IS ACTIVATED. AT LIFT-OFF, $\dot{h}_{ML} = 0$

h_{ML} (G-30)

α_{DE} (G-01)

α_{CG} (I-20)

51 LANDING TABLE DRIVES

LANDING TABLE DRIVES ARE IDENTICAL TO THE LAND MASS SIMULATOR DRIVES CALCULATED IN G-50(Y_{LM}, Z_{LM}).

Y_{LM}, Z_{LM} (G-50)

SHEET 2 OF 4

VISUAL DISPLAY DRIVES

J-   SHEET 3 OF 4

RENDEZVOUS AND DOCKING DISPLAY DRIVE EQUATIONS - LEFT AND RIGHT WINDOW VIEWING

1/20 SCALE MODEL - CSM GIMBAL ANGLE DRIVES

60

$(\psi_c)_{csm} = \tan^{-1}\dfrac{\rho_{12}}{\rho_{11}}$

$(\theta_c)_{csm} = \tan^{-1}\dfrac{\rho_{13}}{\rho_{11}\sin(\psi_c)_{csm} + \rho_{12}\cos(\psi_c)_{csm}}$

$(\phi_c)_{csm} = \tan^{-1}\dfrac{-\rho_{31}\cos(\psi_c)_{csm} + \rho_{32}\sin(\psi_c)_{csm}}{-\rho_{21}\sin(\psi_c)_{csm} + \rho_{22}\cos(\psi_c)_{csm}}$

DO NOT COMPUTE $(\theta_c)_{csm}$ WHEN 1/20 SCALE MODEL IS ACTIVATED

ϵ^* (C-70)

60a

GIMBAL LOCK LOGIC

IF:	THEN:
$\frac{\pi}{2} - \epsilon^* \le (\theta_c)_{csm} \le \frac{\pi}{2}$	$(\psi_c)_{csm}$ = CONSTANT DEFINED WHEN $(\theta_c)_{csm} = \frac{\pi}{2} - \epsilon^*$
$-\frac{\pi}{2} \le (\theta_c)_{csm} \le -\frac{\pi}{2} + \epsilon^*$	$(\psi_c)_{csm}$ = CONSTANT DEFINED WHEN $(\theta_c)_{csm} = -\frac{\pi}{2} + \epsilon^*$

TRANSFORMATION - FROM RENDEZVOUS TABLE AXES (Γ) TO COMMAND AXES

61

$\Gamma_{RK} = [\rho_{ij}]\,\rho_{TABLE}$

$[g_{KE}]^T$ (II-40)

FOR FRONT WINDOW VIEWING

$[\rho_{ij}]_{wf} = [g_{IK_c}][g_{KE}]^T[\gamma_{ij}]$

FOR TELESCOPE VIEWING

$[\rho_{ij}]_{T} = [g_{IK_c}][g_{KE}]^T[h_{em_{T}}]^T[h'_{mn_{wr}}]^T[\gamma_{nj}]$

FOR OVERHEAD WINDOW VIEWING

$[\rho_{ij}]_{wa} = [g_{IK_c}][g_{KE}]^T[h_{em_{wa}}]^T[h'_{mn_{wa}}]^T[\gamma_{nj}]$

$[h_{em_{T}}]_{wa}$ (D-70)

$[h'_{mn_{wa}}]_{wr}$ (J-72)

TRANSFORMATION FROM INERTIAL AXES (Γ) TO CSM BODY BY EULER (g_{IK_c}) INERTIAL MARE - FRAME

62

$g_{11_c} = \cos\psi_c \cos\theta_c$

$g_{12_c} = \cos\theta_c \sin\psi_c$

$g_{13_c} = -\sin\theta_c$

$g_{21_c} = -\cos\phi_c \sin\psi_c + \cos\psi_c \sin\phi_c \sin\theta_c$

$g_{22_c} = \cos\phi_c \cos\psi_c + \sin\phi_c \sin\phi_c \sin\theta_c$

$g_{23_c} = \sin\phi_c \cos\theta_c$

$g_{31_c} = \sin\phi_c \sin\psi_c + \cos\psi_c \cos\phi_c \sin\theta_c$

$g_{32_c} = -\sin\phi_c \cos\psi_c + \sin\psi_c \cos\phi_c \sin\theta_c$

$g_{33_c} = \cos\phi_c \cos\theta_c$

62a

CSM EULER ANGLE LOGIC

IF:	THEN:
CSM IS INERTIALLY STABILIZED	ψ_c = CONSTANT, θ_c = CONSTANT, ϕ_c = CONSTANT
CSM IS [illegible] STABILIZED	$\theta_c = \theta_{c_0} + \int \frac{H_{v/c}}{\Gamma_{RK}^T}\,dt$, [illegible]
CSM IS CONTROLLED BY INSTRUCTOR	$\psi_c = \int \dot\psi\,dt$, $\theta_c = \int \dot\theta\,dt$, $\phi_c = \int \dot\phi\,dt$
[illegible]	[illegible]

$H_{v/c}$ (B-24)

$\Gamma_{v/c}$ (B-47)

$(\dot\theta, \dot\phi, \dot\psi)_c$ (INSTRUCTOR INPUT)

TRANSFORMATION FROM RENDEZVOUS TABLE AXES (Γ) TO LEFT BODY WINDOW AXES (γ_{ij})

63

$\gamma_{11} = \cos\theta_{l_n}$

$\gamma_{12} = \sin\theta_{l_n}\sin\phi_{l_n}$

$\gamma_{13} = -\sin\theta_{l_n}\cos\phi_{l_n}$

$\gamma_{21} = 0$

$\gamma_{22} = \cos\phi_{l_n}$

$\gamma_{23} = \sin\phi_{l_n}$

$\gamma_{31} = \sin\theta_{l_n}$

$\gamma_{32} = -\cos\theta_{l_n}\sin\phi_{l_n}$

$\gamma_{33} = \cos\theta_{l_n}\cos\phi_{l_n}$

θ_{lc}, ϕ_{lc}

OR

θ_{wr}, ϕ_{wr} OR θ_{wa}, ϕ_{wa} (J-71a, 71b)

POST AND TRUNNION CAMERA DRIVE ANGLES FOR LEFT AND RIGHT WINDOWS ONLY

64

$\theta_{lc} = \tan^{-1}\left[\dfrac{\rho'_{x_c}}{\rho'_{z_c}}\right]$; IF: $\rho_{x_c} = \rho_{z_c} = 0$ THEN $\theta_{lc} = 0$

$\phi_{lc} = \tan^{-1}\left[\dfrac{\rho'_{y_c}}{\rho'_{z_c}\cos\theta_{lc} - \rho'_{x_c}\sin\theta_{lc}}\right]$

PARALLAX CORRECTION

64a

$\rho'_{x_c} = \rho_{x_c} - \alpha_{DP}$

$\rho'_{y_c} = \rho_{y_c} - \beta_{DP}$

$\rho'_{z_c} = \rho_{z_c} - \gamma_{DP}$

$\rho'_{cs} = \sqrt{(\rho'_{x_c})^2 + (\rho'_{y_c})^2 + (\rho'_{z_c})^2}$

$(\rho_x, \rho_y, \rho_z)_c$ (F-23)

$(\bar\alpha, \bar\beta, \bar\gamma)_{DP}$ (J-30)

65

SWITCHING LOGIC BETWEEN CSM MODELS

IF:	THEN:
$\rho_{cs} \le \rho'_{cs}$	USE 1/20 SCALE MODEL
$0 \le \rho'_{cs} \le \rho_{cs}$	USE 1/1 SCALE MODEL

ρ_{cs} (J-64)

73

TELESCOPE AND ABOVE WINDOW SWITCH LOGIC

No.	IF:	THEN:
1	$\Lambda_{T_f} \le \Lambda^*_{T_f}$	CSM IS VISIBLE IN EITHER LEFT, RIGHT, OR ABOVE TELESCOPE WINDOW MODES ARE INOPERATIVE. COMPUTE J-70a AND POST AND TRUNNION DRIVES $\phi_{ls_{T}}, \theta_{ls_{T}}$ (J-71a) & INPUT TO J-63. WHEN 1/20 CSM SCALE MODEL IS ACTIVATED TELESCOPE MODES ARE BYPASSED.
2	$\Lambda_{wa} \le \Lambda^*_{wa}$	CSM IS VISIBLE IN ABOVE WINDOW. COMPUTE J-70b AND POST AND TRUNNION DRIVES $\phi_{ls_{wa}}, \theta_{ls_{wa}}$ (J-71b) AND INPUT TO J-63.
3	$\Lambda_{wl} \le \Lambda^*_{wl}$ AND/OR $\Lambda_{wr} \le \Lambda^*_{wr}$	CSM IS VISIBLE IN LEFT AND/OR RIGHT WINDOW. COMPUTE POST & TRUNNION DRIVES ϕ_{lc}, θ_{lc} (J-64) AND INPUT TO J-63.
4	CSM NOT VISIBLE SINCE CONDITIONS 1, 2, 3 ARE NOT SATISFIED.	COMPUTE POST & TRUNNION DRIVE ANGLES CORRESPONDING TO LAST VIEWING MODE WHERE CSM WAS VISIBLE.
5	AT PROBLEM START CONDITIONS 1, 2, 3 ARE NOT SATISFIED.	COMPUTE LEFT & RIGHT WINDOW POST & TRUNNION DRIVE ANGLES θ_{lc}, ϕ_{lc} (J-64) AND INPUT TO J-63.

$\Lambda^*_{wf}, \Lambda^*_{T_f}$ (J-01)

SHEET 3 OF 4

RENDEZVOUS AND DOCKING DISPLAY DRIVE EQUATIONS - TELESCOPE AND ABOVE WINDOW VIEWING

CSM COORDINATES RELATIVE TO LEM WITH RESPECT TO TELESCOPE OR ABOVE WINDOW AXES

h_{ia_T} (D-70)

$h_{ia_{wa}}$ (D-70)

70a

$$\begin{pmatrix}\rho_{x_{T}}\\ \rho_{y_{T}}\\ \rho_{z_{T}}\end{pmatrix} = \left[h'_{ij_{wr}}\right]\left[h_{ja_T}\right]\begin{pmatrix}\rho'_{x_a}\\ \rho'_{y_a}\\ \rho'_{z_a}\end{pmatrix}$$

USE FOR TELESCOPE VIEWING

70b

$$\begin{pmatrix}\rho_{x_{wa}}\\ \rho_{y_{wa}}\\ \rho_{z_{wa}}\end{pmatrix} = \left[h'_{ij_{wl}}\right]\left[h_{ja_{wa}}\right]\begin{pmatrix}\rho'_{x_a}\\ \rho'_{y_a}\\ \rho'_{z_a}\end{pmatrix}$$

USE FOR ABOVE WINDOW VIEWING

POST AND TRUNNION CAMERA DRIVE ANGLES FOR LEM TELESCOPE AND ABOVE WINDOW ONLY

71a

$\theta_{ls_T} = \tan^{-1}\left[\dfrac{-\rho_{x_T}}{\rho_{z_T}}\right]$ $\qquad \phi_{ls_T} = \tan^{-1}\left[\dfrac{\rho_{y_T}}{\rho_{z_T}\cos\theta_{ls_T} - \rho_{x_T}\sin\theta_{ls_T}}\right]$

71b

$\theta_{ls_{wa}} = \tan^{-1}\left[\dfrac{-\rho_{x_{wa}}}{\rho_{z_{wa}}}\right]$ $\qquad \phi_{ls_{wa}} = \tan^{-1}\left[\dfrac{\rho_{y_{wa}}}{\rho_{z_{wa}}\cos\theta_{ls_{wa}} - \rho_{x_{wa}}\sin\theta_{ls_{wa}}}\right]$

TRANSFORMATION MATRIX BETWEEN TELESCOPE OR ABOVE WINDOW OPTICAL AXES AND POST AND TRUNNION AXES

72

$h'_{11_{wj}} = \cos\theta'_{wj}\cos\psi'_{wj} + \sin\psi'_{wj}\sin\phi'_{wj}\sin\theta'_{wj}$

$h'_{12_{wj}} = \cos\phi'_{wj}\sin\psi'_{wj}$

$h'_{13_{wj}} = -\sin\theta'_{wj}\cos\psi'_{wj} + \sin\psi'_{wj}\sin\phi'_{wj}\cos\theta'_{wj}$

$h'_{21_{wj}} = -\cos\theta'_{wj}\sin\psi'_{wj} + \sin\theta'_{wj}\cos\psi'_{wj}\sin\phi'_{wj}$

$h'_{22_{wj}} = \cos\phi'_{wj}\cos\psi'_{wj}$

$h'_{23_{wj}} = \cos\theta'_{wj}\sin\phi'_{wj}\cos\psi'_{wj} + \sin\psi'_{wj}\sin\theta'_{wj}$

$h'_{31_{wj}} = \sin\theta'_{wj}\cos\phi'_{wj}$

$h'_{32_{wj}} = -\sin\phi'_{wj}$

$h'_{33_{wj}} = \cos\theta'_{wj}\cos\phi'_{wj}$

74

POST & TRUNNION EULER ANGLE LOGIC FOR TELESCOPE & ABOVE WINDOW

IF:	THEN:
TELESCOPE MODE IS ACTIVATED (RIGHT CAMERA IS OPERATIVE).	$\phi'_{wr} = -\phi_{wr} + \phi_{a_{T}}$; $\theta'_{wr} = -\theta_{wr} + \theta_{a_T}$; $\psi'_{wr} = \psi_{RAS_{T}}$; $j = l, r, a$
ABOVE WINDOW MODE IS ACTIVATED (LEFT CAMERA IS OPERATIVE).	$\phi'_{wl} = -\phi_{wl} + \phi_{ewa}$; $\theta'_{wl} = -\theta_{wl} + \theta_{ewa}$; $\psi'_{wl} = \psi_{RAS_{wa}}$

ϕ_{wl}, θ_{wr} (J-01)

ϕ_{wl}, θ_{wr} (J-01)

θ_{a_T}, ϕ_{a_T} (J-01)

θ_{ewa}, ϕ_{ewa} (J-01)

$\psi_{RAS_T}, \psi_{RAS_{wa}}$ (J-01)

ANGLE BETWEEN WINDOW OR TELESCOPE OPTICAL AXES AND CSM LINE-OF-SIGHT

75

$(\phi, \theta)_{pf}$ (J-01)

$$\Lambda_{pf} = \cos^{-1}\left[\frac{\rho'_x}{\rho'_{cs}}\sin\theta_{pf} - \frac{\rho'_y}{\rho'_{cs}}\cos\theta_{pf}\sin\phi_{pf} + \frac{\rho'_z}{\rho'_{cs}}\cos\theta_{pf}\cos\phi_{pf}\right]$$

ρ'_{cs} (J-64a), $(\rho'_x, \rho'_y, \rho'_z)$ (J-64a)

VISUAL DISPLAY DRIVES

SHEET 4 OF 4

LEM-CSM SUN ILLUMINATION REQUIREMENTS

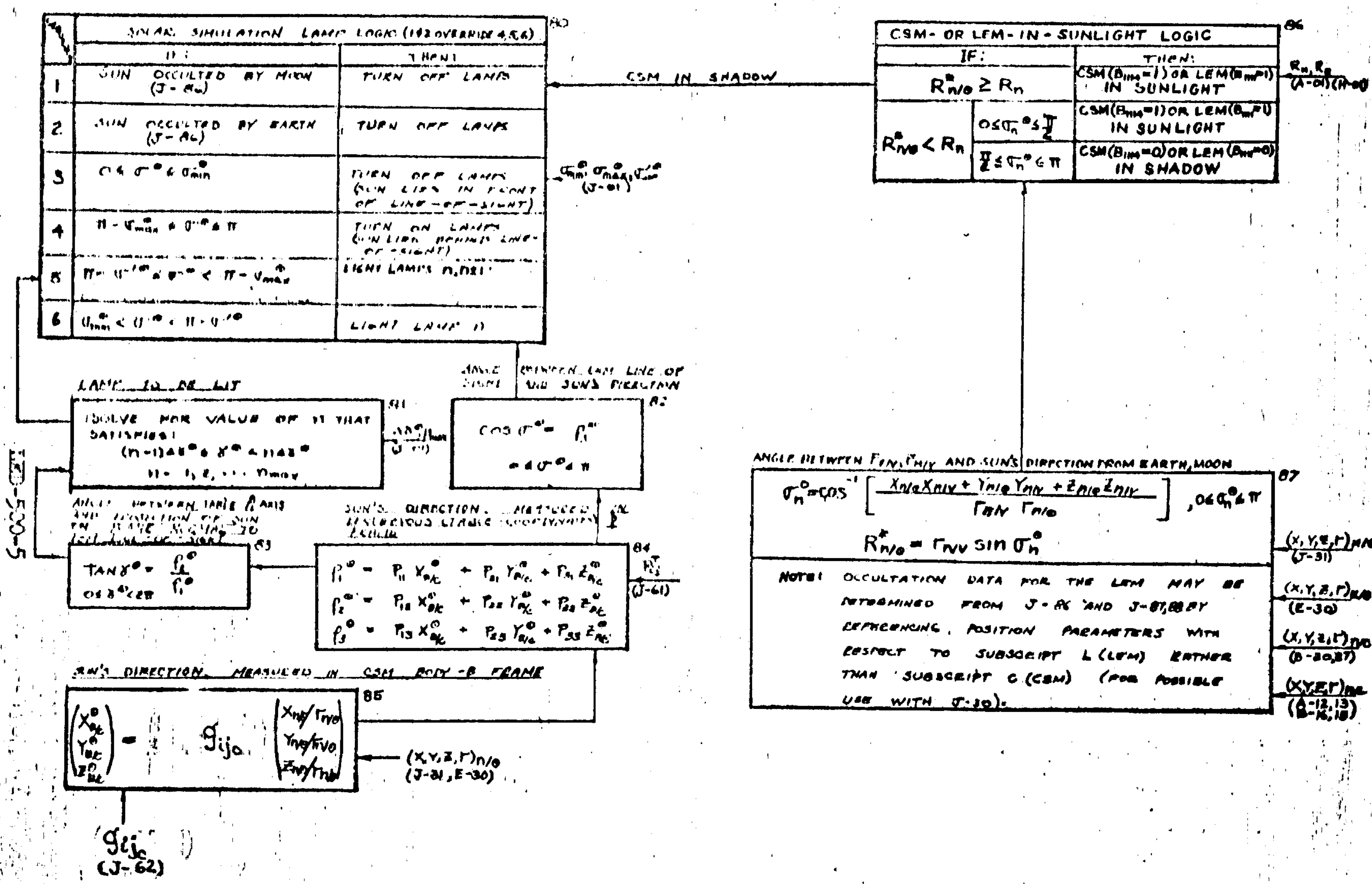

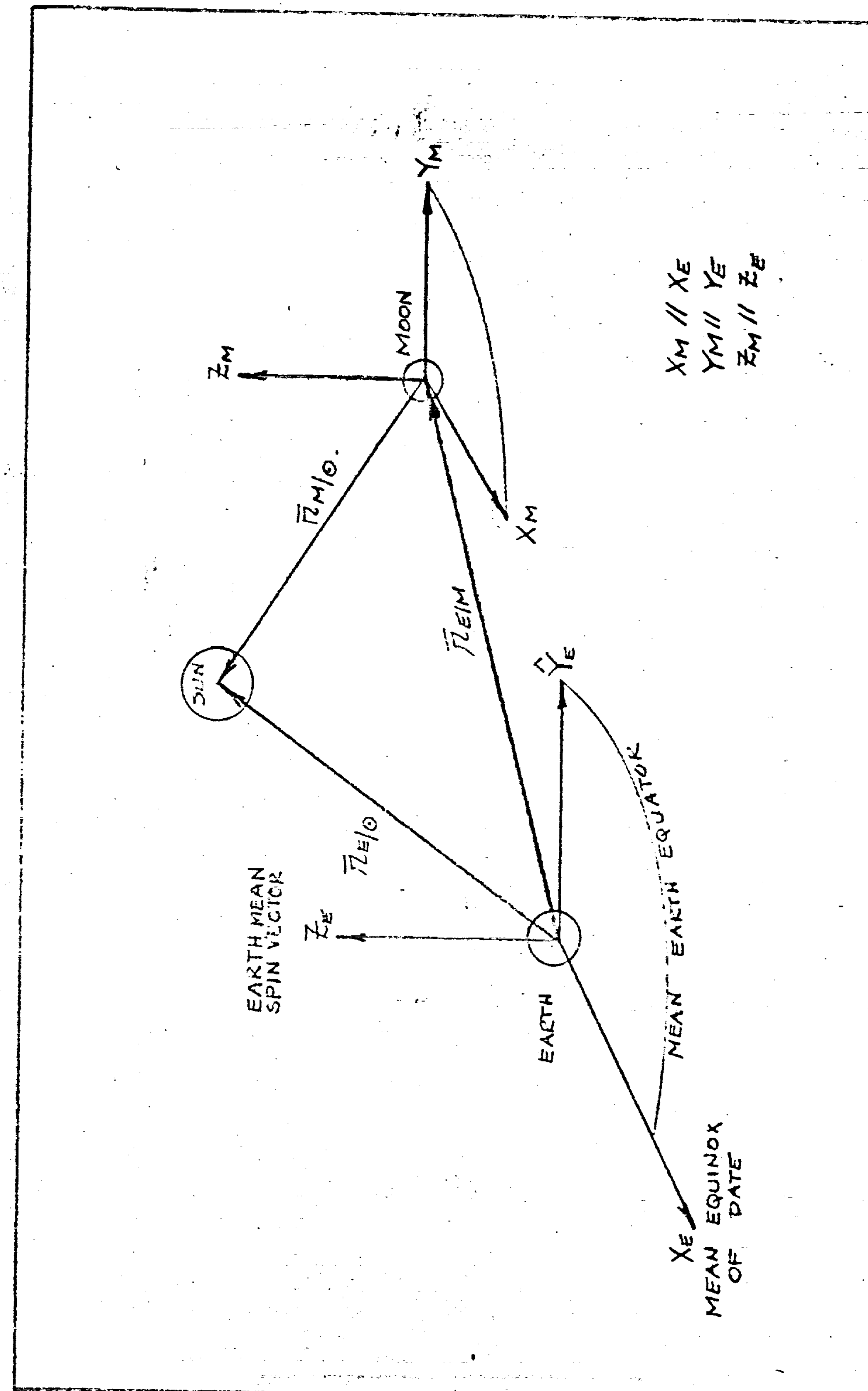

FIGURE-1 INERTIAL EARTH E AND MOON M-FRAME GEOMETRY

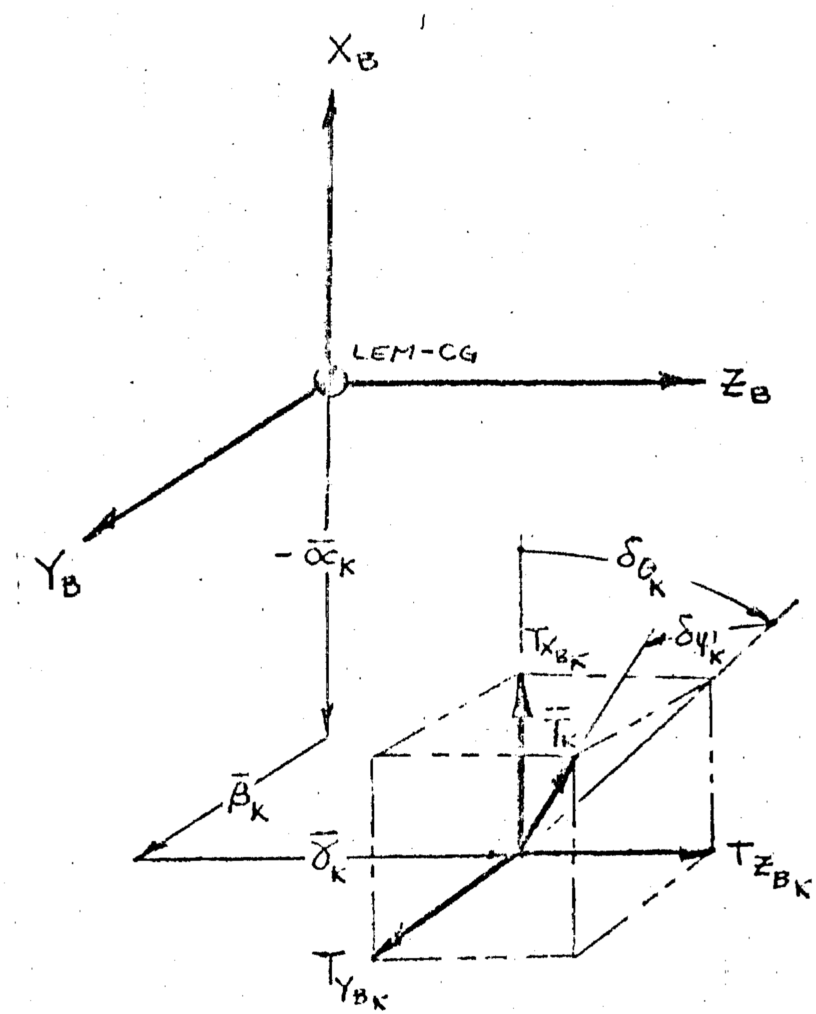

FIGURE-2 MAIN ENGINE THRUST GEOMETRY

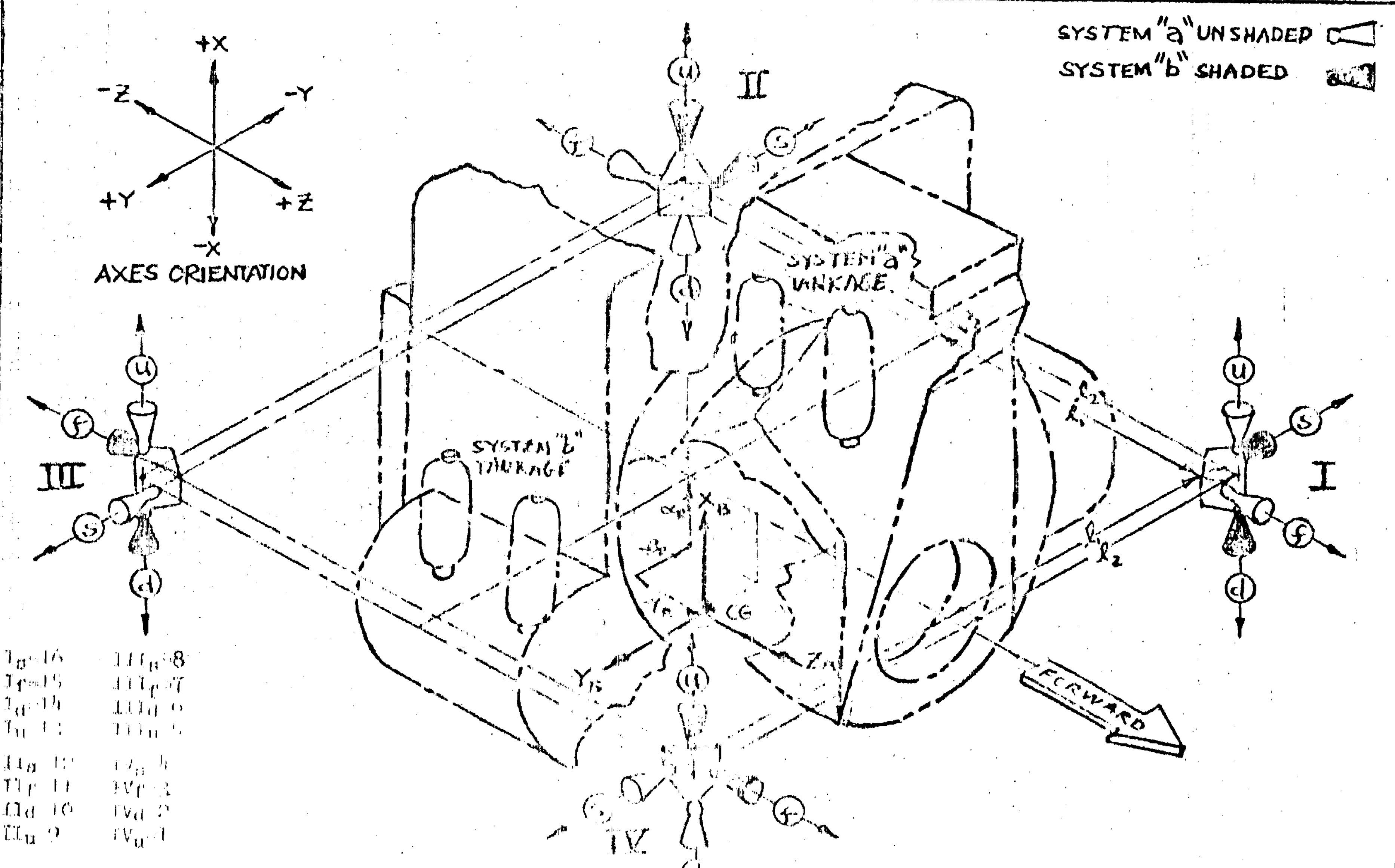

FIGURE-3 LEM RCS THRUSTERS & BODY B-FRAME GEOMETRY

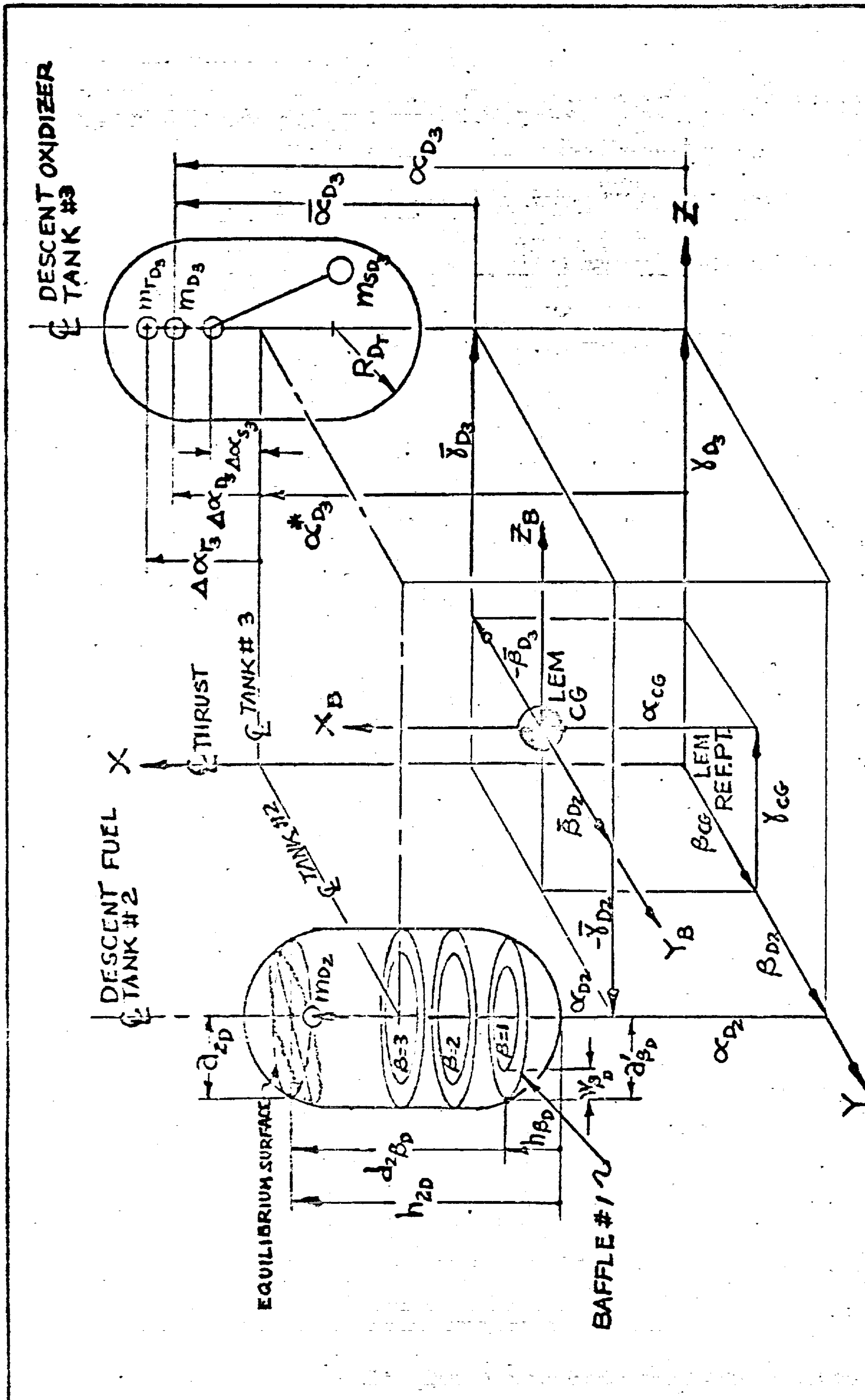

FIGURE-4 DESCENT TANK SLOSH MODEL

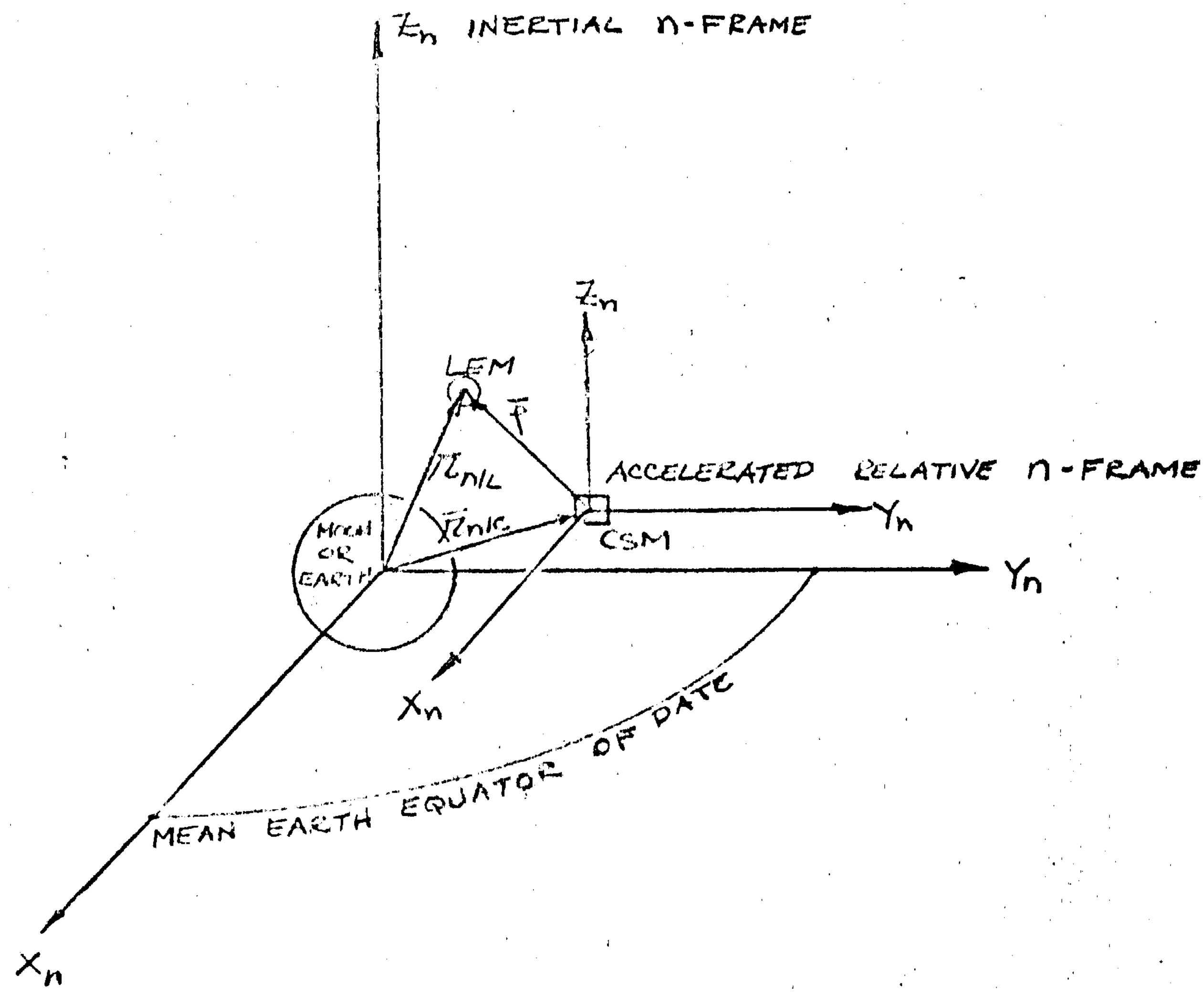

FIGURE 5 - INERTIAL AND RELATIVE M OR E-FRAME SCHEMATIC

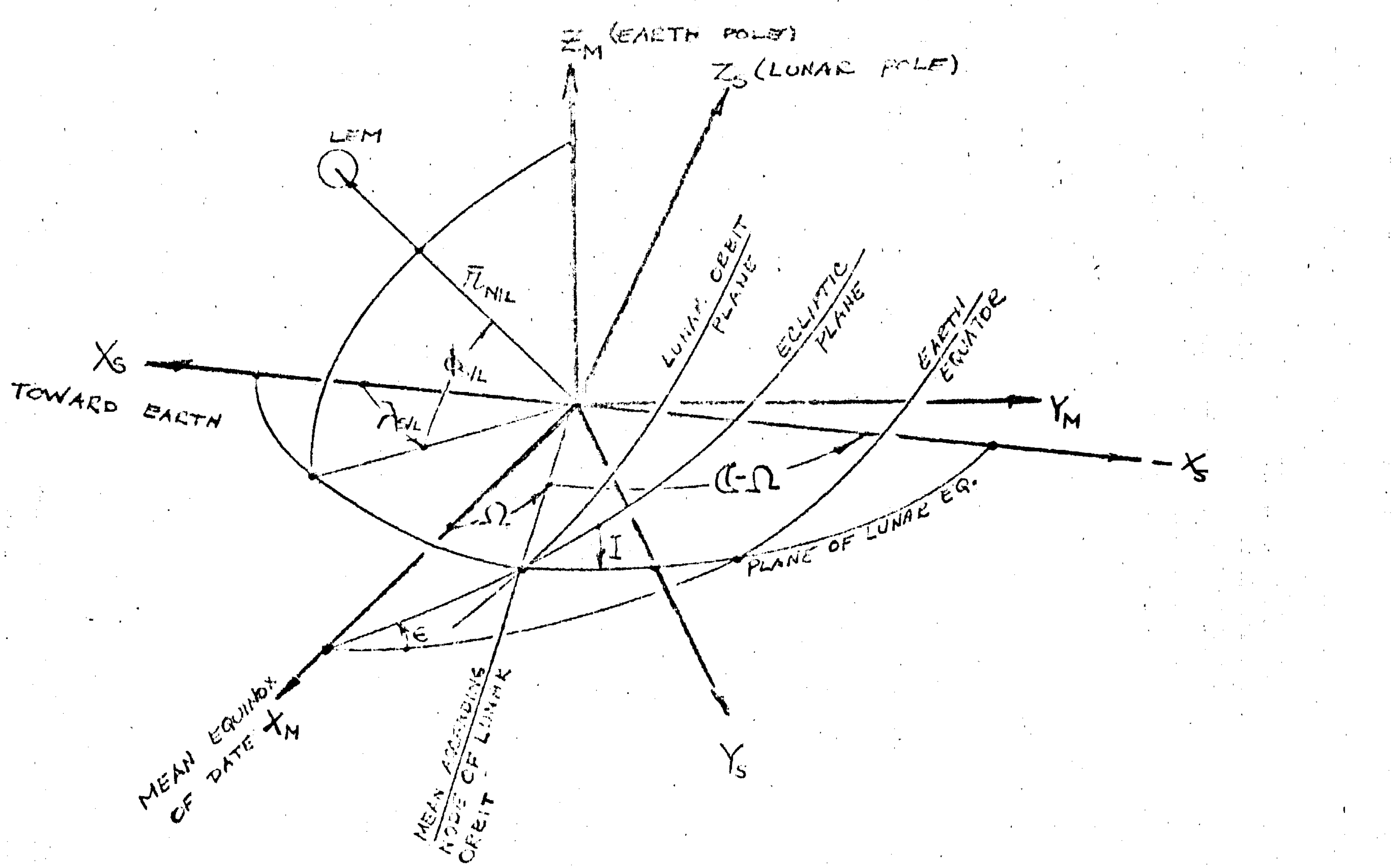

FIGURE-6 RELATION BETWEEN M-FRAME AND SELENOGRAPHIC S-FRAME

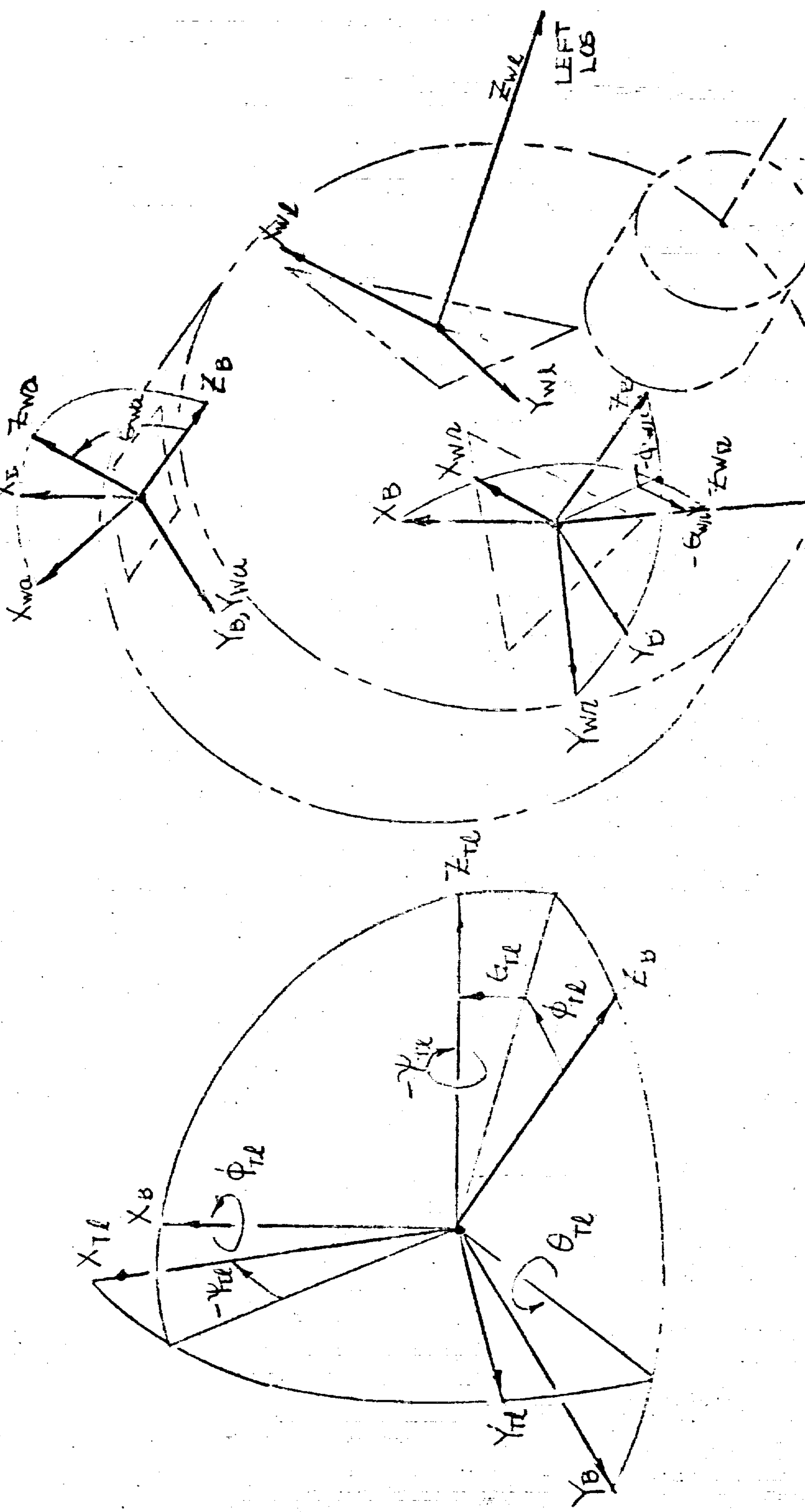

WINDOW OPTICAL AXES

LEFT TELESCOPE OPTICAL AXES

LEM OPTICAL AXES

FIGURE - 1

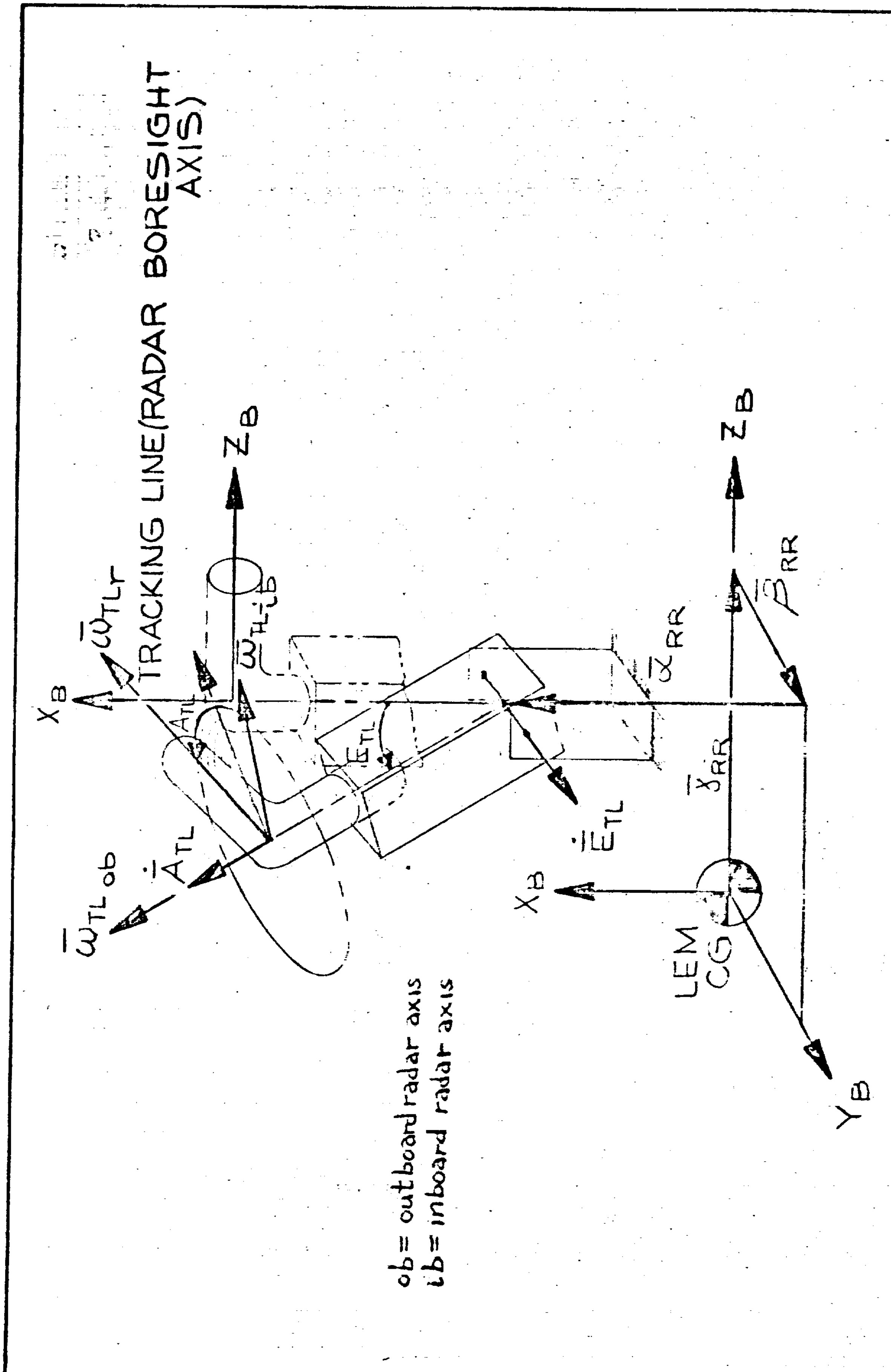

FIGURE 8. RENDEZVOUS RADAR GEOMETRY

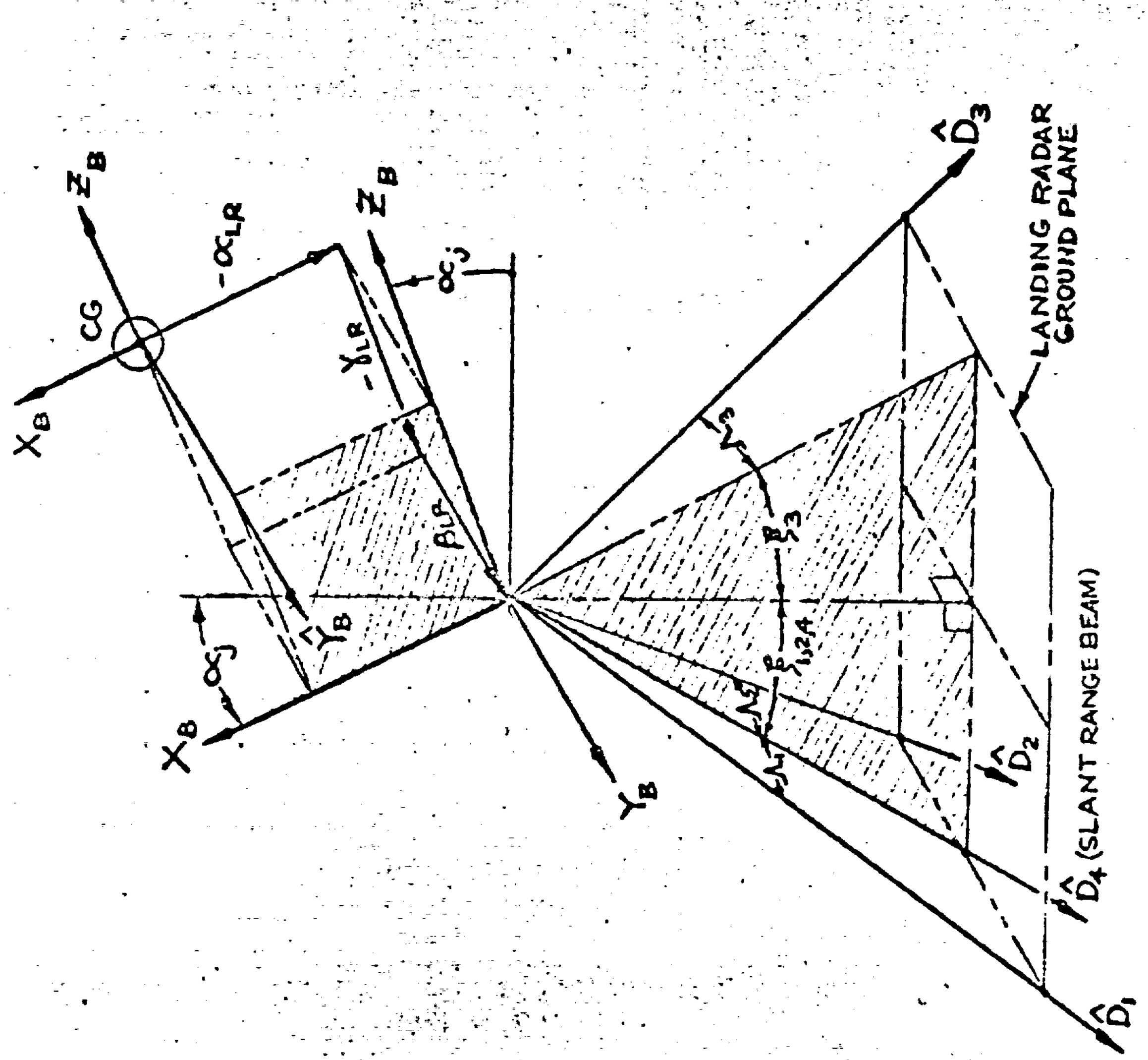

FIGURE-9 LEM LANDING RADAR GEOMETRY

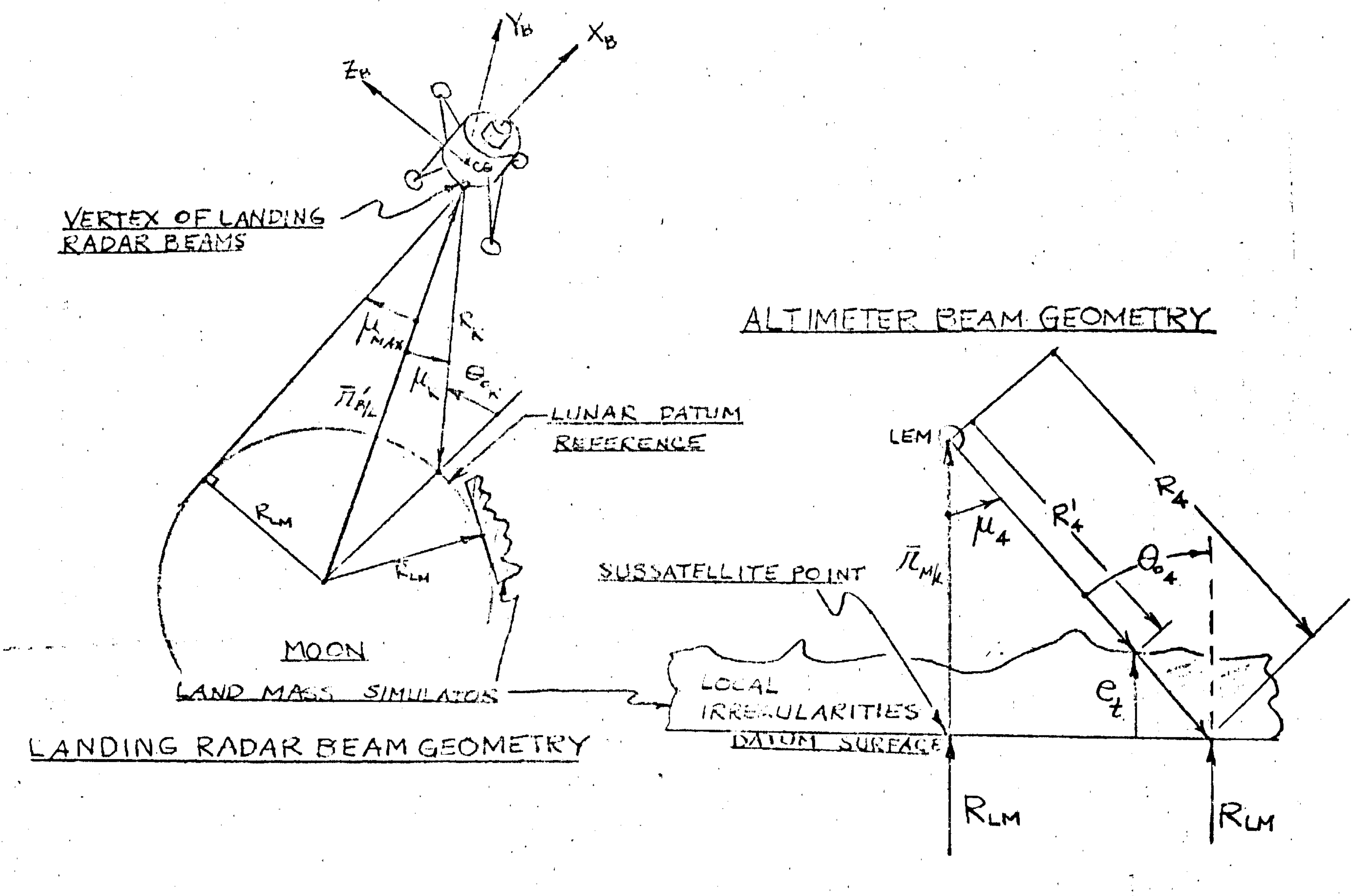

FIGURE-10 LANDING RADAR, LAND-MASS SIMULATOR (BEAM GEOMETRY)

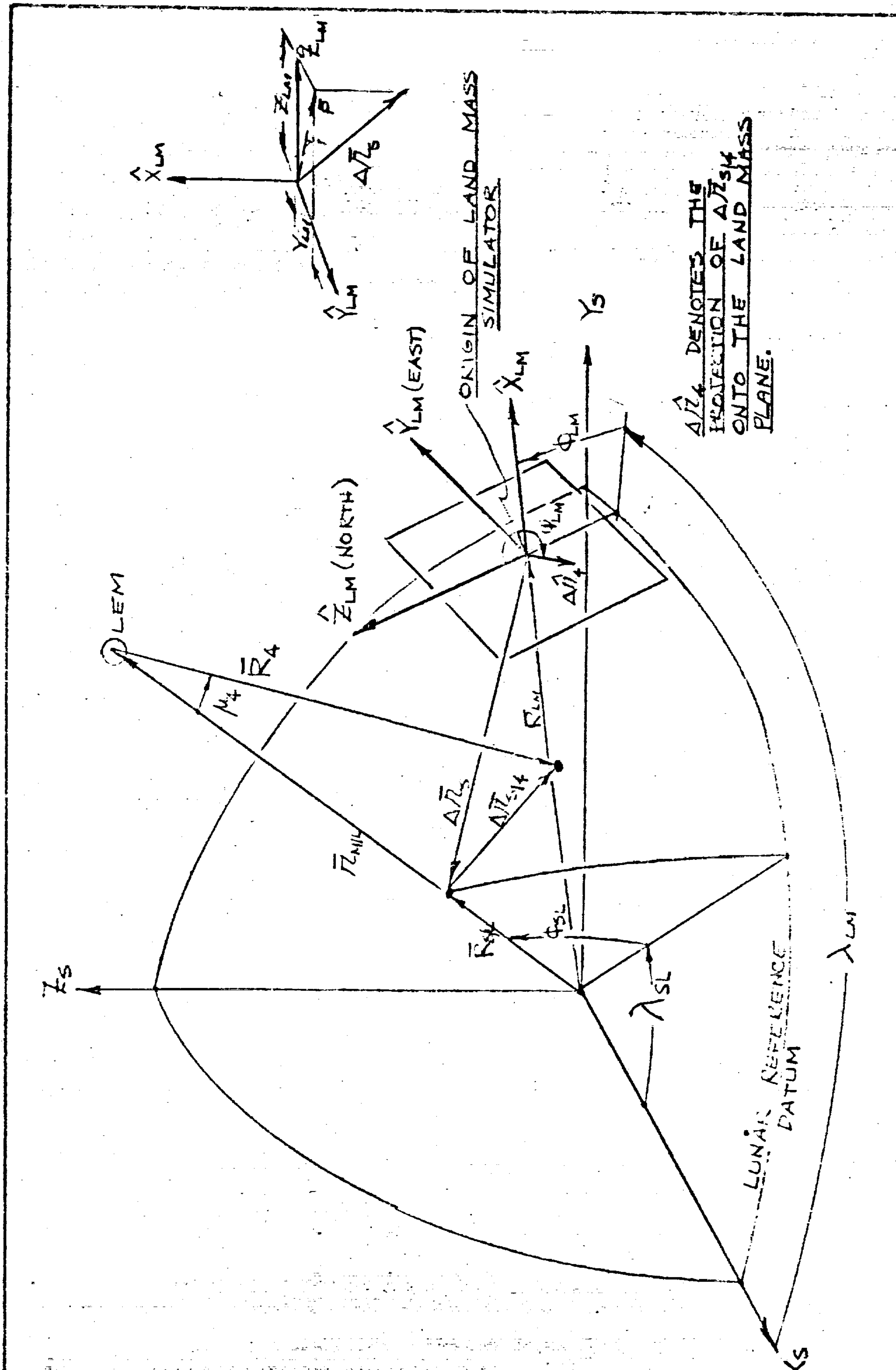

FIGURE-II LAND-MASS COORDINATE GEOMETRY

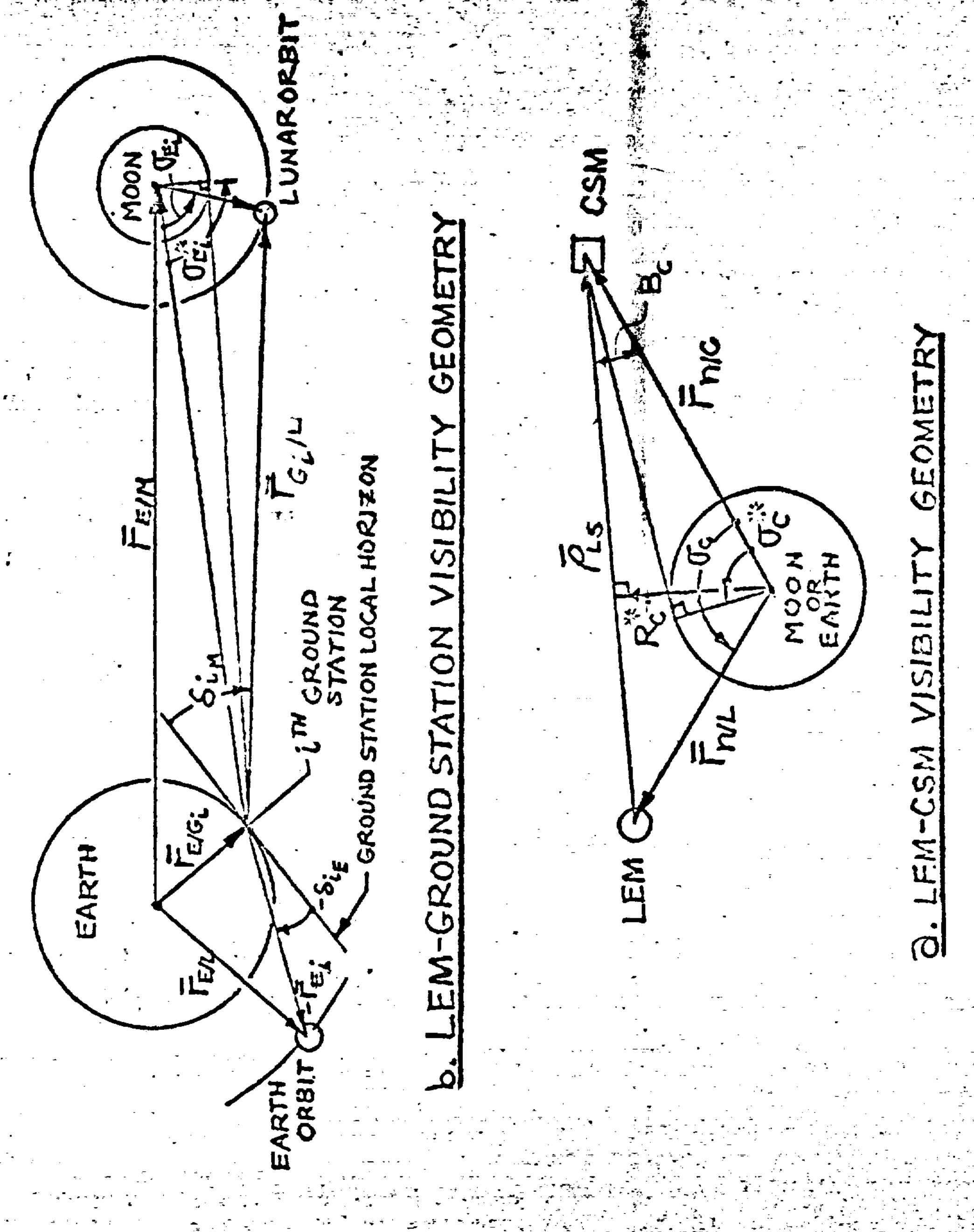

FIGURE-12 COMMUNICATION SCHEMATIC